UNIVERSITY OF CALIFORNIA
RIVERSIDE

Crystalline Open Framework Materials: from Structure to Function

A Dissertation submitted in partial satisfaction
of the requirements for the degree of

Doctor of Philosophy

in

Chemistry

by

Le Wang

December 2012

Dissertation Committee:

Dr. Pingyun Feng, Chairperson
Dr. Christopher A. Reed
Dr. Yadong Yin

The Dissertation of Le Wang is approved:

Committee Chairperson

University of California, Riverside

Acknowledgements

I would like to take this valuable opportunity to express my most sincere gratitude and respect to my advisor Professor Pingyun Feng. I greatly appreciate her inspiring ideas, continuous support and greatest encouragement. And I am deeply touched by her great passion in restless everyday working. This dedication and rigorous attitude toward science always have and will continue to inspire and benefit my research throughout my life.

I also thank my kind collaborators, Prof. Lake; Prof. Wu; Prof. Beyermann and especially our excellent long term crystallography advisor Prof. Bu. Their profound knowledge and insightful suggestions provided me a much wider aspect on research topics. Their kindly help, restricted attitude and active corporation all encouraged me in refining current work and creating new ideas.

During the five years, I have also been very fortunate to have the opportunities to work together with the most talented members in Prof. Feng's group and Prof. Bu's group: Dr. Tao Wu, Dr. Rui Liu, Dr. Xiang Zhao, Dr. Fan Zuo, Dr. Quanguo Zhai, Dr. Yang Liu, Dr. Zhenyu Zhang, Dr, Zhien Lin, Dr. Qipu Lin, Dr. Yang Hou, Dr. Guiyuan Jiang, Dr. Ying Zhang, Dr. Jian Zhang, Dr. Lei Ge, Jikai Liu, Fei Bu, Chengyu Mao, and Koroush Sasan, who help me in many ways.

I am also very grateful to the rest of my dissertation committee, Prof. Christopher

A. Reed and Prof. Yadong Yin, for their valuable comments on my dissertation.

There are many others who deserve many thanks. I would like to thank the staff in Depart of Chemistry for their kindly service and help.

Then, I would give my sincerely thanks to my instruments especially to my autoclaves and flasks for always being with me and producing a lot of fun in our lab. I would give my thanks to the microscope for revealing great results and sharing my joy at the first time. I would also give my sincerely thanks to my desk for fitting me a comfortable place for study from the very first afternoon of my arriving in this country.

Finally, I would like to thank my parents for everything they have done for me. Without their love, encourage and long time support, I would never be so happy in pursuing scientific research.

Dedication

To my Parents

ABSTRACT OF THE DISSERTATION

Crystalline Open Framework Materials: from Structure to Function

by

Le Wang

Doctor of Philosophy, Graduate Program in Chemistry
University of California, Riverside, December 2012
Dr. Pingyun Feng, Chairperson

The open framework materials have emerged as a highly active and rapidly developing domain of research because their rich host-guest chemistry could be utilized to develop promising materials such as absorbents, catalysts, sensors and substrates for mechanistic studies into fundamental surface interactions and catalytic mechanisms.

To better understand, predict and design materials with desired properties and functions, it is often essential to know the detailed structures, crystalline materials with well-defined periodic arrangements that allow for structural studies at the atomic resolution are of special importance. In addition, some properties such as uniform porosity and associated shape- or size-selectivity can be best designed with crystalline materials.

Unlike some other materials such as semiconductors in which properties can be

dramatically altered by simple doping, properties of open-framework materials are closely correlated with their general chemical compositions, and structural and geometrical features. As such, a great emphasis has been placed on creating materials with new crystal structures, in contrast with doping of well-known structure types. Hence the focus of this study is on the introduction of novel chemical-physical functions to the crystalline porous solids by fully exploring and understanding fundamental structural features and their possible correlation to properties and functions.

The first part of this work presented here is on creating pure inorganic framework structures, specifically metal-chalcogenide supertetrahedral-cluster-based frameworks, together with a discussion on their structure-property relationships. A series of such molecular architectures have been built by directed assembly of supertetrahedral clusters that can be viewed as artificial atoms with tunable radii. A new class of “hollowed-out bulk semiconductor” materials has been achieved. Both experimental evaluations and theoretical simulations on some pure phase compounds have been performed. Based on these new structures, the relationship between materials’ structural features and their optoelectronic properties is discussed.

The later parts of the work presented here deal with hybrid porous solids, specifically synthesis, characterizations and novel functions of metal-organic framework materials (MOF). By designed synthesis, one MOF material with unusual 4-level

structural hierarchy was assembled. Its magnetic property was evaluated, revealing an interesting geometry-induced magnetic frustration mechanism. Also, a catalytically active MOF was synthesized and characterized. Most importantly, single-crystal X-ray crystallography has been employed to capture the detailed molecular conformations of reaction intermediates on the active sites, which represents a powerful example of using a MOF-based novel methodology to elucidate catalytic mechanisms.

Table of Contents

List of figures

List of Tables

Chapter 1

An Overview to Crystalline Functional Framework Materials

1.1 Crystalline Framework Material

Crystalline porous solids emerged as a highly active domain of research decades ago together with the technical advances that had taken place in diffractometer instruments and computational methodologies. This growing research area covers a great number of classes to solid state materials including pure inorganic skeletons such as zeolites, metal phosphates, metal chalcogenide frameworks, and also hybrid materials as coordination polymers or more usually called metal organic frameworks (MOFs).

Porous solid materials are interesting to chemists because they generally represent the great potential in host guest interaction which could be utilized in developing them into promising materials such as absorbents, catalysts, sensors and substrates for surfaces interaction mechanism studies. Among these porous solids, the crystalline material is of special importance. As chemistry being a subject studying structure, composition, and inter-exchanging relationship to matters, it is of very necessity to study the detailed structure to substances in helping understanding, predicting and designing materials that are interesting. Crystalline materials with well defined atomic arrangements exactly satisfy the demanded structural resolution and also provide rich chemical information.

The study of crystalline porous materials was initiated as the demand of exact knowing to the existed sponge like rocks, zeolite. However it is of even greater curiosity to understand the formation and possibly further the manipulation on these micro scale channels and cavities. Synthetic control and directed assembling to create porous

molecular architectures have then attracted the attention of materials scientists because of such interest in the creation of nanometer-sized spaces and the novel phenomena in them. Thus the studies to the structure of crystalline frameworks materials has then transformed into a fully qualified field of research with an explosion of papers.[1]

Most of the currently reported research, including much of ours, refers to new phases with crystal structures. Only occasionally are there extensions with very brief indications about the functionality. It is a very necessary step for justifying the richness of chemical information of this research field. Hence the growing interest experienced in the chemistry community towards porous framework materials concerns much more of the increase in chemical-physical functions compared to 'classical' crystalline porous solids.

1. 2 Inorganic Framework Material

1. 2. 1 Zeolite

The earliest studied inorganic microporous solids are zeolite materials, the largest two subclasses of them are the aluminosilicates and the aluminophosphates. Zeolites are crystalline aluminosilicates with primary building blocks of SiO4/AlO4/MO4 tetrahedra. The corner sharing connection mode between adjacent tetrahedra defines 3- dimensional interconnected channels or windows sharing cages in which counter cations are present to balance the local charge. The microporosity is usually achieved by evacuating hydrated water molecules from the counter cations. Noteworthy, the inorganic frameworks are usually very stable upon dehydration. The micro pores within zeolites are often around sub-nanometers that were initially applied as molecular-sieves in small molecule separation and catalysis. After the achievements in synthetic aluminosilicate zeolites,

aluminophosphates and transition metal doped aluminophosphates frameworks were synthesized with much larger pore sizes and novel topologies.[2]

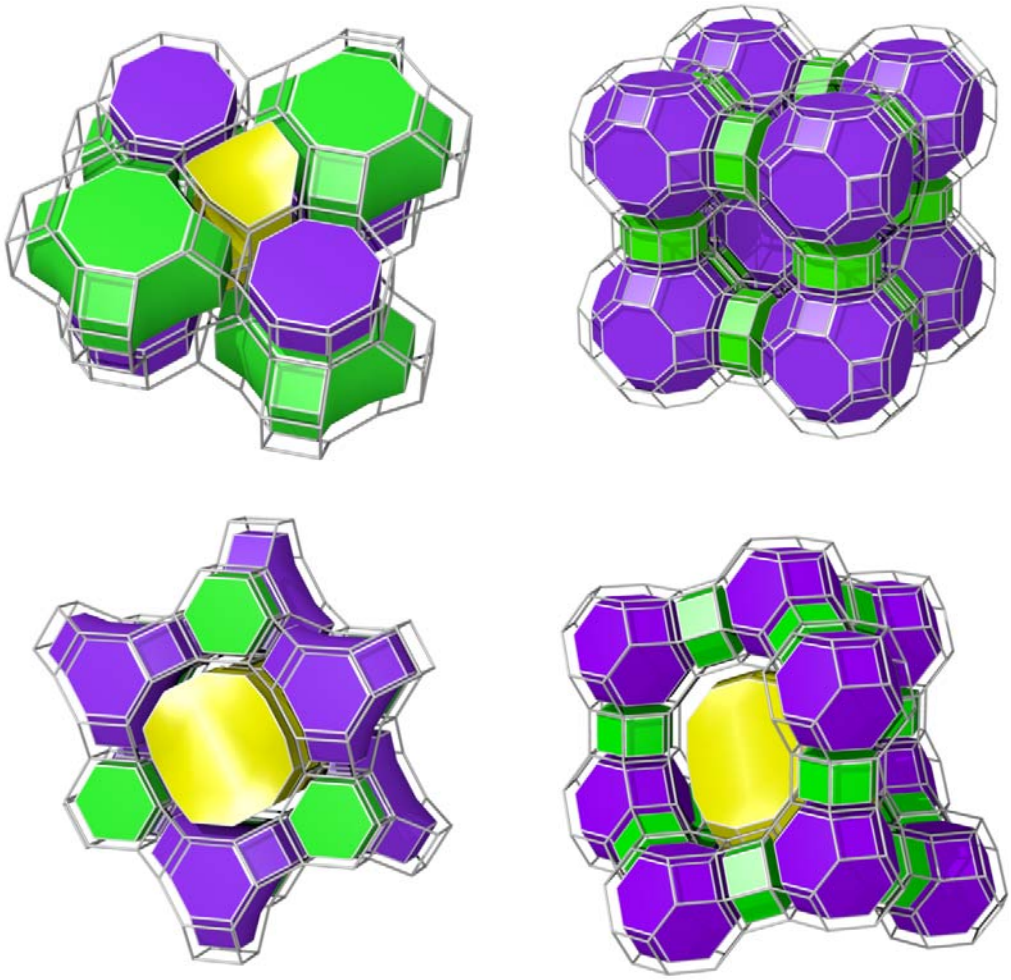

Figure 1.1. Natural tiling and net representations for some common zeolite topologies with large porosity (MER, RHO, GME and FAU).

Zeolite materials generally possess great thermal/hydrothermal stabilities and good survivability in a relatively wide pH range. Hence zeolite materials have already been widely applied as absorbents, molecular sieves and most importantly catalysts on an industry scale. However, zeolite materials are generally composed of fixed anions as

silicates or phosphates and therefore lack the compositional variance. Such fixed silica compositions renders the material to have lower conductivity which greatly limits the materials applications in photoelectrical processes. Meanwhile, the silicate and phosphate tetrahedral building block has an intrinsic limitation in its small dimension and high symmetry that is generally less likely to result in larger porosity and chirality that satisfies the desired spaces for large molecules and enantiomer involved tasks. Thus, zeolite materials tend not to be chosen as functional porous frameworks for these applications.

1. 2. 2 Metal Chalcogenide Open Frameworks

As stated above, research on crystalline porous materials began with oxides because of the natural abundance and interesting chemical properties of zeolites. To mimic the zeolite topologies with a great increase in the pores sizes, dimensional expansions on the 4-connected vertices were made: chalcogenide super clusters with tetrahedral geometries were introduced as a bi-functional building block.[3] These tetrahedral building blocks behave structurally as artificial atoms and are interconnected to form 4-connected skeletons with very large void space. On the other hand, metal chalcogenides are often found to be good semi-conducting materials with intriguing optochemical or electrochemical properties that could integrate multi-functionality such as photoelectric responses or photocatalytic properties together with porosity onto the same piece of material.[4] Moreover, the molecular architecture built by such large artificial atoms is also of great synthetic interest for it reveals fundamental principles of controlled hierarchical directed assembly on a nano scale.

1. 2. 2. 1 Tetrahedral Metal Chalcogenide Cluster Building Units

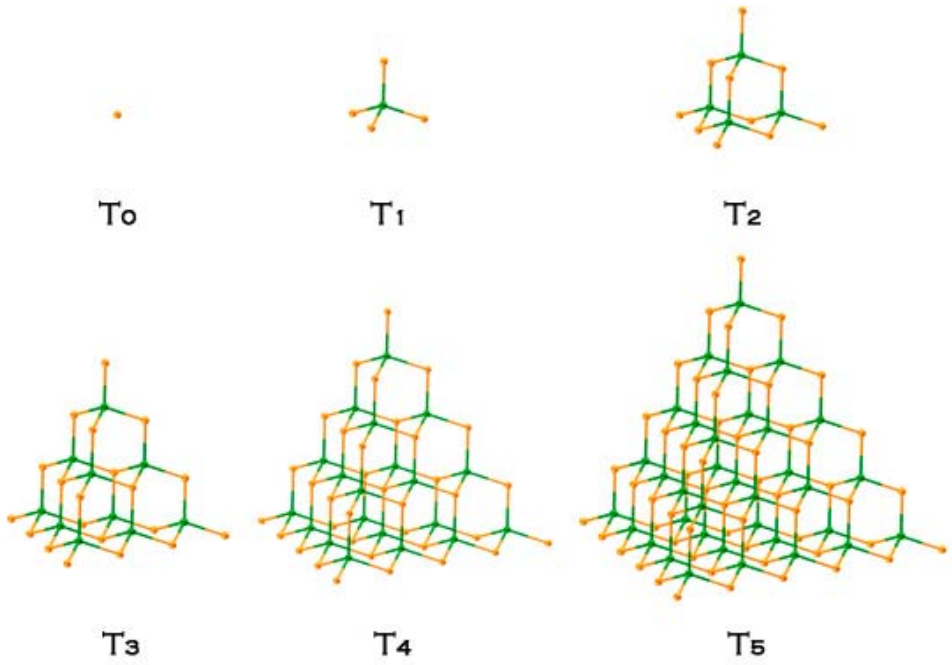

Figure 1.2. Structure and size comparison of Tn clusters. (T0 here just represents a tetrahedrally coordinated vertex like Si in zeolites)

The simplest tetrahedral clusters are supertetrahedral clusters and denoted as T*n*. They can be viewed as delicately shaped tetrahedral fragments of the ZnS blend type lattice. A typical formula for Tn cluster is as shown in Table 1, where *n* is the number of metal layers in each cluster. The number of cations (or anions) within each layer follows a mathematical series: 1, 3, ..., $n(n + 1)/2$. Without considering the cluster condensation by corner sharing, the number of chalcogenides in the clusters in a T*n* cluster is $[6(n - 1) +4]$. Take T2 clusters as an example: the stoichiometry for the T2 cluster would be M_4X_{10}, where X is a chalcogen atom such as S, Se or Te. To note that, the stoichiometry illustrated above is based on isolated clusters. For frameworks built by covalently

connected clusters, the overall stoichiometry of the framework varies depending on the connection mode.[5] Usually, the framework is formed by corner-sharing of all four corners on each cluster, and supertetrahedral clusters behave as exact tetrahedral connection vertices.

Table 1.1. Composition of the Super-supertetrahedral Metal Organic Clusters

Denotation	Metal Ions	Chalcogenide Anions	Examples
T1	1	4	/
T2	4	10	UCR20, UCR21, UCR22
T3	10	20	UCR6
T4	20	35	UCR1, UCR5
T5	35	56	UCR11, UCR16, UCR17

The most common case in corner-sharing mode has a bridging chalcogen atom that is shared by two clusters. This reduces the total number of anions by 2 in the overall framework stoichiometry. Importantly, the coordination number of anions is an important concern in the synthetic design of supertetrahedral clusters. While a T2 cluster consists of only bicoordinated anions, the face center of a T3 cluster is occupied by a tricoordinated anion. On the other hand, the T4 cluster has a chalcogen atom that can be considered as T0 which is tetrahedrally coordinated. For larger clusters, the core atoms have exactly the same coordination environment as in cubic ZnS lattice and in same size and geometry as T(n-4). The T5 cluster is so far the largest known supertetrahedral cluster and occurs in covalent 3D, 2D, and 1D superlattices. Isolated supertetrahedral clusters with size up to T5 with the help of a capping agent have also been achieved.[4a,6,7]

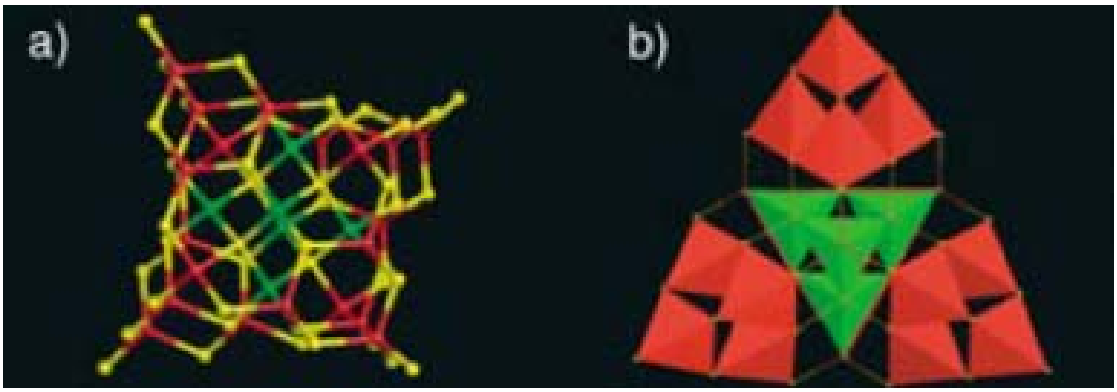

Figure 1.3. The largest synthesized cluster in Pn series: P2.

There is another interesting series of pure inorganic chalcogenide clusters with tetrahedral geometries reported such as pentasupertetrahedral clusters which are denoted as Pn. The general stoichiometry can be derived if each Pn cluster is treated as a higher level of hierarchical assembly between four normal Tn clusters and one anti-Tn cluster (Figure 1.3).[8] However the Pn clusters are not exact fragments of the cubic ZnS lattice. A hexagonal ZnS lattice feature has been introduced between attached surfaces of Tn and anti-Tn. Due to their complicated structural origin, they yield larger obstacles in correlating structure features with framework properties and can not be fully discussed here or in later chapters.

1. 2. 2. 2 Synthetic Control of the Size of Chalcogenide Clusters

Major metal cations applied for constructing chalcogenide clusters are high valent (III, IV) such as Ga, In, Ge, and Sn; and usually a small amount of divalent transition elements such as Zn, Mn, Fe, Co, and Cu. As a crucial synthetic factor in controlling cluster size, reported chalcogenides synthesis usually involved a planned combination of cations with different valences such as (M(III)/M(IV), M(III)/M(II), M(III)/M(I), M(III)/M(IV)/M(II), and M(III)/M(I)/M(IV).[4a, 4d, 5a, 9] The charge on metal cations is an

important factor affecting the size of chalcogenide clusters. This effect is related to Pauling's electrostatic valence rule that states that the valence of each anion is exactly or nearly equal to the sum of the electrostatic bond strength to it from adjacent cations. For cations with uniform tetrahedral geometry, the electrostatic bond strength is often estimated as one quarter of the charge on it. A more accurate calculation of the bond valence makes use of each individual bond length and the empirical model proposed by Brown. Inorganic researchers use the term local charge balance to refer to this situation where the charge of an anion is passivated by its adjacent cations. This local charge balance is in contrast with another term called global charge balance, which we use to refer to the electro-neutralization between the host framework and extra-framework counter ions.

The local charge balancing theory worked every time in our synthetic designs and some guidelines are given below. By applying Pauling's electrostatic valence sum rule, to balance the local charge of the four-coordinated sulfur atom at the center of the T4 or T5 clusters, low valent metals such as Zn or Cu should be employed. In other words, the incorporation of low valent metal ions into the synthesis promotes the formation of larger clusters. Conversely, to shrink the cluster size, higher valent cations such as Ge or Sn would be necessary to force the sulfur into the lower coordination numbers, hence promoting the formation of T2 clusters and inhibiting the formation of the larger clusters such as T4 and T5.

1. 2. 2. 3 Frameworks Built by Metal Chalcogenide Cluster

Because open framework chalcogenides are generally based on the linkage of

negatively charged clusters, there is a natural requirement to apply large sized counter cations to satisfy the global charge balancing. Inspired by the great success of the organic amine templates used in zeolite synthesis, the earliest synthetic work on metal chalcogenide framework synthesis followed the same way. And since the hydrothermal synthesis of open framework chalcogenides seldom starts with molecular clusters as precursors, a basic solution is also found to be greatly favored to the reaction between metal and chalcogen elements.

As such, the initial process usually involves redox chemistry and formation of clusters. It further becomes a very complicated system with ions and clusters of various types and sizes that coexist in the same solution. Equilibria between various clusters in solution would shift to favor one or more clusters when crystallization involving these clusters occurs. One very good example of a system that demonstrates the selective crystallization of different clusters is the Cu-In-Ge-S mixture containing amine molecules. The presence of both M(I) and M(III) ions in a solution allows the formation of T5 ($Cu_5In_{30}S_{56}$) clusters, however the M(III)/M(IV) combination favors T2(In_3GeS_{10}) clusters. In our work, by using appropriate amine molecules, several structures involving them can be crystallized into a superlattice within the same bottle. All three phases UCR-20 (pure T2 cluster based), CIS-52 (T5-T2 cluster mixed) and UCR-16 (pure T5 cluster based) were formed using the same template amine counter cation despite the very different cluster sizes. This experiment demonstrates well the complicated equilibria of amine-directed selective crystallization.

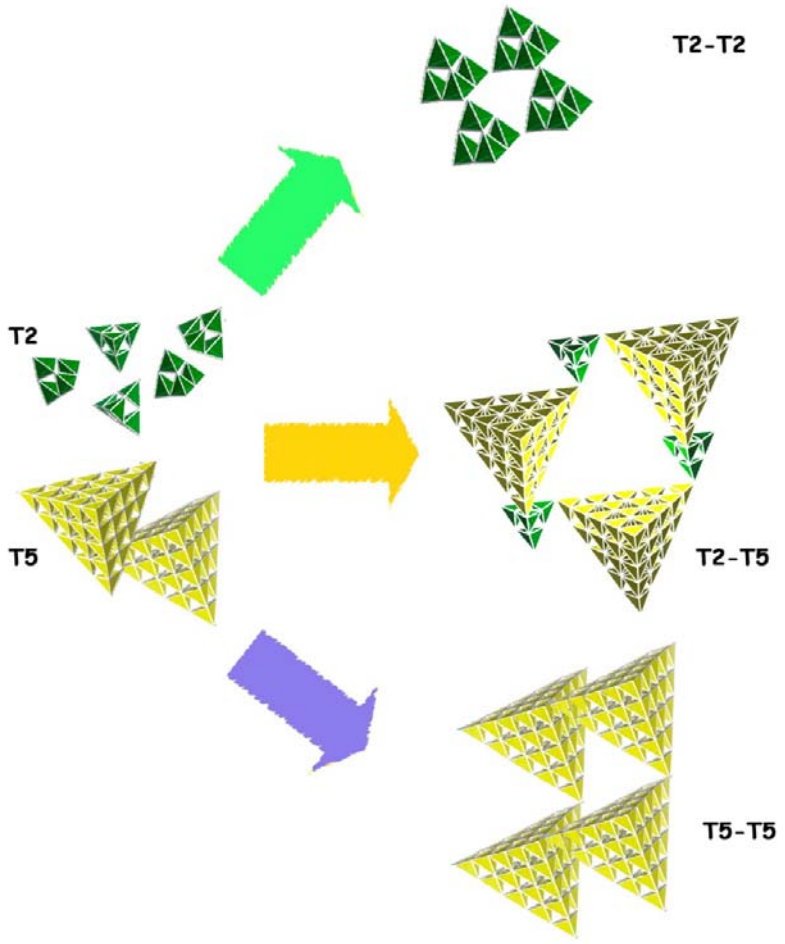

Figure 1.4. Selective crystallizations in solution with different sized clusters.

Upon applying numerous variants of organic amines and other inorganic cations as structure-directing agents to different combinations of metal chalcogenide systems, many inter-cluster connection modes and overall topologies were achieved. Some of these topologies could be synthesized with different composition and even different cluster size. Most of them possess large solvent-accessible void spaces which potentially could be evacuated to generated very large pore sizes though with special treatments as ion exchange. Some of the achieved topologies are shown below.

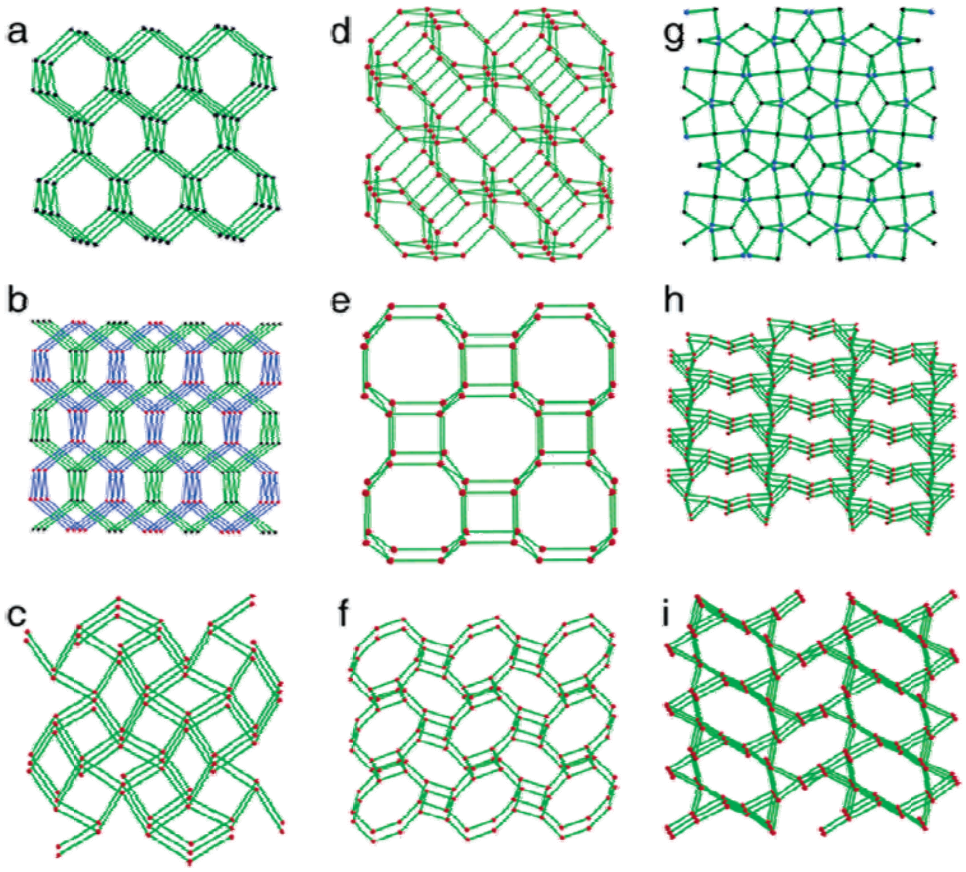

Figure 1.5. Examples of 3D framework topologies formed from tetrahedral clusters: (a) single diamond; (b) double diamond; (c) UCR-1; (d) SOD; (e) CrB4; (f) ABW; (g) cubic-C3N4; (h) ICF-24; (i) ICF-25. Except for the cubic-C3N4 type topology, all others are 4-connected 3D nets with each sphere representing a tetrahedral node that can be occupied either by a single tetrahedral atom or in chalcogenides by a tetrahedral cluster. For the cubic-C3N4 type, blue spheres are three-connected sites and black spheres are 4-connected sites.

1. 2. 2. 4 Selected Functionalities of Metal Chalcogenide Frameworks

A great number of metal chalcogenide open frameworks have been reported. These open frameworks have shown great compositional richness and especially astonishing topological features. Moreover, many of them have shown interesting chemical physical properties with promising applications.

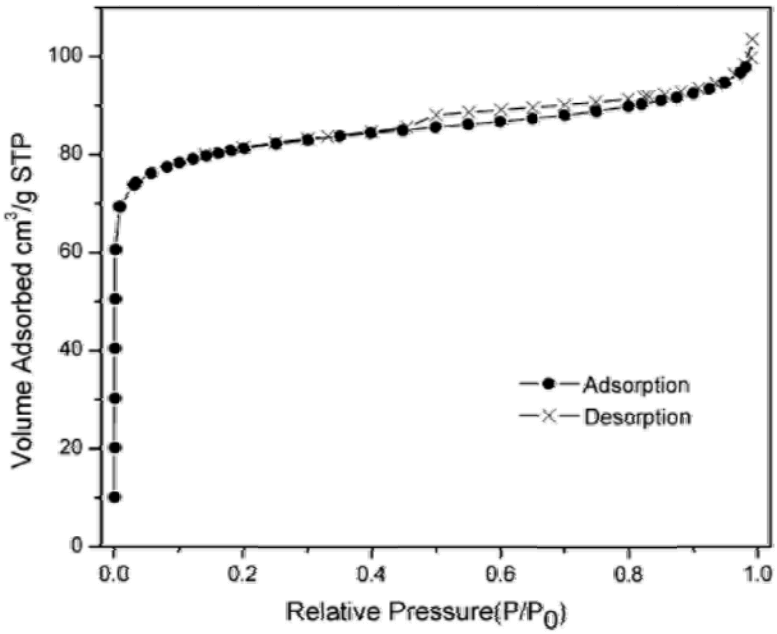

Figure 1.6. Nitrogen adsorption and desorption isotherms measured at 77 K for the Cs+-exchanged UCR-20GaGeS-TAEA. The ion exchange was performed at 373 K for 60 h and then dried at 353 K for 2 h. Prior to the measurement, the sample was degassed at 373K for 10 h.

Due to their porous nature, they are good candidates for adsorbing small molecules. However only a few open framework chalcogenides are known to show microporosity through gas adsorption because of the pore blocking by amine templates. Also, their generally relatively low thermal stability above 500^{o}C prohibits completely remove organic guest molecules through calcination. For a typical framework, as high as 70% of nitrogen, 40% of carbon and 80% of hydrogen could be removed from the framework by direct calcination at 350^{o}C in nitrogen. However, carbonization left behind carbon that blocks the pores and makes them inaccessible. Luckily, ion exchange is among the most common properties of open framework solids, especially when the framework is heavily charged. This property has been shown for a number of open framework sulfides, in

which protonated amine molecules can be exchanged with inorganic cations such as Na+. Delicately conducted exchange experiments with Cs+ ions led to an almost complete removal of amine molecules. The Cs^+ exchanged UCR-20GaGeS-TAEA framework exhibits the type I isotherm characteristic of a microporous solid. This sample has a high BET surface area of 807 m^2/g and a micropore volume of 0.23 cm^3/g despite the presence of much heavier elements (Cs-Ga-Ge-S).[4a]

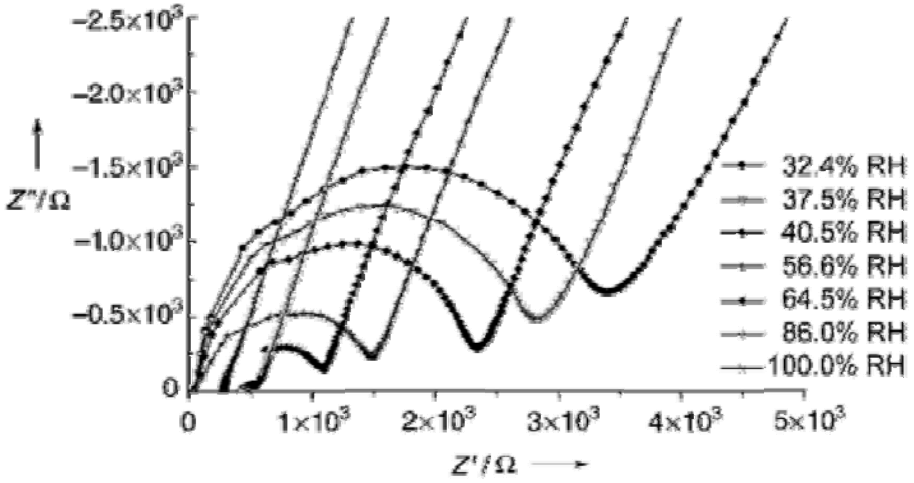

Figure 1.7. The ac impedance plots of metal chalcogenide open framework material at room temperature and different relative humidities. (ICF-26)

On the other hand, as heavily charge frameworks with fairly large pore size, metal chalcogenide frameworks are good ionic conductors for light ions with good mobilities. Even though the overall conductivity of chalcogenides may consist of contributions from both electronic and ionic conductions that allow their application as solid electrolyte, they can still serve as model compounds for conducting mechanisms. The intrinsic advantage of a hollowed framework is that it tends to lower the electronic conductivity because of the more localized electronic states within clusters while exposing the ionic contribution.

Hence these 3D chalcogenides containing mobile alkali metal cations has led to a new class of fast ion conductors. These crystalline inorganic chalcogenides integrate zeolite-like architecture with high anionic framework polarizability and high concentrations of mobile cations.[4b] These structural features are particularly desirable for enhancing ionic conductivity. At room temperature and under relative humidity of 30% or higher, the specific conductivity of these materials is comparable to or exceeds previously known crystalline sodium or lithium conductors. In general, the conductivity increases with increasing humidity. The highest specific conductivity achieved among open framework chalcogenides is 0.15 Ω^{-1} cm^{-1} at room temperature and under 100% relative humidity.

By sharing the same composition with semiconducting materials, most open framework chalcogenides have been shown to display photoluminescence with tunable emission wavelengths ranging almost continuously from 450 to 600 nm. The electronic band gaps of these chalcogenides are generally smaller than open framework oxides and many of them are in the visible range. This makes it possible to explore these open framework materials for applications ranging from solar cells to photocatalysis with visible light. In our preliminary work, some of these open framework chalcogenides have been found to be highly active as visible-light photocatalysts for the reduction of water into hydrogen.[4e]

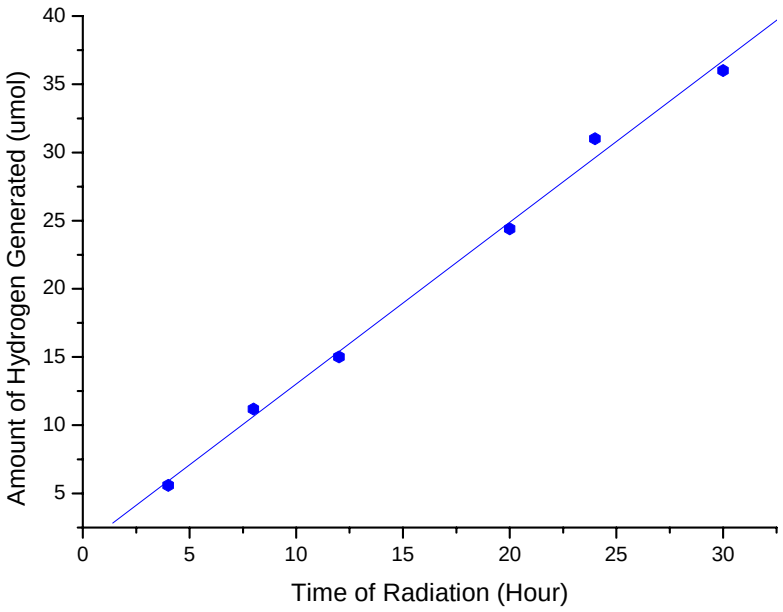

Figure 1.8. Photocatalytic activity for hydrogen generation of CIS-11.

1. 3 Hybrid Frameworks: Metal-Organic Frameworks

1. 3. 1 General Description

Coordination polymers, more often called metal-organic frameworks, cover a large class of hybrid crystalline porous materials that are composed of inorganic parts like single metal ions, metal-oxo oligomeric clusters, or metal-oxo polymeric chains that are joined by organic ligand struts via coordinate bonds.[1b, 10] These types of porous crystalline solids are hybrid materials compared to traditional pure inorganic porous materials like zeolites and they have obvious advantages in structural and compositional diversity. Unlike the only topology control method to the connection between tetrahedral units only by template counter cations in zeolite synthesis, the MOF materials adopt their topology largely based on the pre-designed organic ligands. The organic building blocks

not only provide ease and great versatility in topology directing on a synthetic aspect, they also carry complicated symmetry elements and enrich the structure with chemical information such as molecular or space chirality. More importantly, compared to bridging oxygen atoms organic linkers are much better spacers. They tend to create larger void spaces for host-guest interactions with bulkier molecules, not to mention their capability of in introducing specific binding affinities by grafting functional groups. Therefore, MOF materials are believed to have many potential applications such as gas storage, separation, sensing and catalysis.

During the past decade, MOF material synthesis has become one of the most interesting research areas and has experienced an explosion of different compounds. Some of them present astonishingly beautiful structures and show interesting properties at the same time. Figure 1.9 illustrates several of the most studied MOFs in exemplifying the material's beauty.[1a, 10a, 11] All the metal nodes or metal oxo-clusters constructing the polymeric framework have discrete counterparts in oganometallics and are quite commonly seen. Hence, it is usually believed this type of material is formed by pre-assembled oligo-metal-ligand clusters in the same configuration, and these fragments are defined as sub-building units (SBU). As a result, the conceptual structure design becomes more realistic in this MOF system since by assembling an organic ligand with special symmetry elements and the appropriate SBUs, the final topology can be very close to what is desired.

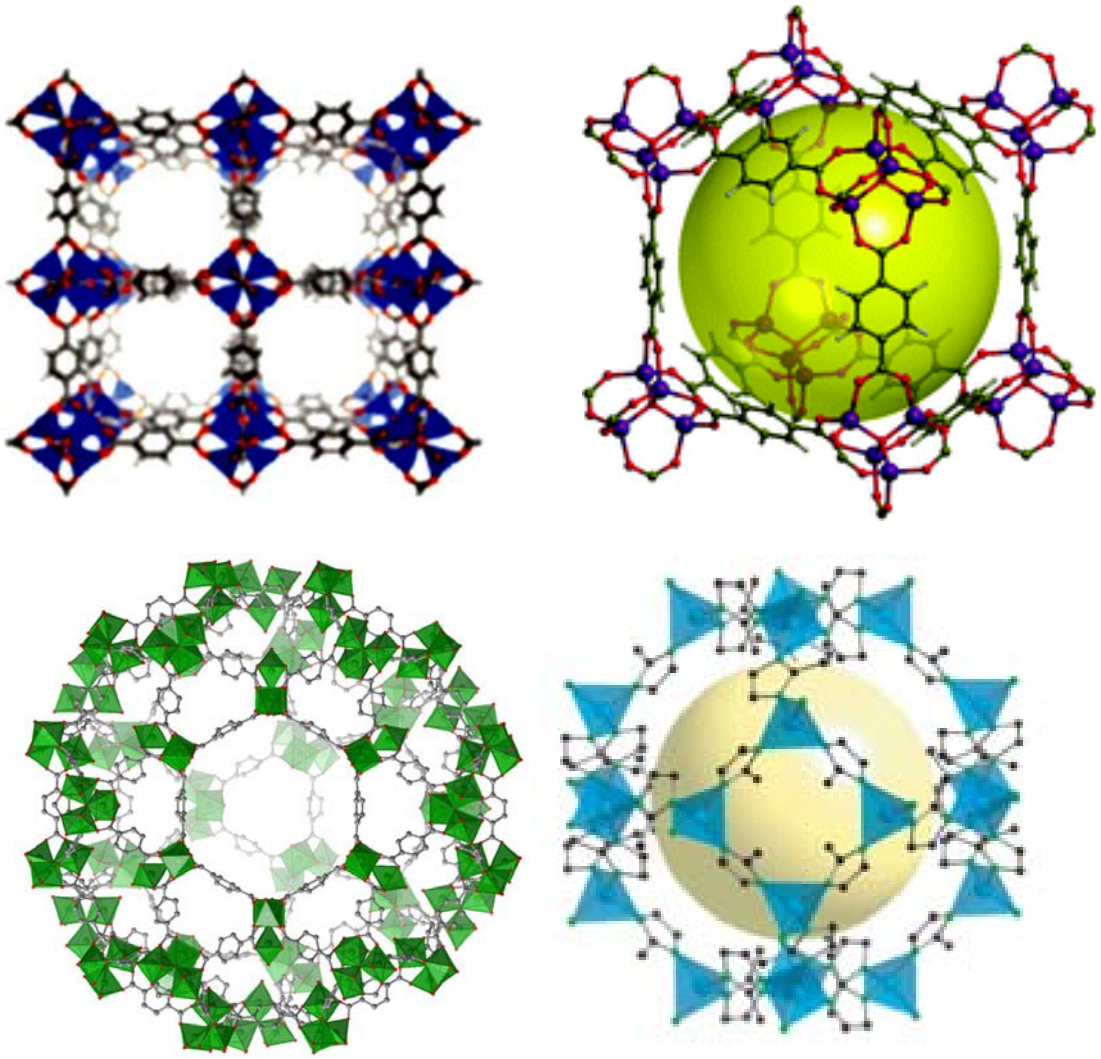

Figure 1.9. An illustration of four examples of most studied MOFs: HKUST-1, MOF-5, MIL-101, ZIF-8.

1. 3. 2 Material Design

1. 3. 2. 1 General Idea for Synthesizing MOFs

As stated above, coordination polymers or MOFs contain two central components, nodes and linkers. They are the principle factors in defining the framework being constructed. In addition to the two major components, other auxiliary components, such as adsorbed solvents, counteranions, and nonbonding guests or template molecules may

also affect the total topology of the material. And in designing material, the important characteristics for nodes and linkers are the number and orientation of their binding sites (coordination numbers and coordination geometries).

Metal-containing units are formed at the time of synthesis under specific temperature and pH designed to produce the desired SBU. Their shape and connection numbers defines the way of extension where they connect to organic linking components. Among the various metals applied to construct MOFs including Zn(II), Cu(II), Fe(III), Ni(II), Co(II), Cr(III), Mn(II), Mg(II), In(III) and Zr(IV), the most porous structures are often formed by some high symmetry sub-building units shown below.

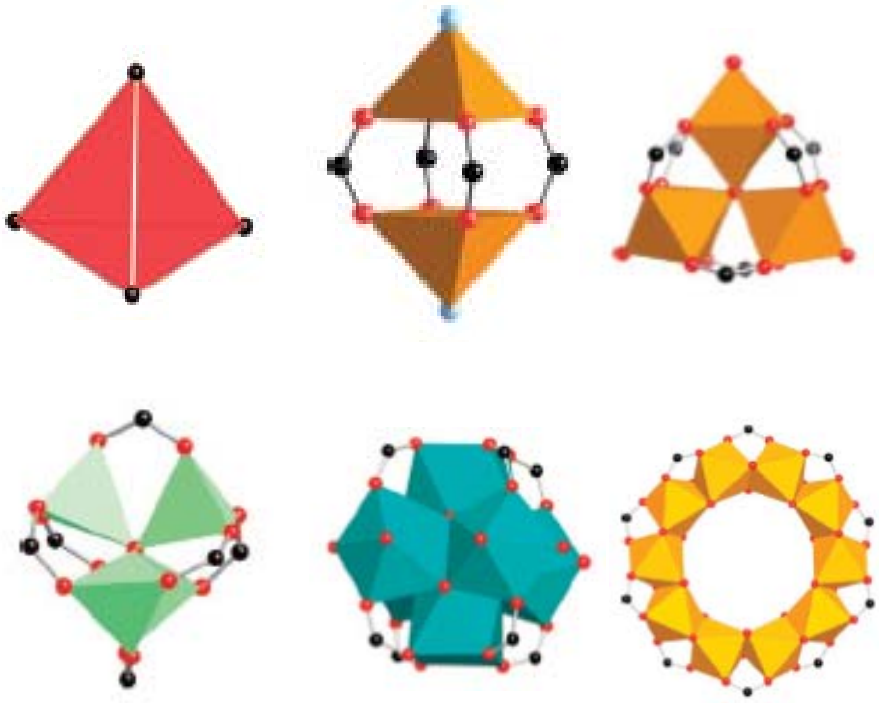

Figure 1.10. An illustration of most common SBUs in MOF. The SBUs are selected from some famous structures namely: ZIF-8; HKUST-1; MIL-101; MOF-5; UIO-66 and MIL-125.[12]

On the other hand, organic SBUs are mostly pre-synthesized with particular

geometry and functional groups. The essence of material design in MOF system is the combination of an accessible metal-containing SBU with a variety of organic SBUs to yield the predicted structure. In particular, these may result in a series structures with the same underlying net with systematically tuned porosity and functional groups. The most frequently used ligands are carboxylic acids and polypyridines as shown below.

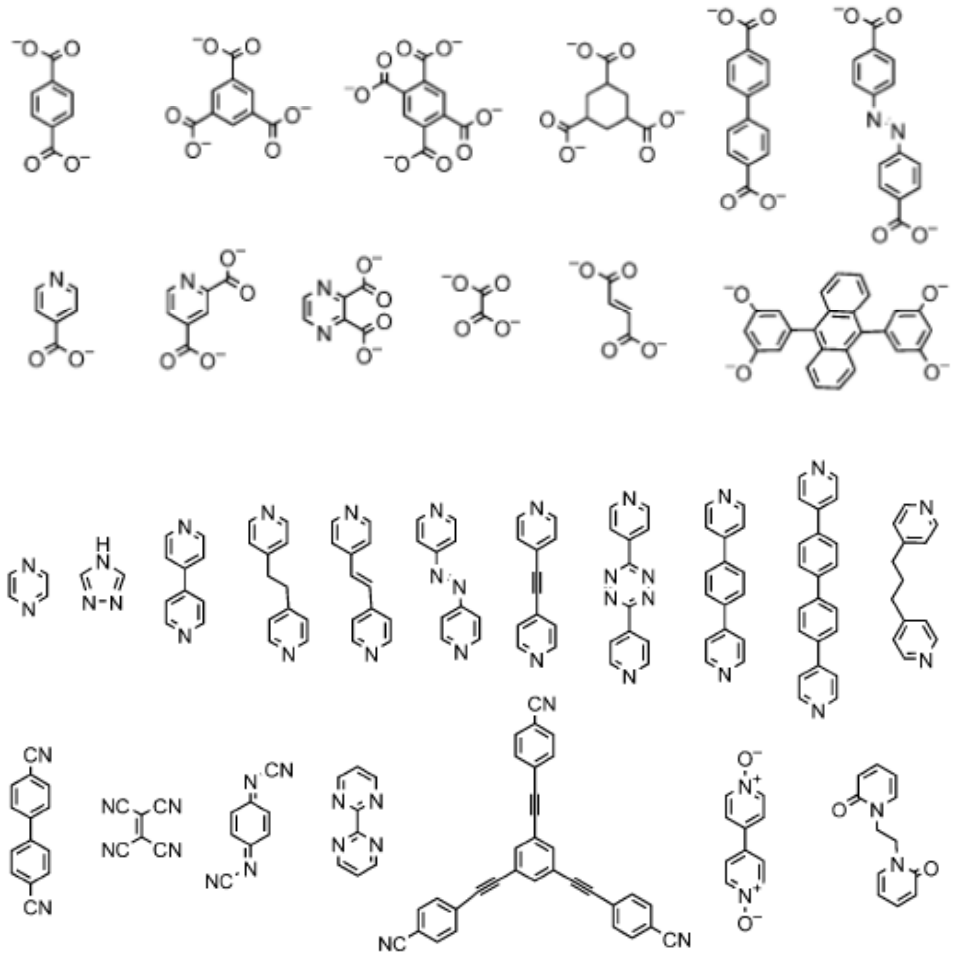

Figure 1.11. Some most used organic ligands in MOF synthesis.

1. 3. 2. 2 Synthesizing MOFs with Special Binding Sites

Other than creating the desired global properties such as topology and porosity, in

order to graft more functionality onto the framework, more specific local chemical environment needs to be controlled during synthesis. The existence of strongly directed specific interactions between metal and substrate provides selective adsorption, retention time bias and even potential catalytic activity, and greatly promotes the material's capacity in gas storage, separation and catalysis. Hence, a very common task in MOF synthesis is to generate open-metal sites, or unsaturated metal sites.

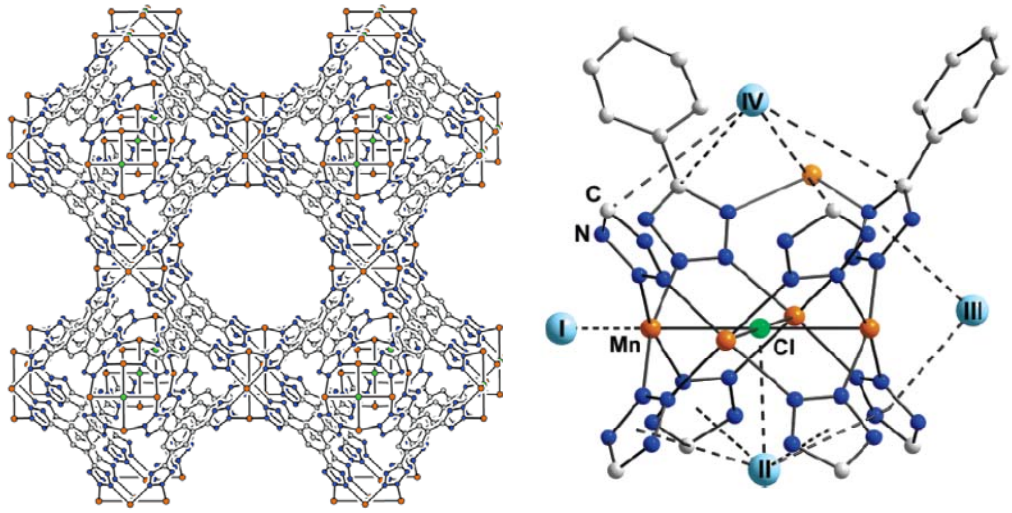

Figure 1.12. An illustration of overall framework and the potential binding sites.

The first general method is to use labile molecules that adsorbed on metal nodes which could potentially be removed under vacuum or heat leaving behind unsaturated metal sites. These previously occupied metal sites create further specific binding sites for targeted guest molecules. Labile neutral ligands introduced to generate unblocked metal sites, in most cases, are solvent molecules. The first example of this strategy was illustrated with HKUST-1, in which the copper sites are known to reversibly lose their coordinated apical water molecule upon thermal activation, thus leaving an accessible

coordination vacancy on the Cu. A more complex example is found in the material described by Dinca et al.,[13] in which DMF solvent molecules occupy metal sites inside sodalite-like cages constructed from square-planar Mn_4Cl tetramer and tritopic ligands. Upon exchanging the DMF molecules by methanol and evacuating at 423 K, the resulting material shows exposed Mn(II) sites. These evacuated unsaturated Mn(II) centers greatly improved the hydrogen binding affinity. Indeed, the idea of utilizing open metal sites to increase the hydrogen binding affinity and storage capacity has proved to be true in many other cases.

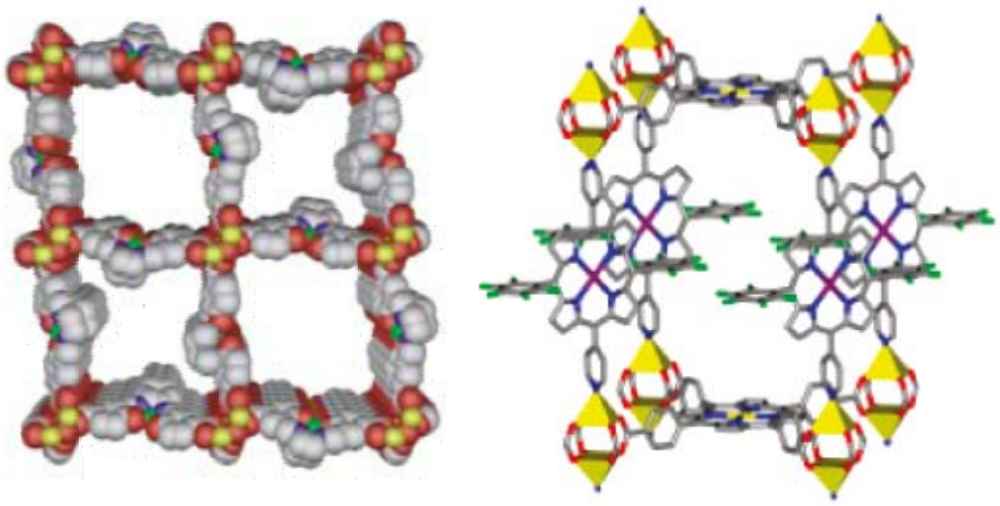

Figure 1.13. Structural illustrations of two MOFs composed of metallorganic ligands.

Another widely applied methodology to generate open-metal sites is the use of metallorganic ligands as linkers. The entirr MOF material is turned into an ordered 3-D array of unsaturated metallorganic coordination complexes. This method has been applied in preparation of a number of frameworks. The earliest work was presented by Kitagawa and co-workers in preparing an MOF using a preassembled Cu(II) metalloligand, which

further coordinated to Zn(II) cations through one of the carboxylate groups to form a framework with 1D channel where Zn(II) simply acted as structural nodes. Similarly, salen ligands with a variety of metals were used, again with Zn(II) cations at the nodes.[14] Unfortunately, these frameworks were not able to expose the metal sites because of π − π stacking between aromatic rings. It was very recently that researchers realized a way of fully exposing the active sites. The Hupp group reported a series of compounds with metallo-porphyrin ligands with an extended 3-D skeleton using Zn(II) carboxylates dimers as connection nodes.[15] As well separated and stand alone ligand struts, the open metal sites are accessible to guest molecules in void spaces in the 3-D channels.

1. 3. 3 Selected Functions of MOF Materials

1. 3. 3. 1 Gas Storage Properties

For the various potential applications of MOF materials, it is natural that these sponge solids are good absorbents for small molecules. Indeed, MOF materials possess extremely large surface areas and tunable pore diameters that well meet the requirements for adsorbents. Moreover, the crystalline nature gives them uniformly defined surface properties and hence uniform binding affinities for molecules being adsorbed. The uniform surface properties and binding energies make the specific adsorption and controlled release possible. Thus MOF materials are widely accepted as good candidates of gas storage material for gathering these features.

The earliest works on gas storage were reported by Kitagawa's and Yaghi's groups. From these early studies until today, fuel storage has been constantly in the spotlight. Gas fuels with low storage density and those subject to explosions, including H_2, CH_4 and

C_2H_2, were of great concern in the MOF community ever since. It is already widely accepted that gas storage capacity is a general property and is one of the most important criteria in evaluating a certain framework. Nowadays, gas adsorption data is reported in almost every publication.

Though gas storage capacity is a general property to MOF materials, there are still challenging topics such as increasing storage efficiency, defining the adsorption sites and mechanistic studies. Storage efficiency is not only affected by surface areas and pore volumes. Binding energy of gas molecules to the framework is crucial. Most research today is putting more and more emphasis onto surface property modification while pursuing larger surface areas and porosity. One of the most accepted methodologies for achieving high gas adsorbing affinities is to generate open metal sites, as stated in 1.3.2.2. For binding sites and mechanism studies, other than to theoretical simulation, neutron diffraction is employed for observing potential adsorption sites and provides deeper understanding.

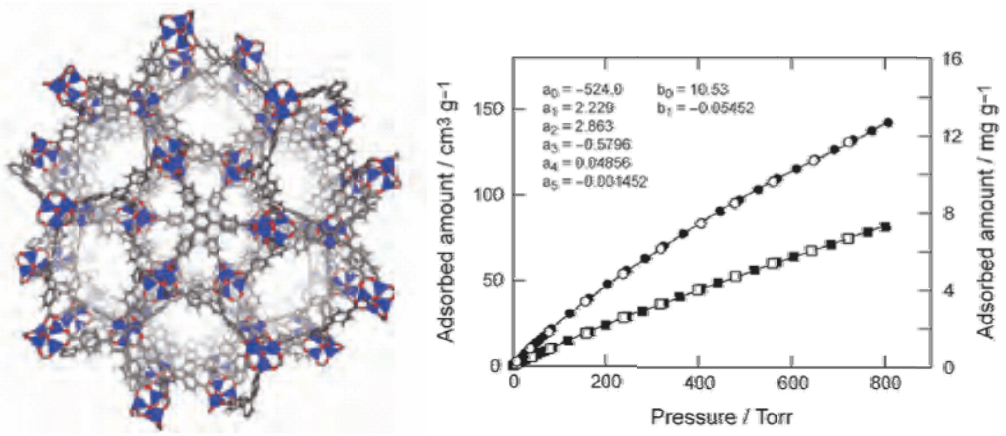

Figure 1.14. Structure of a bench mark material for hydrogen storage (MOF-177) and its adsorption isotherm under 77K and 87K.

1. 3. 3. 2 Separation of Small Molecules

Generally, as crystalline porous solids with defined channels and uniform window openings, MOFs are promising candidates for small molecule separations due to their adjustable pore sizes and controllable surface properties. Based on possible mechanisms, both experimental and theoretical work on selective adsorptions property of MOF materials have been reported.

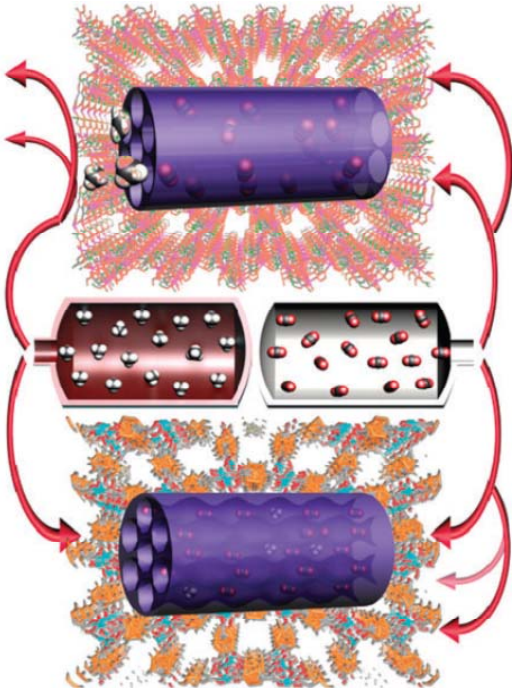

Figure 1.15. An illustration for pore size selective permeability in porous MOFs. Up: Small sized pore could exclude large guest. Down: Large pore could accept both guests.

One of the most common separation mechanisms is size selectivity. Size-selective, adsorption based molecular sieving effect has been confirmed in several MOFs. The size selective adsorption of H_2 but N_2 due to size exclusion is widely observed in MOF material studies. Recently, a detailed study was reported by Zhou's group using the material PCN-17,[16] which has a porous structure containing large cages linked by

relatively small apertures. The interpenetration and sulfate bridging in PCN-17 reduce its window size to 3.5 Å leading to selective adsorption of H2 and O2 over N2 and CO. This material may thus have applications for the separation of N2 and O2, or the separation of H2 from CO in fuel-cell applications. Usually this size selective adsorption bias, and therefore the induced separation, requires a rigid framework since the swelling and breathing in soft framework systems allows intake of both large and small guests, making it the hard to distinguish the difference of size.

However, as a quite common feature, breathing effects and pore structure swelling have been seen in many MOF materials. Especially for separation tasks that involve substrates with similar sizes, physical property-based molecular sieving can not serve the purpose any longer. Hence, selective adsorption-based separation would have to rely on different affinities of different substrates. Then surface modification or specific binding to MOF materials would be essential. As stated above in 1.3.2, creating open metal sites is a good choice for greatly enhanced specific binding. A recent example following this idea to induce affinity bias to similar sized substrates was reported by the Long's group.[17] A Cr(III) structural analogue of HKUST-1 was synthesized and the structure retained its porosity after open metal site exposure. The Cr(III) open metal sites showed great affinity to oxygen over nitrogen with a selectivity factor of 22. Reversible oxygen over nitrogen adsorption was demonstrated based on affinity bias with an energy cost in the deoxygenating process.

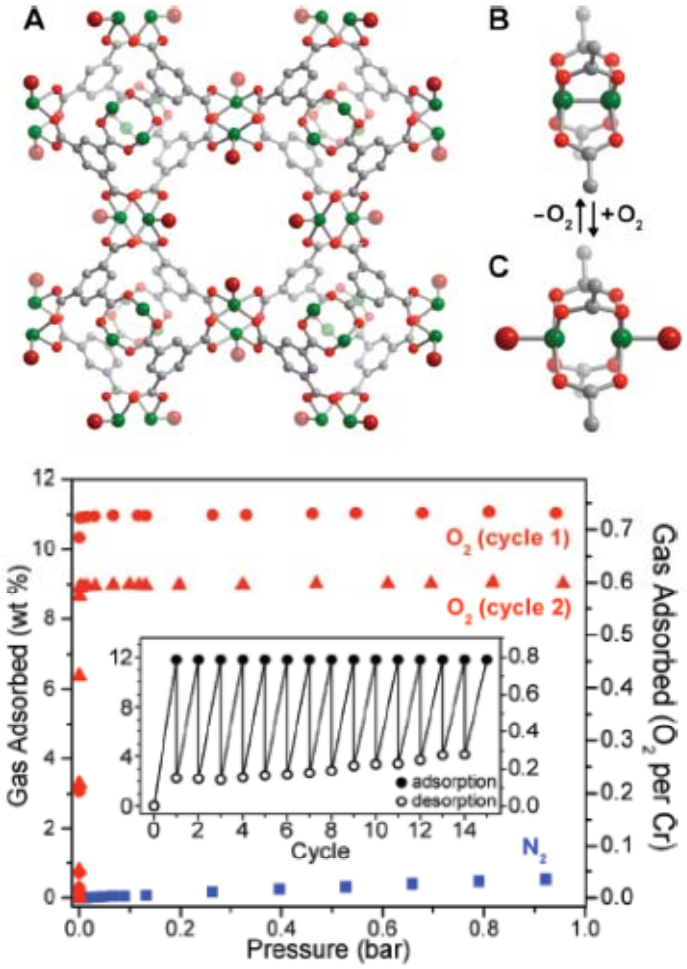

Figure 1.16. Overall structure and local adsorption site for oxygen and oxygen adsorption selectivity over nitrogen at room temperature.

1. 3. 3. 3 Guest Encapsulation

"Nature abhors a vacuum." Void space within porous solids always favors the tendency to capture guest molecules. MOFs as crystalline porous materials always tend to have molecules confined in their channels and have a high potential to form a specific assembly owing to the restricted geometry of the void space. Especially, the adsorption enhancement by the overlapping of the interaction potentials from the opposing and

neighboring channel walls would regulate the molecule orientation in a 3-D manner. Hence, extensive studies have focused on synthetic strategies that give regular, highly-ordered pore or channel structures that control the orientation and conformational properties of confined guest molecules.

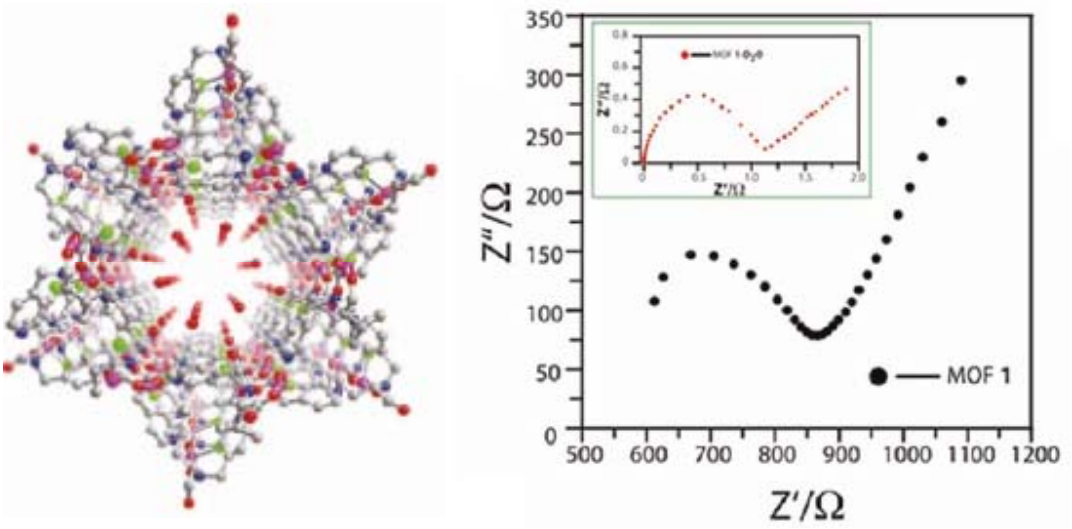

Figure 1.17. Water molecule saturated 1-D pore channel and impedance spectra.

Among these studies, the formation of a low-dimensional assembly, especially 1D chain type alignment has drawn great attention. Initiated by Kitagawa's group, recent studies have utilized the aligned molecular chains to facilitate proton conductivity. Following this idea, a very interesting example was presented by Banerjee's group.[18] A MOF material with 1-D channel has been saturated with water molecule on its pore wall. Upon this proton donor adsorption, impedance spectra on the powder sample have revealed the material possesses moderate proton conductivity due to the helical water chain. And many other 1-D frameworks presenting the ionic conductivity induced by adsorbed proton conductors were reported.

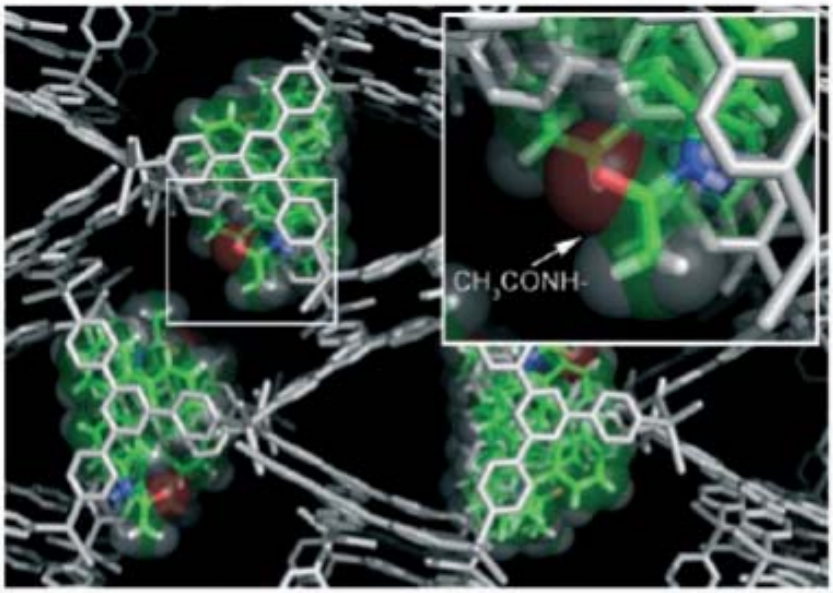

Figure 1.18. Global packing and local configuration of captured guest molecules within $[(ZnI_2)_3(C_{18}N_6H_{12})_2]_n$ crystals.

Molecules being trapped in 3-D MOF materials with orientation regulation are also reported. The earliest reports were presented by the Fujita's group.[19] The framework with 3-D connected channels was connected through Zn(II) cations by tripodal ligands of tris(4-pyridyl)triazine. A series of compounds with large conjugated system were in-situly introduced to the system during framework formation process. Interestingly, with such intentionally introduced π - π interactions, the flat guest molecules were "sandwiched" into the adjacent pore walls of tris(4-pyridyl)triazine as shown below. And due to the strong adsorption enhancement by overlapping interaction potentials from the channel walls, the guest molecules took rather ordered orientation that are able to be determined through crystallography.

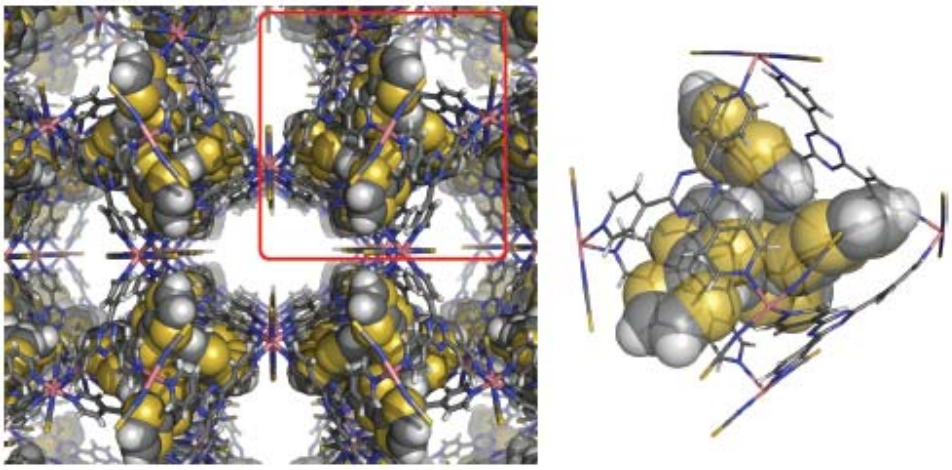

Figure 1.19. Global packing and local configuration of enriched TTF molecules in $\{[Co(SCN)_2]_3(C_{18}N_6H_{12})_2\}_n$ crystals.

Some more recent research works from the same group have further demonstrated other than to single target,[20] it is possible that multiple guest molecules to be regulated with a preferred conformation in each confined chamber of MOF material. The framework material with 3-D inter-connected large and small cages was realized with the same ligand of tris(4-pyridyl)triazine and Co(II) cations. After submerging crystals into of TTF, the latter selectively enriched in smaller cages in a very high concentration. After demonstration the capability of holding electron deficient TTF molecules in the smaller cages, the authors further loaded electron rich C_{60} to the larger cages. A proposed electron transfer conductor systems could be expected though the experiments has not yet been performed.

Other than to ordered small molecules, much large metallic nano clusters of transition metals (though in this case without any ordering), such as Pt have been entrapped into MOF structures to promote the materials functionality. While many other

works that reported encapsulation of nano sized metal clusters as active material for hydrogenation and coupling reactions, and only utilized the pore structure regulation of MOF for size selectivity. A novel work recently reported by Lin's group has trapped Pt nano clusters into UIO-66 type of framework.[21] The latter composed of Zr oxo-clusters which is photo active in hydrogen generation from water with the help of co-catalyst. Upon such modification of loading Pt nano particles as co-catalyst, the authors have then achieved moderate hydrogen generation capacity on a functional MOF with emphasis on photoelectric properties.

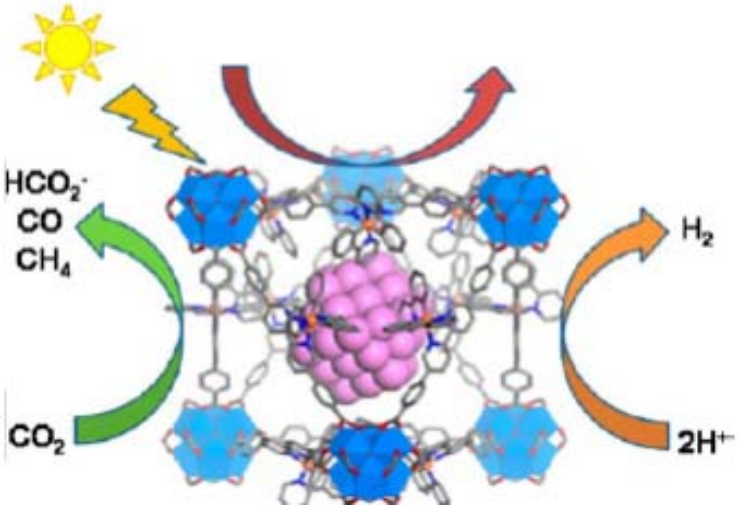

Figure 1.20. An illustration of Pt nano particle assisted MOF based photo catalysis.

Importantly, a porous host promotes the formation of a specific assembly and uniform dispersion of guest molecules, which could not be easily achieved under other conditions. This allows researchers to achieve an ideal nano-reactorfor studying specific arrangement of molecules and mechanisms.

1. 4 Author's Contribution

Other than to structural novelties, extending functionalities of the crystalline

porous materials is of study focus in the work presented hereby.

In Chapter 2, a series metal chalcogenide supertetrahedral cluster based frameworks were synthesized. Most of them shares great similarity in building units both structurally and compositionally. The pure inorganic molecular architectures are built by directed assembling of supertetrahedral clusters as artificial atoms with organic amine templates. A new class of so named “hollowed bulk phase” materials are achieved and enriched the metal chalcogenide framework family. Both experimental evaluation and theoretical simulations on some pure phase compounds are conducted. Based on these new structures, the relationship between material’s structural feature and its optoelectrical properties is discussed.

Chapter 3 and chapter 4 are focusing on hybrid porous solids. Novel MOFs synthesis, characterizations and novel functions are presented.

In chapter 3, a magnetic active MOF material is discussed. The designed synthesis to its extremely unusual 4-level hierarchical assembly is described. More importantly, the material is found to be in magnetic frustration which is rarely studied in MOf materials, this interesting property of geometry induced magnetic frustration is discussed and possible mechanistic scenarios are made.

Chapter 4 is describing a novel idea of utilizing MOF material for reaction intermediate capturing. A challenging synthetic task of synthesizing early transition metal MOF single-crystals is accomplished. Detailed structural information and gas adsorption behaviors are studied. Size selective epoxidation to a series of olefin substrates by the framework has been performed. Single-crystal X-ray crystallography is employed to

capture the detailed molecular conformation of pre-catalytic stage and intermediate stage on the active sites. X-ray data provided trustworthy clues for reaction mechanism. And such observed results are in well agreement with both theoretical calculation and literature proposed mechanism. Hence a novel methodology of simple one-step molecular catalysis mechanism study is illustrated as a radical perspective.

1. 5 References

(1) (a) Eddaoudi, M.; Moler, D. B.; Li, H. L.; Chen, B. L.; Reineke, T. M.; O'Keeffe, M.; Yaghi, O. M., Accounts Chem Res 2001, 34, 319-330; (b) Kitagawa, S.; Kitaura, R.; Noro, S., Angew Chem Int Edit 2004, 43, 2334-2375; (c) Ferey, G., Chem Soc Rev 2008, 37, 191-214.

(2) (a) Kokotailo, G. T.; Lawton, S. L.; Olson, D. H.; Olson, D. H.; Meier, W. M., Nature 1978, 272, 437-438; (b) Hansen, S., Nature 1990, 346, 799-800; (c) Feng, P. Y.; Bu, X. H.; Stucky, G. D., Nature 1997, 388, 735-741.

(3) (a) Krebs, B.; Henkel, G., Angewandte Chemie-International Edition in English 1991, 30, 769-788; (b) Dance, I.; Fisher, K., Prog Inorg Chem 1994, 41, 637-803; (c) Scott, R. W. J.; MacLachlan, M. J.; Ozin, G. A., Curr Opin Solid St M 1999, 4, 113-121.

(4) (a) Zheng, N. F.; Bu, X. G.; Wang, B.; Feng, P. Y., Science 2002, 298, 2366-2369; (b) Zheng, N. F.; Bu, X. H.; Feng, P. Y., Nature 2003, 426, 428-432; (c) Zheng, N.; Bu, X. H.; Vu, H.; Feng, P. Y., Angew Chem Int Edit 2005, 44, 5299-5303; (d) Wu, T.; Wang, X. Q.; Bu, X. H.; Zhao, X.; Wang, L.; Feng, P. Y., Angew Chem Int Edit 2009, 48, 7204-7207; (e) Wang, L.; Wu, T.; Zuo, F.; Zhao, X.; Bu, X. H.; Wu, J.

Z.; Feng, P. Y., J Am Chem Soc 2010, 132, 3283-+.

(5) (a) Wang, C.; Li, Y. Q.; Bu, X. H.; Zheng, N. F.; Zivkovic, O.; Yang, C. S.; Feng, P. Y., J Am Chem Soc 2001, 123, 11506-11507; (b) Zhang, Q. C.; Liu, Y.; Bu, X. H.; Wu, T.; Feng, P. Y., Angew Chem Int Edit 2008, 47, 113-116.

(6) Cahill, C. L.; Gugliotta, B.; Parise, J. B., Chem Commun 1998, 1715-1716.

(7) (a) Li, H. L.; Laine, A.; O'Keeffe, M.; Yaghi, O. M., Science 1999, 283, 1145-1147; (b) Li, H. L.; Kim, J.; Groy, T. L.; O'Keeffe, M.; Yaghi, O. M., J Am Chem Soc 2001, 123, 4867-4868.

(8) Zheng, N. F.; Bu, X. H.; Feng, P. Y., Angew Chem Int Edit 2004, 43, 4753-4755.

(9) Bu, X. H.; Zheng, N. F.; Li, Y. Q.; Feng, P. Y., J Am Chem Soc 2002, 124, 12646-12647.

(10) (a) Ferey, G.; Serre, C., Chem Soc Rev 2009, 38, 1380-1399; (b) Corma, A.; Garcia, H.; Xamena, F. X. L., Chem Rev 2010, 110, 4606-4655; (c) Wilmer, C. E.; Leaf, M.; Lee, C. Y.; Farha, O. K.; Hauser, B. G.; Hupp, J. T.; Snurr, R. Q., Nat Chem 2012, 4, 83-89.

(11) Ockwig, N. W.; Delgado-Friedrichs, O.; O'Keeffe, M.; Yaghi, O. M., Accounts Chem Res 2005, 38, 176-182.

(12) O'Keeffe, M.; Yaghi, O. M., Chem Rev 2012, 112, 675-702.

(13) Dinca, M.; Dailly, A.; Liu, Y.; Brown, C. M.; Neumann, D. A.; Long, J. R., J Am Chem Soc 2006, 128, 16876-16883.

(14) Kitaura, R.; Onoyama, G.; Sakamoto, H.; Matsuda, R.; Noro, S.; Kitagawa, S., Angew Chem Int Edit 2004, 43, 2684-2687.

(15) Farha, O. K.; Shultz, A. M.; Sarjeant, A. A.; Nguyen, S. T.; Hupp, J. T., J Am Chem Soc 2011, 133, 5652-5655.

(16) Li, J. R.; Kuppler, R. J.; Zhou, H. C., Chem Soc Rev 2009, 38, 1477-1504.

(17) Murray, L. J.; Dinca, M.; Yano, J.; Chavan, S.; Bordiga, S.; Brown, C. M.; Long, J. R., J Am Chem Soc 2010, 132, 7856-+.

(18) Sahoo, S. C.; Kundu, T.; Banerjee, R., J Am Chem Soc 2011, 133, 17950-17958.

(19) (a) Haneda, T.; Kawano, M.; Kawamichi, T.; Fujita, M., J Am Chem Soc 2008, 130, 1578-+; (b) Kawamichi, T.; Kodama, T.; Kawano, M.; Fujita, M., Angew Chem Int Edit 2008, 47, 8030-8032.

(20) Inokuma, Y.; Arai, T.; Fujita, M., Nat Chem 2010, 2, 780-783.

(21) Wang, C.; deKrafft, K. E.; Lin, W. B., J Am Chem Soc 2012, 134, 7211-7214.

(22) (a) Cahill, C. L.; Parise, J. B., Chem Mater 1997, 9, 807-811; (b) Cahill, C. L.; Ko, Y. H.; Parise, J. B., Chem Mater 1998, 10, 19-21.

(23) Li, H. L.; Eddaoudi, M.; Laine, A.; O'Keeffe, M.; Yaghi, O. M., J Am Chem Soc 1999, 121, 6096-6097.

(24) Manos, M. J.; Malliakas, C. D.; Kanatzidis, M. G., Chem-Eur J 2007, 13, 51-58.

(25) Li, H. L.; Kim, J.; O'Keeffe, M.; Yaghi, O. M., Angew Chem Int Edit 2003, 42, 1819-1821.

Chapter 2

Metal Chalcogenide Nanocluster Chemistry: Structure-Property Correlations

2.1 Introduction

Metal chalcogenide open frameworks built from tetrahedral clusters represent a unique family of materials that beautifully demonstrate the bottom-up self-assembly of nanoclusters with precisely defined size and composition.[1,2,3,22,7a, 23] Such metal chalcogenide open frameworks preserve the structural feature of condensed phase semiconductors within a framework of three-dimensional (3-D) porous architectures. As such, they are capable of integrating uniform porosity with various physical properties such as semiconductivity, photoluminescence, photocatalytic activity, and thermoelectric property which make them potentially useful for different applications.[4a-c, 4e,24]

While different types of chalcogenide clusters are synthesized, the supertetrahedral Tn series of clusters (n is the number of MX_4 tetrahedra along each tetrahedral edge) represent a unique family of tetrahedral clusters whose structures can be described as the exact fragment of well-known condensed phase of cubic ZnS lattice.[4a, b, 4d, e, 5a, 9] Whereas such kind of "fingerprints" of its own condense phase analog could hardly be traced in any other crystalline framework materials (which usually built up from thin atomic layers, poly- or oligomeric chains). As such, the Tn series of metal chalcogenide clusters based open frameworks stand on a unique boundary that bridges the condensed phase material to the open structure. This would provide us a great opportunity to incorporate multiple

functions onto the same material in a way that still preserves the original properties carried by condensed phases.

Furthermore, these Tn clusters can be used as artificial tetrahedral atoms for the construction of crystalline molecular, supramolecular, and covalent superlattices. A most common mode of linkage between adjacent supertetrahedral clusters uses a bicoordinated corner S^{2-} site (or Se^{2-}) as the bridging linker. In general, the linkage leads to various 3-D open framework architectures based on the artificial atoms assembly. Naturally, tri and tetra connection cross-linkers would greatly flourish the available framework topologies however they are quite rare cases.[4e, 5b] Hence achieving different connection modes and direct them into more complicated structure is of great importance however still quite challenging.

As a topology-rich chemical system, together with intriguing photoelectric property, Tn cluster based frameworks could provide a good platform for us to achieve tunable properties in the same composition by varying the framework structures. As our research lies at the boundary between framework materials and the condense phase, a question arises: how and to what extent would the framework topological features contribute to the change in materials' photoelectric properties? Although it is a common belief that the material's electron state is defined by the periodic potential field in which it sits. However, no previous work reported had stressed this issue in detail. The purpose of this research work is to develop better understanding about how these structural variances may affect the physicochemical properties in this type of cluster based framework material, both experimentally and theoretically. And hopefully this could

serve as the pioneer work to provide new synthetic pathways for property engineering.

In the work presented here, we mainly focus on one of the AIBIIICVI ternary chalcopyrite compounds -- CuInS2 which is both iso-valence-electronic and "isomorphous" with cubic ZnS. This material has stimulated technological interests both as electroluminescent and as photovoltaic material with high theoretical solar cell efficiency, and has been intensively studied during the past decade. And other than the well-known fact that copper is the essential element to ensure the band gap is in the visible light region. The presence of copper in cluster chemistry has other advantages. From the structural viewpoint, the copper is essential for stuffing up the larger-sized clusters because of the local valence requirement which is well recognized in literature. And as will be explained later, the presence of copper at the corner of the cluster will result in novel local connectivity and new overall topology. (Note: the compounds were named as CIS (Cu-In-S) series.)

2.2 Methods

2. 2. 1 General Consideration

To try to understand the underlying correlation between electron states and the framework structural features, building up a large structure library is of great necessity. Hence great emphasis is placed on the material synthesis in this work. Earlier research in our group has established that the cluster frameworks could be synthesized either by solvothermal method or by hydrothermal method; and the resulting structure can be controlled by the template counter cations (also called structure directing agents) and the solvent. By employing solvothermal or hydrothermal synthetic approaches, a large

number of experiments using different templates and various solvent have been screened and a number of compounds sharing similar composition however with different topologies were synthesized.

2. 2. 2 Material Synthesis

Indium (Aldrich), CuI (Aldrich), sulfur powder (Aldrich), dibutylamine (DBA) (Acros), trimethylenedipiperidine (TMDP) (Aldrich), 2-amino-ethylene-4-piperidine (AEP) (Aldrich), 1,1'-dipiperidinmethane (DPM) (Aldrich), dipropylamine (DPA) (Aldrich), hexamethaleneimine (HMI) (Acros), isopropylcyclohexylamine (iPcHA) (Aldrich), Ethylene glycol (EG), 3,5-Lutidine (Alfa-Aesar), all chemicals were used as purchased without any further purification.

2. 2. 2. 1 Synthesis of CIS-1

The CIS-1 reported in this study could be synthesized by reacting a mixture of In powder (120mg), CuI (30 mg), S (120 mg), in a solution of 2.0g TMDP, 2.0g of ethylene glycol and 2.0g water under 190^{o}C for 7 days, large lemon yellow crystal beautifully yielded together with brown powders and black aggregates. The powdered impurity compounds yielded could be drifted away by washing using water and ethanol.

2. 2. 2. 2 Synthesis of CIS-5

The CIS-5 reported in this study could be synthesized by reacting a mixture of In powder (120mg), CuI (30 mg), S (90 mg), in a solution of 2.0g AEP, 2.0g of ethylene glycol and 2.0g water under 190^{o}C for 7 days, octahedral orange yellow crystal beautifully yielded together with brown powders and black aggregates. The powdered impurity compounds yielded could be drifted away by washing using water and ethanol.

2. 2. 2. 3 Synthesis of CIS-8

The CIS-8 could be synthesized by reacting a mixture of In powder (90mg), CuI (30 mg), S (120 mg), in a solution of 4.0g DBU, 2.0g of ethylene glycol and 1.0g water under 150^{o}C for 7 days, cubic orange yellow crystal beautifully yielded together with brown powders and black aggregates. The powdered impurity compounds yielded could be mostly drifted away by washing using water and ethanol.

2. 2. 2. 4 Synthesis of CIS-11

The CIS-11 reported in this study could be synthesized by using different template molecules. By reacting a mixture of In powder (180mg), CuI (30 mg), S (170 mg), in a solution of 4.0g dibutylamine, 2.0g of ethylene glycol and 3.0g water under 150^{o}C for 5 days, large octahedral lemon yellow crystal beautifully yielded together with brown powders and black aggregates. The powdered impurity compounds yielded could be drifted away by washing using water and ethanol, the crystalline sample collected after such purification varied for each batch from 80mg to 100 mg. And the quality of single crystal could be improved by adding 1.0g of 3, 5-Lutidine as co-solvent. Single crystal for XRD structure analysis was picked from this batch. This material could also be reproducibly synthesized by reacting water (2.0g) and ethylene glycol (2.0g) solution mixture of Indium (120mg), CuI (30mg), sulfur powder (90mg), and isopropylcyclohexylamine (0.6g) under 190^{o} C for 7 days. The product was yielded as orange yellow tetrahedral crystals and other block polyhedrons with less amount of amorphous powder.

The crystal using DBA as template has better morphology and better crystallinity,

and the crystal using iPcHA as template has better yield. Data of the powder–XRD pattern, TGA information, solid state UV-Vis reflectance spectra, and photocatalytic activity tests are all from the sample using DBA as template with co-solvent of 3, 5-Lutidine.

2. 2. 2. 5 Synthesis of CIS-28

The CIS-36 could be synthesized by reacting a mixture of In powder (120mg), CuI (30 mg), S (90 mg), in a solution of 2.0g DPM, 2.0g of ethylene glycol and 1.0g water under 190^{o}C for 7 days, very large orange yellow block crystal beautifully yielded together with brown powders and black aggregates. The powdered impurity compounds yielded could be mostly drifted away by washing using water and ethanol.

2. 2. 2. 6 Synthesis of CIS-36

The CIS-36 could be synthesized by reacting a mixture of In powder (120mg), CuI (30 mg), S (90 mg), in a solution of 1.3g DPA, 2.0g of ethylene glycol and 1.0g water under 190^{o}C for 7 days, hexagonal yellow crystals could be picked from the major phase of CIS-28 with brown powders and black aggregates. The powdered impurity compounds yielded could be mostly drifted away by washing using water and ethanol.

2. 2. 2. 7 Synthesis of CIS-51

The CIS-51 could be synthesized by reacting a mixture of In powder (120mg), CuI (30 mg), S (90 mg), in a solution of 0.8g HMI, 2.0g of ethylene glycol and 1.0g water under 190^{o}C for 7 days, pillar like yellow crystals could be picked from the major phase of CIS-28 with brown powders and black aggregates. The powdered impurity compounds yielded could be mostly drifted away by washing using water and ethanol.

2. 2. 2. 8 Synthesis of CIS-52

The CIS-52 reported in this study is synthesized under solvothermal conditions. The autoclaves are loaded first with powder reactants in sequence as follows: indium powder (180mg), sulfur powder (170 mg), copper iodide (40 mg), GeO_2 (40 mg), and TMDP (4, 4'-trimethylenedipiperidine) (2.0 g). To the powder mixture a further co-solvent ethylene glycol (3.0 g) was added to increase the final solution viscosity. Finally deionized water (2.0 g) is added and the viscous mixture was left to vigorous stir for 15 min. Then the Teflon autoclaves are sealed in steel bomb and heated under 190^{o}C for 7 days with no special cooling programming. Orange-yellow prismatic crystals of CIS-52 formed together with orange-yellow UCR-16 and colorless UCR-20 with small amount of amorphous powder with yield of 22% based on indium source (the yield calculation is based on hand selected CIS-52 crystals).

2. 3 Structure Descriptions

The first group of materials is named “hollowed-out bulk phase” materials. It refers to a class of structures which could be depicted as the remaining frameworks with a set of atoms imaginarily hollowed out from the original condense phase super cell which is set as standard reference, however with all the remaining atoms preserving its original position. My latest research effort has resulted in the creation of several phases in this class including CuInS-11, CuInS-28, CuInS-51 and CuInS-66 as described hereafter.

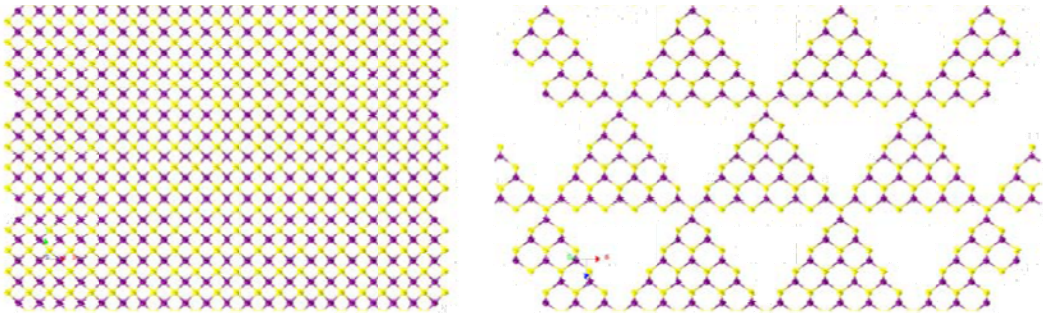

Figure 2.1. Projection views from different direction of CIS-11.

As the first example shown in this class of materials, it is very impressive that CIS-11 structure can be described as being derived with an imaginary top-down approach by starting with a macroscopic piece of crystal with the cubic ZnS structure and periodically carving out octahedral and half of the tetrahedral boxes of atoms (Figure 3). Thus, all the atoms in this CIS-11 unit cell could be found at the exact positions in a 125-fold (5×5×5) ZnS zinc blende super cell with the rest of atoms being absent periodically. In other words, in such an imaginary top-down process, exactly 64.8% of the total 1000 atoms in the 5×5×5 zinc blende super cell are etched out, with only 352 remaining atoms aligned as four supertetrahedral T_5 clusters. Consistent with such a removal of 64.8% atoms, the calculation by PLATON indicates that there is 60.2% extra-framework void space, which is filled by fully disordered extra-framework species.

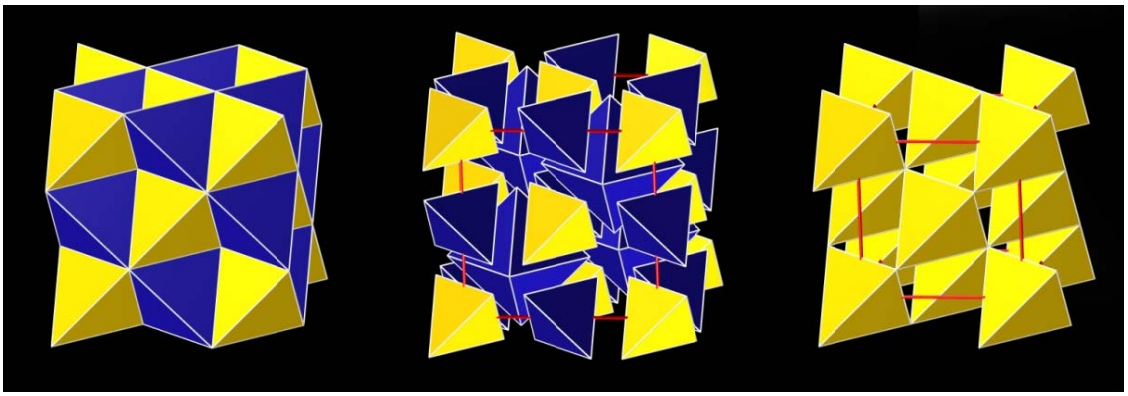

Figure 2.2. An illustration showing hollowed-out and remaining blocks in a fragment of condensed zinc blende phase. The yellow tetrahedra represent the remaining T5 clusters, while the blue tetrahedra and octahedra represent the hollowed-out space. (Left: fully filled space by tetrahedra and octahedral; middle: separated blocks for better view; right: remaining blocks of atoms after removing the evacuated blocks)

Although the T_5 cluster building block itself already carries the fingerprint of the condensed phase (cubic ZnS in this case), an additional level of preservation in this "hollowed-out bulk" structure with all atomic sites preserved throughout the crystal is highly unusual. Such a precise atom-to-atom match between a condensed phase and an open-framework phase is another outstanding feature of CIS-11, and this structural feature follows with the other compounds in this class.

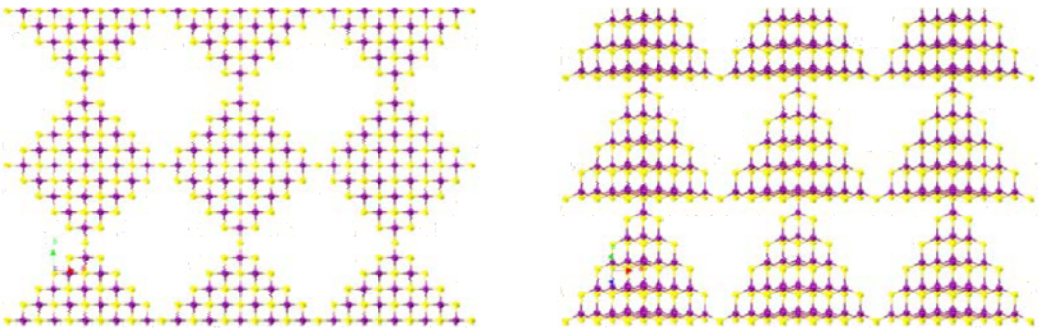

Figure 2.3. Projection views from different direction of CIS-28.

CIS-28 is a 2-D fishing-net like (4-4 net) layered structure that also has a perfect atom to atom match with the "original" condensed phase. The adjacent T5 clusters are

aligning with their edges parallel to each other and sharing the corner sulfur atoms in a 2-connecting mode as shown in the graph.

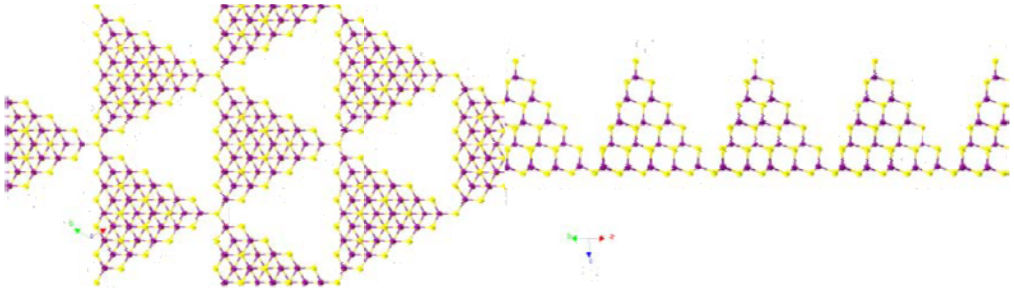

Figure 2.4. Projection views from different direction of CIS-36.

CIS-66 as a third member in this family not only represnts the same “hollowed out bulk” feature and the same evacuated space, but also shows interesting connections. The structure is joined together by three-connected corner sulfur atoms that rarely seen. Each T5 cluster can be viewed as tetrahedral blocks sitting on the same plane while sharing the corner with the other two in a hexagonal closed packing mode. Each two set of layers are pointing to each other with a daggling corner sulfur atom in a staggered fashion and fill out the space and forms this 2-D strucutre.

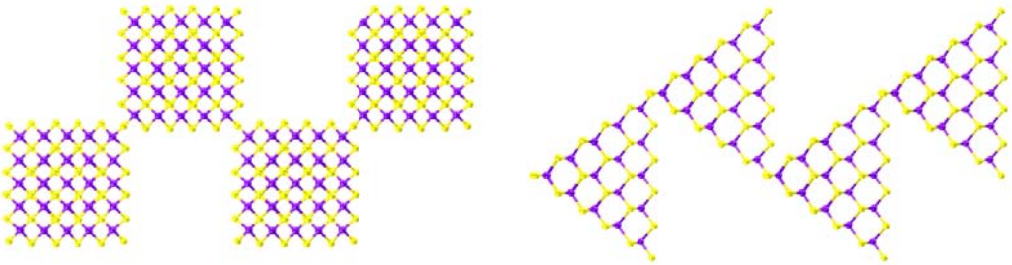

Figure 2.5. Projection views from different direction of CIS-51.

The fourth member in this class of material is CIS-51. To our surprise, CIS-51 is a

1-D T5 cluster chain with only two corners joining the structure however the other two remained as daggling bare S atoms or protonated as thio groups. The low dimensional cluster based structure is not often seen because of the general tendency in condensation. Though recently we have reported isolated T5 clusters, however there is still no 0-D T5 structures formed without the help of capping agent. CIS-51 is so far the lowest dimension in pure inorganic molecular architecture that we could achieve.

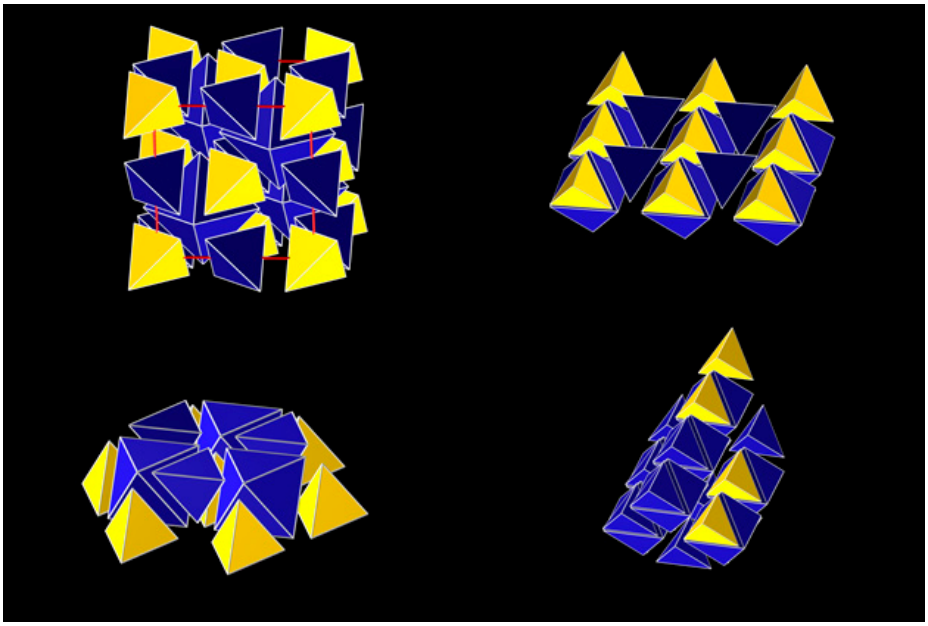

Figure 2.6. An illustration of the idea of "hollowed-out bulk" phase. Blue parts are to be evacuated.

All the four structures in the "hollowed-out bulk" series ideally share the same framework density. A well known geometric fact is the fully filled space could be divided into closely packed octahedra and two fold of tetrahedra. And in the imagined evacuating process, they all lose one set of tetrahedral spaces and one set of octahedral spaces from the imagined super cell hence the ideal void space ratio without considering the packing distances between different layers or chains (Figure 2.6).

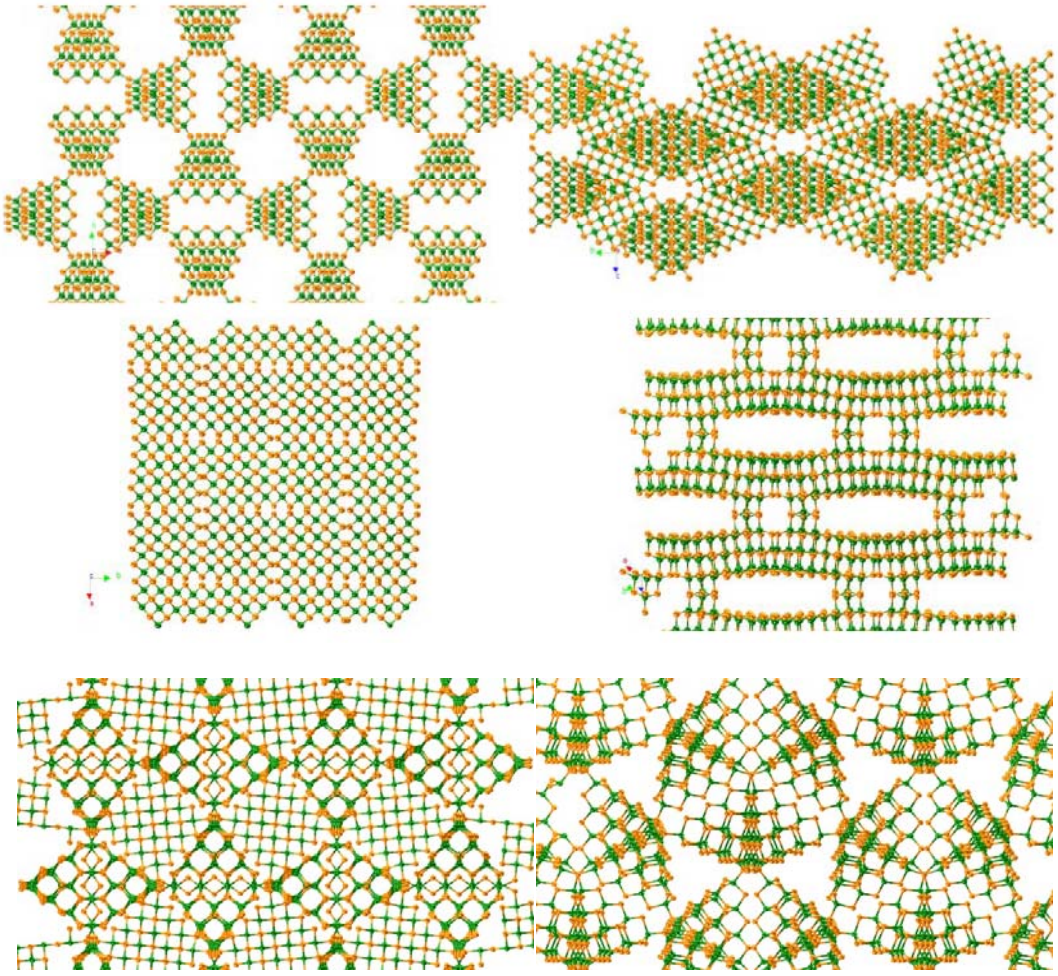

Figure 2.7. Structures of CIS-1, CIS-5 and CIS-8 projected from different axis.

A second group of framework materials, CIS-1, CIS-5 and CIS-8 are based on T4 clusters. In contrast with hollowed-out bulk phase described above, these structures, the features of the condense phase is only preserved within super tetrahedral cluster, however, on the overall view, the systematic position switch and deviation from the reference imaginary super cell is observed as a result by twisting and rotating the secondary building units. These three new phases, CuInS-1, CuInS-5 and CIS-8 as shown below have adopted the topology of UCR-1, UCR-5, and UCR-8 whi ch were reported before in

other compositions. Hence the structural description would be omitted hereby.

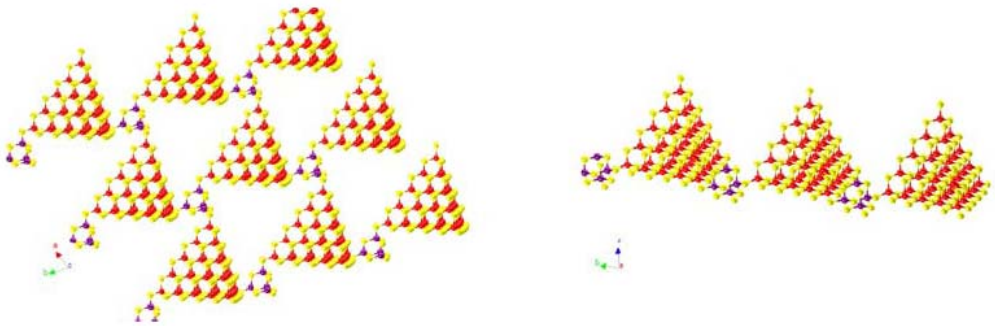

Figure 2.8. CIS-52 structure projected from different views.

The last compound CIS-52 is particularly interesting. Other than the two classes of structures reported above, which are both composed of uni-sized cluster building block, this CIS-52 framework is formed by different sized clusters. The T5 and T2 clusters co-crystallized here are the largest gap we could achieve up to so far in mixed cluster systems.

2. 4 Detailed Case Studies

2. 4. 1 CIS-11

2. 4. 1. 1 General Characterizations on CIS-11

As a well known semiconducting material in its bulk phase, the cluster based CIS framework also shows visible light absorption and appears orange which is slightly blue shifted from its bulk phase. This blue shift is inconsistent with nano confinement effect.

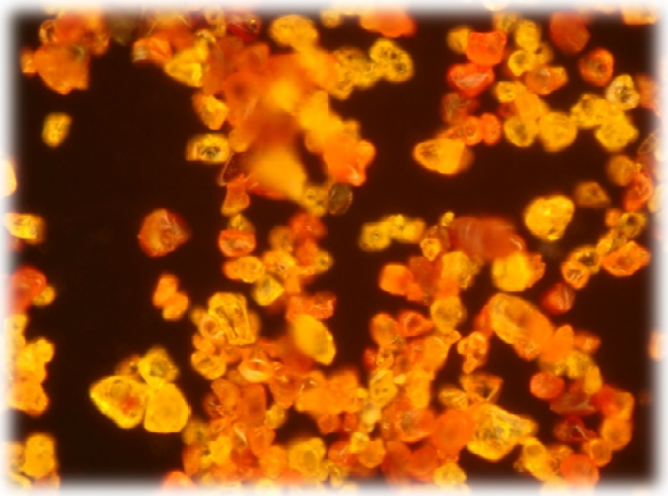

Figure 2.9. An optical image of crystals synthesized.

Powder phase XRD proves the material is pure phase, and other experiments performed on the same batch is not disturbed by impurities.

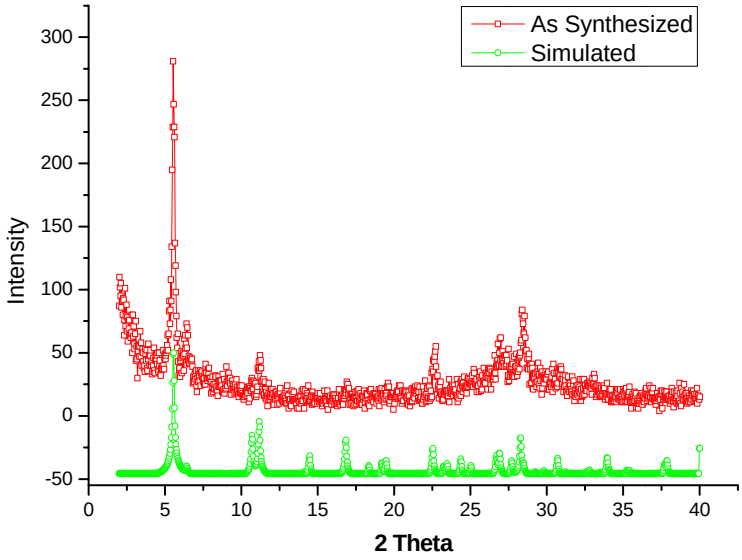

Figure 2.10. Measured and simulated powder XRD patterns for CIS-11.

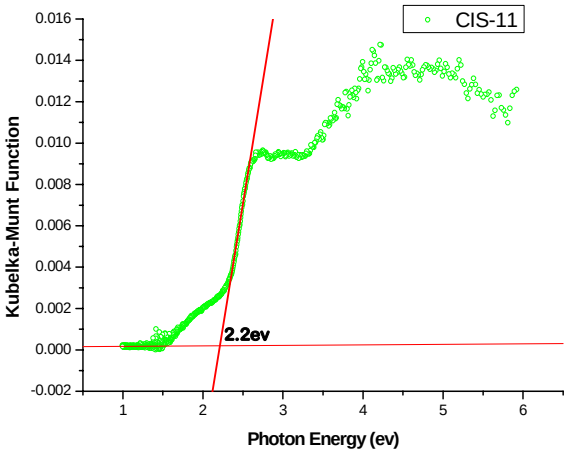

Figure 2.11. The solid state UV-Vis absorption spectrum of CIS-11.

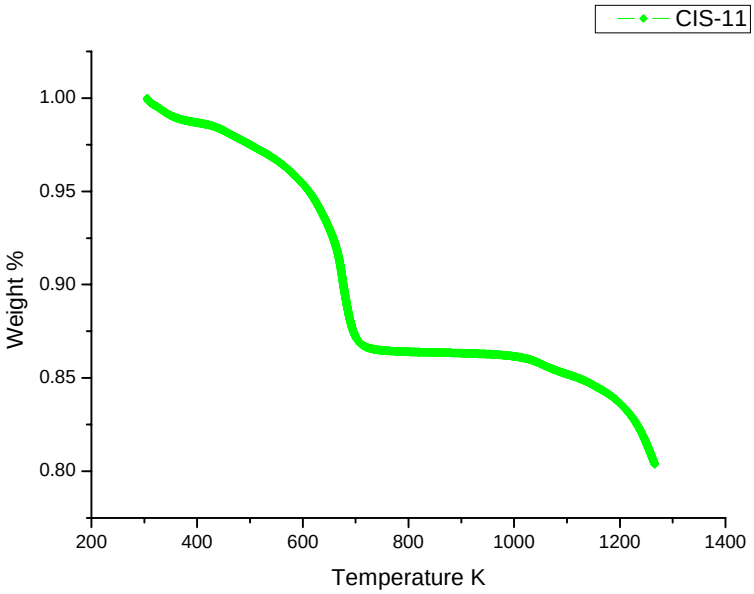

Figure 2.12. TGA plot of CIS-11 heated under nitrogen atmosphere.

TGA experiment was performed on STDQ-600 with initial temperature of 300K increased to 1200K with 10K per minute under nitrogen environment with a flow rate of 100 micro liters per minute.

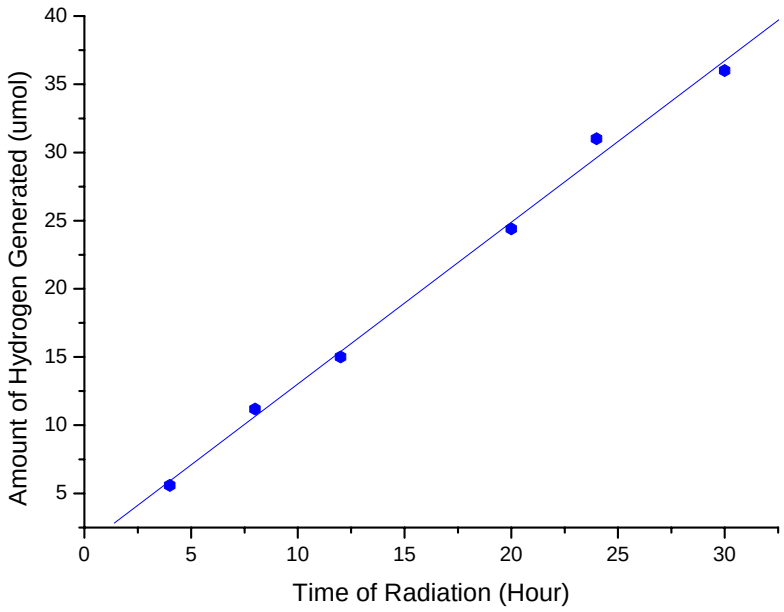

Figure 2.13. Photocatalytic activity for hydrogen generation of CIS-11.

The photocatalytic hydrogen evolution reaction with sacrificial reagent of Na_2S was performed in a quartz round bottom flask, and the incident light from 300w Xe lamp was filtered by both optical filter with cutoff >400nm and an IR filter. In a typical reaction, 200mg of CIS-11 crystals are suspended into 270ml of 0.5 M Na_2S aqueous solution under vigorous stir. The hydrogen could be generated steadily with a rate of 3.8 $\mu mol \cdot h^{-1} \cdot g^{-1}$ without any co-catalysts. The catalysts remained active for at least 72 hours with a turnover numbers of 3.7; however, the evolution rate slowed after 40 hour, which may indicate the decomposition of the material under long radiation.

2. 4. 1. 2 Structural Analysis

Other than to the hollowed-out bulk feature as a pure imagination, the unique way of assembly of these artificial atoms T5 clusters is of great importance in synthesis aspect.

In here, a very fascinating structural feature of CIS-11 is its dual hierarchical architecture. CIS-11 is one of the rare examples in inorganic structures representing the expansion of the same packing mode on the atomic scale to a secondary hierarchy on nano-scale; because other than the difference in dimensions (component T_5 vs. whole super-T_∞), the arrangement and orientation of the tetrahedral metal atoms within the T_5 cluster are exactly identical to the arrangement and orientation of T_5 clusters in the whole crystal.

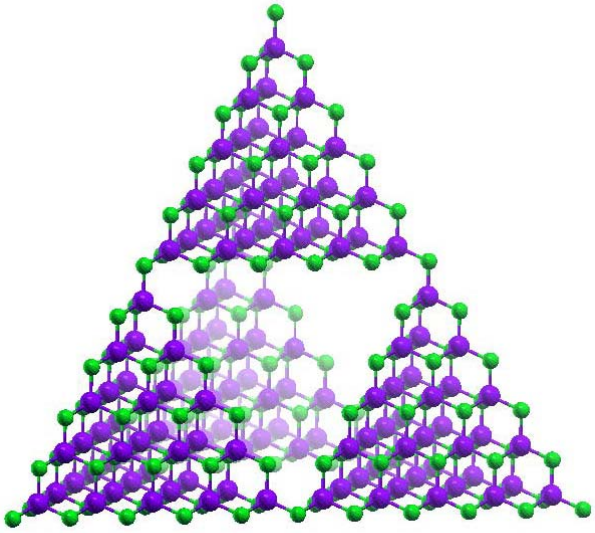

Figure 2.14. Four T5 clusters, M35S53 (M= Cu+ or In3+) organized into a secondary supertetrahedron with an infinite order. The super- supertetrahedral cluster is only drawn as T5,2 even though the actual structure is T5,∞. Purple: Metal; Green: Sulfur.

The formation of this super-$T_{5,\infty}$ cluster relies on a structural feature that was not previously found in open-framework chalcogenides built from tetrahedral clusters. This unprecedented structural feature is the four-coordinated corner sulfur atom (Figure 2). This 4-coordinated vertex is ideally tetrahedral and has an M-S-M angle of 109.5^o. As a result, the corner tetrahedral S^{2-} sites and T_5 clusters (serving as pseudo-tetrahedral atoms)

interconnect to create a 3-D framework. In comparison, in previously reported chalcogenide 3-D frameworks, supertetrahedral clusters are linked with bi-coordinate corner S^{2-}/Se^{2-} sites into 4-connected networks and in only one case with tri-coordinate S^{2-} sites into the C_3N_4-type topology.

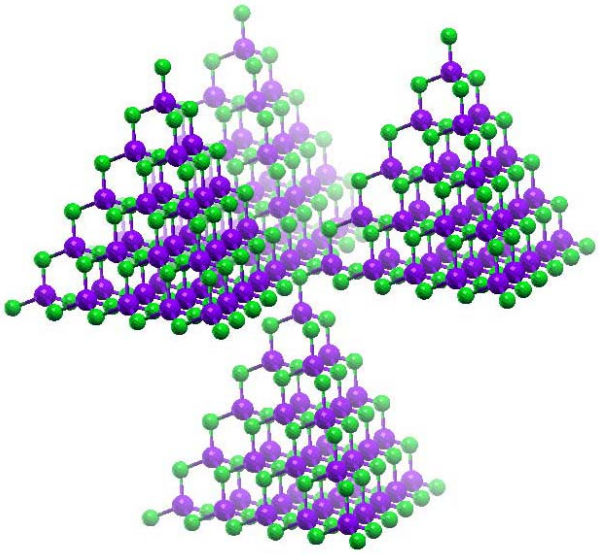

Figure 2.15. One four-coordinated corner sulfur atom joining four T5 clusters into tetrahedral geometry, which further extends into 3-D infinite framework in CIS-11. Purple, Metal; Green: Sulfur.

Following Pauling's electrostatic valence rule and consistent with previously reported structures, each corner sulfur atom and four core sulfur sites of T_5 clusters in CIS-11 are assigned an average of two Cu (I) and two In (III) sites to balance the local charge of tetrahedral S^{2-} sites. The crystallographic refinement further supports such an assignment of the Cu (I) and In (III) around the tetrahedral sulfur. The shorter metal-sulfur bond length of 2.25 Å, compared with the typical In-S bond length of 2.4 - 2.5 Å is another indication of the partial copper sites around the tetrahedral S^{2-} atom.

As CIS-11 with the $T_{5,\infty}$ structure is currently the only synthesized member in a series of 3-D porous frameworks that can be represented as $T_{n,\infty}$. The common condensed ZnS type structure can be represented as $T_{1,\infty}$. The synthesis of the $T_{5,\infty}$ structure reported here hints at a tantalizing possibility of synthesizing other members of the $T_{n,\infty}$ family. Assuming Pauling's valence rules, the framework compositions of other members of $T_{n,\infty}$ (n= 2, 3, 4) series of structures based on the Cu-In-S composition are listed in Table 1 and Figure 2.16.

Table 2.1. Composition, charge and percent of removed atoms for $T_{n,\infty}$ series of structures based on Cu(I)-In(III)-S composition.

Structure	framework composition	charge per supertetrahedral cluster	percent of removed atoms in n×n×n super cell
$T_{1,\infty}$	$(CuInS_2)_{1/2}$	0	0
$T_{2,\infty}$	$Cu_2In_2S_7$	-6	31.3%
$T_{3,\infty}$	$Cu_2In_8S_{17}$	-8	50.0%
$T_{4,\infty}$	$Cu_4In_{16}S_{32}$	-12	59.4%
$T_{5,\infty}$	$Cu_7In_{28}S_{53}$	-15	68.4%
$T_{n,\infty}$	$M_{(n)(n+1)(n+2)/6}S_{[(n+1)(n+2)(n+3)/6]-3}$		$1-[(n+1)(n+2)(2n+3)-18]/12n^3$

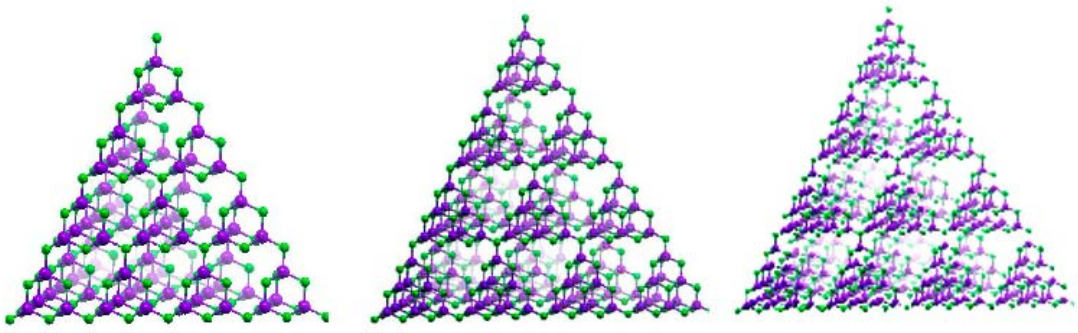

Figure 2.16. Imaginary structures of super-super tetrahedra of T2, ∞ T3, ∞ T4, ∞. Because of the limitation of the page size, only T2,4, T3,4, and T4,4, which are fragment of T2, ∞ T3, ∞ T4, ∞ are shown here.

2. 4. 1. 3 Optoelectrical Property Studies

The synthesis of CIS-11 in the Cu-In-S domain is in part inspired by its similarity

to the composition of copper indium sulfide ($CuInS_2$), which is one of the most intensively studied semiconductor materials for high-efficiency solar cell applications. CIS-11 possesses a band gap of approximately 2.2 eV determined by solid state UV-Vis reflectance spectra with Kubelka-Munk methods, which indicates the material retains the semiconducting property of the corresponding condensed phase. The relative blue shift of the optical band gap compared to the condensed $CuInS_2$, which usually shows a band gap of 1.53 eV,[14] is also reasonable because the electrons are more localized due to the periodic absence of about two-thirds of atoms, and are primarily confined within the nano-sized T_5 building block. CIS-11 also shows photocatalytic activity for hydrogen evolution from water in the presence of Na_2S sacrificial reagent in the visible-light region.

2. 4. 1. 4 Perspectives

This CIS-11 as "hollowed-out bulk" material provides an ideal platform for exploring how the material's property may change upon periodically losing inside atoms from a bulk single crystal. Theoretically, differing from shrinking particle size by chopping apart outside atoms under the guidance of quantum confinement effect, another route of property engineering by periodically removing lattice atoms is also possible. Structures similar to CIS-11, but based on T_2, T_3, T_4 clusters with comparable compositions (i.e., $T_{n,\infty}$ with n=2, 3, 4, Table 1) would be promising candidates for tuning the properties of $CuInS_2$ material, and the work reported here suggests that the realization of such materials is feasible, which would serve to demonstrate a new principle in the property engineering of semiconducting materials

2. 4. 2 CIS-52

2. 4. 2. 1 General Characterizations on CIS-52

2. 4. 2. 1. 1 Qualitative Elemental Analysis

EDAX data was collected on a Philips XL30 scanning electron microscope. The extra Pt peaks were from sputtering Pt for processing of EDAX measurement. The data clearly reveals the presence of all kinds of metals composed in CIS-52. Though EDAX only provides qualitative results, the indium metal is in predominant amount comparing to the copper and germanium which possess much smaller peak intensity. This is in good consistence with the crystallographic result.

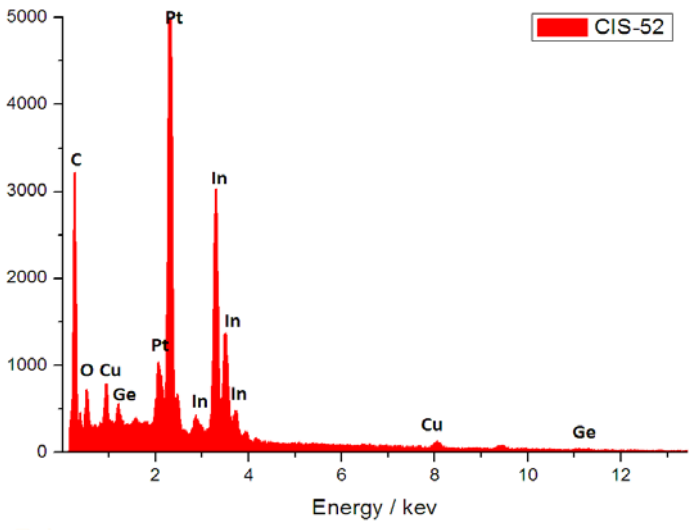

Figure 2.17. The energy dispersive X-ray (EDAX) spectroscopy of CIS-52.

2. 4. 2. 1. 2 Solid-state UV-Vis Absorption Spectra

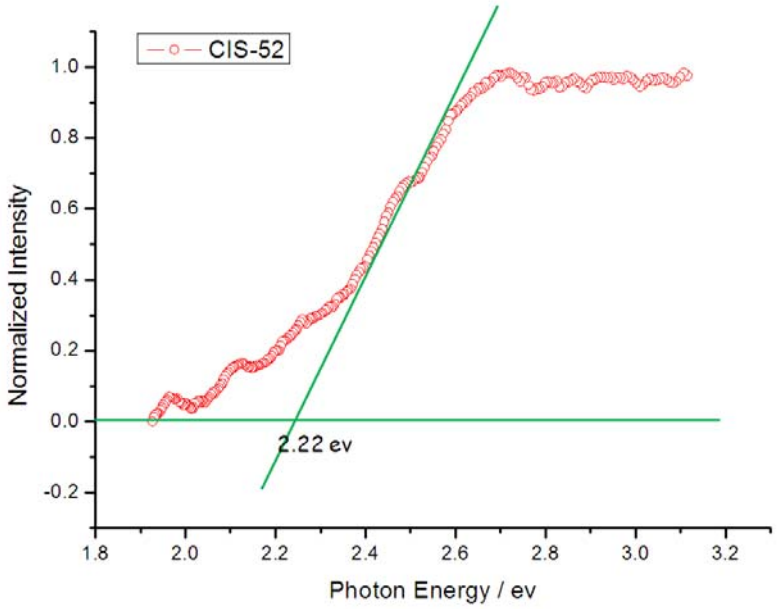

Figure 2.18. Solid-state UV-Vis absorption spectra for CIS-52.

The measured solid-state UV-Vis absorption spectra was taken based on the manually picked crystals of CIS-52.

2. 4. 2. 1. 3 Theoretical Simulation

Theoretical calculation on Density states of CIS-52 and its proposed isomer is performed by extended Huckel theory. All the negative charges are pacivated by Na cations that are arbitrarily generated in ex-framework space. The refined atomic positions are listed below.

Table 2.2. Atomic positions of modeling structures.

ISO structure to CIS-52 a= 24.4960 b= 24.4960 c= 20.0000 α =90.000 β =90.000 γ =120.000				CIS-52 a=21.3738 b=23.9400 c=29.1969 α =72.211 β =68.980 γ =64.472			
S	-8.79455	-7.98443	-4.41043	S	3.8803	11.13512	-7.07168
S	-0.31516	12.14182	-4.41043	S	5.14037	0.53053	12.10062
S	12.87499	-5.26467	-4.41043	S	7.45397	10.22173	-5.91658
S	13.50309	-7.44048	-1.20773	S	-3.7927	-7.4907	-6.68772

S	10.04853	-2.54491	-4.41043	S	4.94038	12.24636	-3.59056
S	-4.08377	11.05392	-4.41043	S	-0.2267	-8.47543	-5.26476
S	11.30474	-6.89653	1.99499	S	-2.83507	-6.66274	-2.89852
S	9.10638	-6.35258	-4.41043	S	8.29572	11.3124	-2.14508
S	7.22206	0.17487	-4.41043	S	9.91661	8.03587	-0.76341
S	6.27992	-3.63282	-4.41043	S	-9.06539	6.15867	-3.39724
S	10.67663	-4.72072	-1.20773	S	8.46552	6.88863	-4.40782
S	-2.51352	12.68577	-1.20773	S	8.72814	6.23165	2.48202
S	2.49688	-4.70685	-4.35043	S	-7.7883	2.50831	-2.74086
S	4.3956	2.89463	-4.41043	S	5.95999	3.95525	-4.71697
S	-1.27384	-5.78402	-4.41043	S	7.55577	4.42266	5.70842
S	-5.02594	-6.89653	-4.41043	S	-6.65126	-1.18504	-2.01209
S	7.85018	-2.00096	-1.20773	S	3.34013	1.0859	-4.86203
S	3.45346	-0.91305	-4.41043	S	6.28991	2.58514	8.92168
S	1.56914	5.61439	-4.41043	S	-5.64759	-4.96084	-1.32326
S	5.02371	0.71882	-1.20773	S	0.87564	-1.87293	-5.23741
S	0.62699	1.80673	-4.41043	S	7.52293	-1.21862	9.62069
S	-0.31516	-2.00094	-4.41043	S	-11.4569	-3.04118	7.14452
S	2.19725	3.43858	-1.20773	S	-9.15695	-4.89932	4.64851
S	-4.08379	-3.08886	-4.41043	S	-6.85041	-6.79615	2.12514
S	-3.14162	0.71882	-4.41043	S	-8.26995	-7.9729	-1.50693
S	-2.19947	4.52649	-4.41043	S	-11.9316	-7.18768	-2.55451
S	-1.25751	8.33416	-4.41043	S	-15.5813	-6.42064	-3.50503
S	-6.91026	-0.36908	-4.41043	S	2.10296	-5.74508	-4.42283
S	-7.8524	-4.17677	-4.41043	S	-0.37539	-3.76762	-1.92763
S	-5.96808	3.43858	-4.41043	S	0.8765	-2.76161	1.68622
S	4.08156	-3.08886	-1.20773	S	2.25051	-1.65327	5.16331
S	-5.02593	7.24625	-4.41043	S	3.64282	-0.50421	8.62674
S	-0.62921	6.15835	-1.20773	S	5.87756	13.07668	-0.1561
S	0.32415	-4.14893	-1.20773	S	-1.49618	-4.67013	-5.74417
S	-3.4553	8.87811	-1.20843	S	11.14893	9.71711	-4.22147
S	1.25509	-0.36908	-1.20773	S	-10.1665	4.291	-0.02337
S	-3.45568	-5.26467	-1.20773	S	-11.6089	3.11695	-3.67502
S	-1.57137	2.35068	-1.20773	S	7.32703	5.05672	-1.03449
S	-2.51354	-1.45699	-1.20773	S	10.00967	2.49327	3.14859
S	-7.2243	-6.35258	-1.20773	S	-9.03983	0.65584	0.65365
S	-4.39782	5.07044	-1.20773	S	-10.4742	-0.49025	-3.03902
S	-5.34	1.26278	-1.20773	S	7.24159	0.22128	-3.9705
S	-6.28216	-2.54489	-1.20773	S	4.71619	2.15668	-1.2994
S	-2.82757	6.7023	1.99499	S	6.06697	3.22222	2.18467
S	5.60998	-1.47716	1.98033	S	8.76136	0.6681	6.35729
S	-2.19947	4.52649	5.19769	S	-10.3099	-1.15736	3.86048
S	-0.00107	3.98247	1.99557	S	-7.89051	-2.94999	1.40629

S	-1.57137	2.35068	8.40041	S	-9.37424	-4.13804	-2.30327
S	2.82535	1.26278	1.99499	S	-13.0571	-3.40061	-3.23368
S	-0.94326	0.17487	1.99499	S	4.68174	-2.66203	-4.23246
S	1.88321	-2.54491	1.99499	S	2.1397	-0.74173	-1.57906
S	-3.76972	2.89463	1.99499	S	3.5088	0.32879	1.87659
S	-1.88543	-3.63282	1.99499	S	4.82579	1.45431	5.35074
S	-5.65404	-4.72072	1.99499	S	6.06624	-2.42389	6.10123
S	-4.71189	-0.91305	1.99499	S	-12.9797	-4.26779	3.59449
S	3.45346	-0.91305	5.19769	S	-10.6514	-6.06257	1.11188
S	0.62699	1.80673	5.19769	S	-14.2827	-5.31235	0.16512
S	-0.31516	-2.00094	5.19769	S	3.36964	-4.60356	-0.81221
S	-3.14162	0.71882	5.19769	S	4.69004	-3.51887	2.65363
S	-0.94326	0.17487	11.60311	S	8.53318	1.28141	-0.34057
S	-4.0838	-3.08884	5.19769	S	6.00993	-1.51576	-0.56258
S	1.25509	-0.36908	8.40041	S	7.27447	-0.49382	2.78769
S	-2.51352	-1.45699	8.40041	S	-11.761	-2.27274	0.32573
In	13.50309	-7.44048	-3.60975	In	10.41382	7.65181	-3.13421
In	-2.51353	12.68579	-3.60975	In	9.33248	5.88552	0.14394
In	11.30474	-6.89653	-0.40705	In	-9.6446	4.02816	-2.47112
In	7.85018	-2.00096	-3.60975	In	7.89374	4.7482	-3.48036
In	5.02372	0.7188	-3.60975	In	8.09669	4.07398	3.36819
In	2.19726	3.43856	-3.60975	In	-10.9258	2.145	0.81775
In	5.62727	-1.47126	-0.42165	In	-8.48899	0.34684	-1.77828
In	4.08156	-3.08886	-3.60975	In	-9.7975	-1.46567	1.50228
In	0.31295	-4.17677	-3.60975	In	-7.38518	-3.27763	-1.00821
In	1.25509	-0.36908	-3.60975	In	5.47504	1.05699	3.05662
In	3.40436	-0.94154	2.76647	In	-11.1731	-2.55586	-1.96409
In	1.84768	-2.57064	-0.44427	In	4.15079	-0.00513	-0.37784
In	-0.6293	6.1582	-3.60975	In	-12.3152	1.0324	-2.65426
In	-3.45567	8.87811	-3.60975	In	5.3634	1.84887	-3.68682
In	-4.39782	5.07044	-3.60975	In	6.83986	2.28039	6.59137
In	-2.51351	-1.45701	-3.60975	In	-10.0447	-6.33094	-1.29028
In	-5.33998	1.26278	-3.60975	In	2.83569	-1.87501	2.81075
In	-0.02526	3.97431	-0.43437	In	5.33003	-3.65684	0.31742
In	-2.85012	6.69574	-0.44073	In	-13.7236	-5.59075	-2.22927
In	-3.45566	-5.26467	-3.60975	In	1.50312	-2.95572	-0.64865
In	-7.22441	-6.35239	-3.60975	In	3.97936	-4.81907	-3.22188
In	-6.28216	-2.54489	-3.60975	In	0.35493	-4.05099	-4.26276
In	-1.91865	-3.66616	-0.46681	In	-2.02952	-6.94605	-5.18942
In	-5.68499	-4.76168	-0.48935	In	9.16584	11.03166	-4.42659
In	-3.80388	2.85855	-0.45703	In	5.81536	11.967	-5.84553
In	1.18146	-0.41185	5.95459	In	2.7804	-1.06632	-3.97559
In	-2.24029	4.49804	2.75057	In	5.65598	0.36041	9.67566

In	0.57991	1.78029	2.75851	In	8.06786	-1.52394	7.28958
In	-3.20601	0.63208	2.71651	In	-11.0084	-3.35473	4.79196
In	-4.1566	-3.17336	2.68297	In	-8.61387	-5.19887	2.3064
In	-1.58048	2.21533	5.94157	In	-6.41994	-7.025	-0.25343
In	-2.60463	-1.56053	5.90421	In	4.22097	-0.77505	6.31064
In	-1.04147	0.11785	9.14271	In	6.66313	-2.58303	3.75912
Ge	10.67663	-4.72072	-3.60975	Ge	6.63264	12.90447	-2.30435
Cu	-0.97575	0.14114	-0.45065	Cu	9.1956	0.36504	3.99239
Cu	-0.39477	-2.06297	2.72453	Cu	6.53252	-1.80236	-2.89048
Cu	-4.73779	-0.96704	-0.47321	Cu	-12.3755	-4.38012	1.28161
Cu	-1.57137	2.35068	-3.60975	Cu	6.73836	2.86735	-0.13143
Cu	2.7996	1.25289	-0.42801	Cu	7.84363	-0.75766	0.55981

2. 4. 2. 2 Synthetic Design

Most framework structures are built from clusters of the same order. For example, supertetrahedral $Cd_4In_{16}S_{35}^{14-}$ T4 clusters are known to crosslink through four corner S^{2-} sites to form two-fold interpenetrating diamond-type structures, as well as novel structure types as found in UCR-1 and UCR-8. In comparison, the structures built from different-sized supertetrahedral clusters are much less known, and the structural contribution from the non-uniform building blocks to the band structure is rarely discussed. One interesting example of mixed-Tn-cluster frameworks is a 3D diamond-type framework formed from Ga-S T3 clusters and Zn-Ga-S T4 clusters (the difference in the order of clusters, $\Delta n = 1$). The synthesis of framework structures simultaneously possessing different-sized supertetrahedral clusters is highly desirable because it creates additional compositional and structural possibilities that can be utilized to achieve a new level of property engineering.

One of the greatest challenges in developing structures with multi-building blocks is the potential phase separation into structures containing only each separate component.

It is conceivable that structures with two or more different building blocks would likely aggregate into complicated repeating units that are generally more difficult for the molecular recognition and self-repairing processes during crystallization. The growth of hetero-cluster frameworks further faces the competition from the formation of many synthetic "default" structures with single-sized clusters, which are well known as exemplified by the T2-cluster-based structure (e.g. UCR-20),[4a] the T4-cluster-based structure (e.g., CdInS-44),[25] and T5-cluster-based structure (e.g., UCR-16).[9] Thus, the synthesis of the material with non-uniformly-sized sub-building units, instead of macroscopic phase separation into simpler phase, is intellectually fascinating and experimentally challenging.

We recently reported one structure built on T2-T4 clusters (the difference in the order of clusters, $\Delta n = 2$).[4d] It has a new zeolite-type topology and demonstrates a new possibility for the co-existence of different building blocks in one structure with topology other than the diamond type by introducing size mismatch in the tetrahedral vertex. CIS-52 is the most extreme case known to date in which a 2D extended framework is constructed from the largest known supertetrahedral cluster (T5) and the smallest supertetrahedral building blocks (T2, not considering the simplest and ubiquitous T1 unit such as InS_4) (the difference in the order of clusters, $\Delta n = 3$).

In the synthetic design of the covalent architecture built from supertetrahedral clusters, the local charge balance, especially surrounding the anionic species (S^{2-} in this case) plays a very essential role in defining the size of the cluster. According to Pauling's electrostatic valence sum rule, to balance the local charge of the four-coordinated sulfur

atom at the center of the T5 clusters, low valent metals such as Zn or Cu should be employed. In other words, the incorporation of low valent metal ions into the synthesis promotes the formation of larger clusters. Conversely, to shrink the cluster size, higher valent cations such as Ge or Sn would be necessary to force the sulfur into the lower coordination numbers, hence promoting the formation of T2 clusters and inhibiting the formation of the larger clusters such as T4 and T5.

And at the same time, we explored an unprecedented trimetallic sulfide system with three charge-complementary metal species, Cu(I), In(III), and Ge(IV). In this case, we can consider the In-S as the base system. The introduced Cu(I) favors the formation of T5 clusters while the addition of Ge(IV) assists the growth of T2 clusters. The resulting trimetallic synthetic system undoubtedly possesses much more complexity and flexibility that can lead to multiple competing crystallization processes in which other competing phase such as UCR-20 and UCR-16 may be formed in the synthetic system. Indeed, both T2-T2 (UCR-20) and T5-T5 (UCR-16) structures could be found to crystallize, together with the targeted T2-T5 in the presence of the same amine template.

2. 4. 2. 3 Structural Analysis

As stated above, the most exceptional structural features of CIS-52, is that the largest and the smallest metal chalcogenide supertetrahedral clusters crystallize together within the same lattice. The huge gap between two supertetrahedral clusters is as large as 77 atoms in the total number of atoms and 13.8 times of difference in terms of volume (an edge ratio of 2.42 between T5 and T2 gives a volume ratio of $2.42^3 = 13.8$). In this

structure, the T2 and T5 clusters are of 1:1 ratio and connect with each other by sharing a bicoordinated corner sulfur atom. Each T2 cluster is connected to 3 T5 clusters and vice versa. Three T2 and three T5 clusters are further assembled into a six-membered ring. Notably, the ratio between two cluster building units differs significantly from the previously reported OCF-42, which is composed of T2: T4 clusters in the 4:1 ratio. Unlike the T2 tetramer aggregates in OCF-42 that could compensate for the size difference between discrete T2 and T4 clusters, the smaller isolated T2 clusters in CIS-52

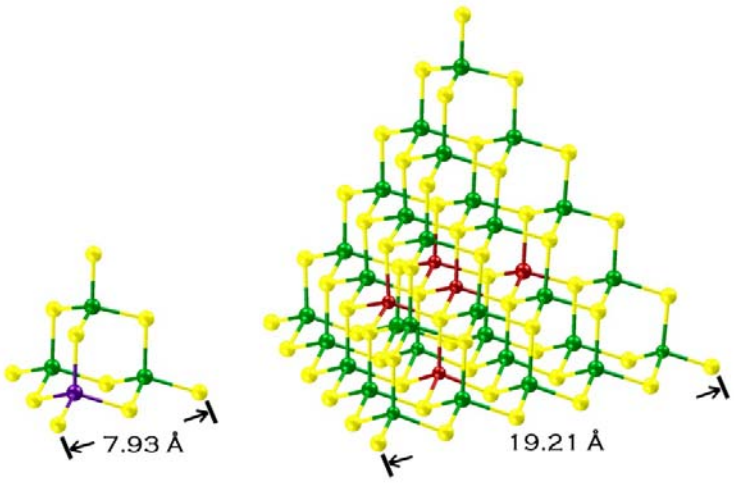

Figure 2.19. The size difference between T2 and T5 supertetrahedral clusters. Yellow: S; Green: In; Purple: In/Ge mixed sites; Red: In/Cu mixed sites.

are evenly dispersed between large T5 clusters and the resulting large size mismatch leads to a huge void space near the edge and the center of the ring which approaches 2 nm in diameter. Since these tetrahedral cluster nodes are only 3-connected the fourth corner sulfur atoms all point to the axial direction to the ring system, leading to a 2-D honeycomb net. The adjacent layers of these hexagonal nets are further packed in a staggered fashion with dangling corner of the tetrahedron pointing to each other.

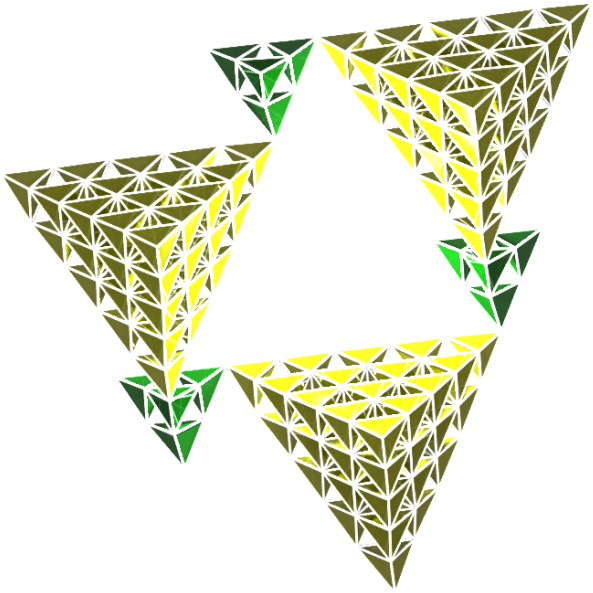

Figure 2.20. Three T5 and three T2 supertetrahedral clusters assembled into a six-membered ring by sharing sulfur atoms on the corner.

The synthetic success of CIS-52 not only proved that two kinds of clusters with huge difference in terms of size and charge could be assembled together under the templating effect of protonated amine molecules with suitable charge density, but also revealed an unusual structure with unprecedented combination of chemical elements involving Cu, In, and Ge all in one crystal. A search of the Cambridge Structural Data shows that no phase containing Cu, In, and Ge is known. The presence of these different metal ions and their well-refined crystallographic positions are supported by single crystal X-ray crystallography and EDAX analysis (Figure 2.17). Our results also show that the different metal ions that tend to have phase separation macroscopically could be brought together by incorporation into separate clusters first, and then by further assembly though sulfur bridges. Such nano-scale separation into crystallographically

ordered different-sized clusters seems to promote the co-assembly of various components and lessen the chances for macroscopic phase separation.

2. 4. 2. 4 Structure and Property Correlations

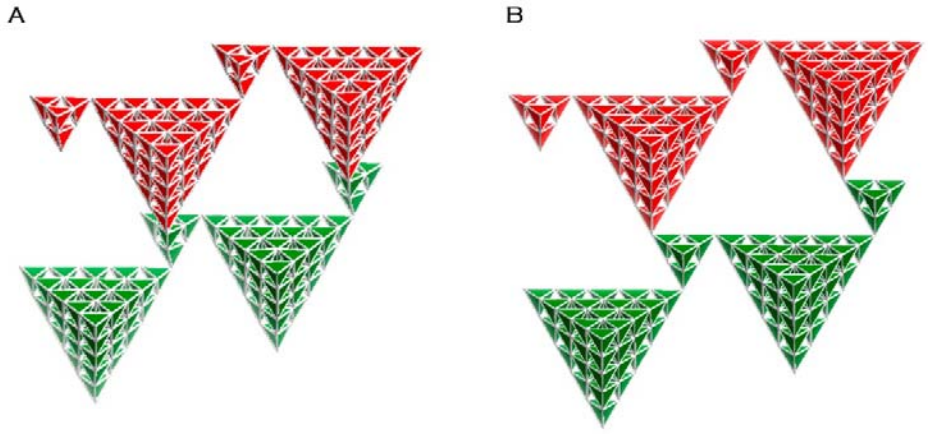

Figure 2.21. Structural difference between stacking mode of supertetrahedral clusters in CIS-52 and its isomer. A: stacking aggregations of the synthesized CIS-52; B: coplanar aggregation of the clusters in the imagined isomer.

The creation of the molecular architectures from different-sized building blocks has a general implication in property engineering based on the manipulation of artificial atoms. One common concern in this system is whether the material's property is equally highly sensitive to the change in aggregation modes of the nano-scaled artificial atoms as to the change on the atomic scale. Therefore, UV-Vis spectrum of CIS-52 was measured from selected single crystals to evaluate its band gap. The measured band gap of 2.2eV (Figure 2.18) is almost the same as that of the purely T5 constructed structures with the same Cu-In-S composition. This result shows even with introduction of T2 clusters into the framework, the optical band still carries T5 framework character. The corner sulfur atom connecting different clusters as the only channel is limited and ineffective for electronic

states to overlap between adjacent clusters. Thus the material tends to exhibit an optical gap that closely resembles that of discrete building units.

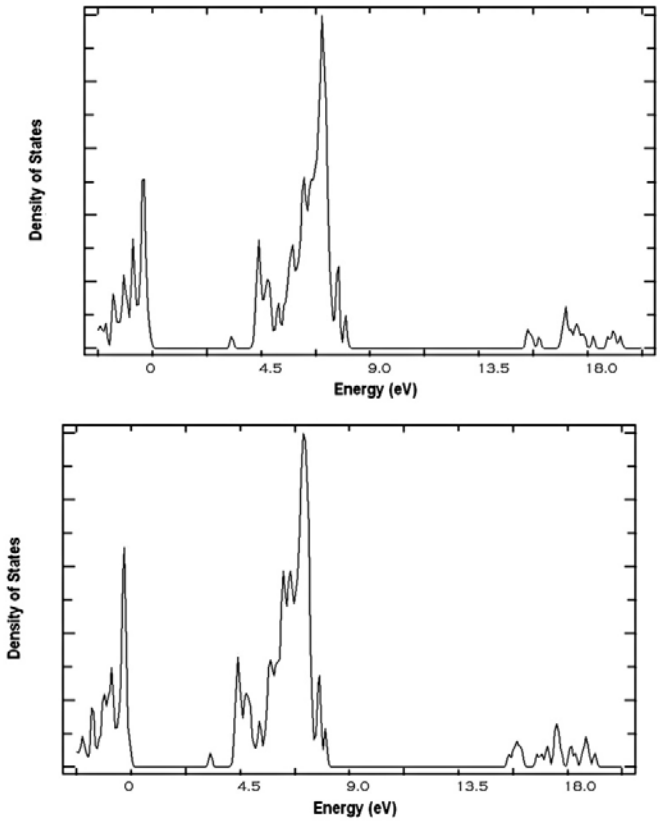

Figure 2.22. Density of state plot of CIS-52 and CIS-52-iso.

We further carried out theoretical calculation to support our findings. Since CIS-52 is the only obtained structure of the T2-T5 system, we had to build one imagined comparable iso-structures which preserves most of the local structural feature of the CIS-52 with only difference in packing modes without any change on connection between clusters, (exactly the same components within each supertetrahedral clusters, the same dihedral angles on the bridge sulfur atom, and the same ratio between the T2 and T5 units) as shown in Figure 2.21. Theoretical simulations for both structures were

performed on the same basis set with extended Hückel theory considering the calculation cost by using Caesar calculation package.[18] The atom positions of the model calculated are listed in Table 2.2. The calculated DOS plots (Figure 2.22) show that for both structures, the conduction band bottom is dominated by Cu d orbitals and the valence is mostly contributed from the S p orbitals, which is consistent with our common understandings about semiconductors. However, there is no big difference in total DOS between two isomers, which indicates the electronic states in this type of material are indeed highly localized within the clusters and the states coupling between connecting corners is quite weak. Preserving the local structural feature and yet changing the long range order, as in this case, by shifting the stacked packing mode to the co-planar packing mode between the T2-T5 chains would not have significant effects on band structure. This result also indicates the possibility of keeping the electronic properties undisturbed by utilizing the same ratio and size of the cluster building blocks no matter how different in the connection mode. In other words, the optical band of the cluster based materials is highly dependent on its local structure feature (cluster size, cluster composition), and not severely affected by its overall topology. And this allows the tuning in porosity and pore geometry while retaining the same optoelectrical property.

2. 4. 2. 5 Concluding Remarks

In conclusion, a supramolecular architecture composed of the largest and the smallest supertetrahedral clusters has been successfully synthesized. Its component complexity indicates the mixed building blocks strategy could incorporate different metal ions (that usually distribute in separate phases) into the same lattice by local nanoscale

phase separation (instead of macroscopic phase separation into different crystalline phase).

2. 5 Conclusion and Perspectives

Conclusively, supertetrahedral clusters based molecular architectures represent optical gaps that strongly dependent to their local structures and compositions within clusters other than to the inter-cluster relationships. This provides opportunity of property engineering by cluster assembly to possibly orthogonalize the band gap from the structural features as coordination number, overall topology, packing density and other long range ordering.

2. 6 References

(1) (a) Dance, I.; Fisher, K., Prog Inorg Chem 1994, 41, 637-803; (b) Krebs, B.; Henkel, G., Angewandte Chemie-International Edition in English 1991, 30, 769-788; (c) Scott, R. W. J.; MacLachlan, M. J.; Ozin, G. A., Curr Opin Solid St M 1999, 4, 113-121.

(2) (a) Cahill, C. L.; Parise, J. B., Chem Mater 1997, 9, 807-811; (b) Cahill, C. L.; Ko, Y. H.; Parise, J. B., Chem Mater 1998, 10, 19-21.

(3) (a) Li, H. L.; Eddaoudi, M.; Laine, A.; O'Keeffe, M.; Yaghi, O. M., J Am Chem Soc 1999, 121, 6096-6097; (b) Li, H. L.; Laine, A.; O'Keeffe, M.; Yaghi, O. M., Science 1999, 283, 1145-1147.

(4) (a) Zheng, N. F.; Bu, X. G.; Wang, B.; Feng, P. Y., Science 2002, 298, 2366-2369; (b) Zheng, N. F.; Bu, X. H.; Feng, P. Y., Nature 2003, 426, 428-432; (c) Zheng, N.; Bu, X. H.; Vu, H.; Feng, P. Y., Angew Chem Int Edit 2005, 44, 5299-5303; (d)

Wang, L.; Wu, T.; Zuo, F.; Zhao, X.; Bu, X. H.; Wu, J. Z.; Feng, P. Y., J Am Chem Soc 2010, 132, 3283-+.

(5) Manos, M. J.; Malliakas, C. D.; Kanatzidis, M. G., Chem-Eur J 2007, 13, 51-58.

(6) (a) Wang, C.; Li, Y. Q.; Bu, X. H.; Zheng, N. F.; Zivkovic, O.; Yang, C. S.; Feng, P. Y., J Am Chem Soc 2001, 123, 11506-11507; (b) Bu, X. H.; Zheng, N. F.; Li, Y. Q.; Feng, P. Y., J Am Chem Soc 2002, 124, 12646-12647; (c) Wu, T.; Wang, X. Q.; Bu, X. H.; Zhao, X.; Wang, L.; Feng, P. Y., Angew Chem Int Edit 2009, 48, 7204-7207.

(7) Zhang, Q. C.; Liu, Y.; Bu, X. H.; Wu, T.; Feng, P. Y., Angew Chem Int Edit 2008, 47, 113-116.

(8) Li, H. L.; Kim, J.; O'Keeffe, M.; Yaghi, O. M., Angew Chem Int Edit 2003, 42, 1819-1821.

Chapter 3

Hierarchical Assembly of Super-Supertetrahedral Metal-Organic Clusters and Spin Frustration Study

3.1 Introduction

The use of molecular building blocks is a powerful method in the synthesis of solid state materials.[1, 2] In the areas of metal-organic frameworks (MOFs) and metal-organic polyhedra (MOPs), the "node and spacer" approach involving molecular building blocks of various combinations is very successful in constructing the targeted open architectures. Compared to traditional dense solid state materials, molecular building blocks such as organic linkers and metal clusters exhibit a much greater diversity and provide new opportunities for generating materials with high porosity.

More recently, supramolecular building blocks have been found to be a potent way for achieving hierarchical assemblies that allow a new level of control over structural properties and pore structures. This method, as highlighted by the use of MOPs as building units, beautifully demonstrates the self-assembly on a supramolecular scale by larger and more sophisticated aggregates of multi-metal nodes and organic linkers.[2] Compared to molecular building blocks, these supramolecular cages or clusters can dramatically scale up the pore architecture, and very often they also possess well-defined coordination geometry, which bestow a certain degree of predictability in the synthetic design.[3, 4] On the other hand, so far there are much fewer examples of supramolecular building units, compared to molecular building units. Hence creating new rationally

designed supramolecular building blocks is of increasing importance.

Most interestingly to us is the fact that even among supramolecular building units, it is possible to have multiple levels of hierarchies. For example, in metal chalcogenide chemistry,[5] four InS_4 molecular tetrahedra can form an In_4S_{10} supertetrahedral cluster (known as T2) by corner sharing. Such T2 clusters, by themselves, can form 3D porous frameworks with zeolite-like topologies such as sodalite.[6a] Yet, it is also known that four T2 clusters can form a closed super-supertetrahedral clusters with the same T2 configuration, $In_{16}S_{34}$ (known as super-supertetrahedral T2,2 cluster).[6a] Similar formation of hierarchical superstructures is also known for larger clusters (e.g., the assembly of four T4 $Cd_4In_{16}S_{35}$ clusters into the T2 configuration of $Cd_{16}In_{64}S_{134}$, denoted as T4,2 cluster).[6b] In comparison, while supramolecular tetrahedral building units are also found in MOFs, as exemplified by $[(Cr_3O)_4(BTC)_4]$ and $[(Cr_3O)_4(BDC)_6]$ cages in MIL-100 and MIL-101, as well as dense clusters like $Cu_5(btz)_6(L)_4$ and $Co_5(btz)_6(L)_4$;[7, 8] a higher level of assembly into super-supertetrahedron-like cluster has so far remained elusive in MOFs. The work presented here was just started with targeting the multi-level complexity in MOF system.

3.2 Synthetic procedures and general characterization

3.2.1 Ligand Synthesis

Methyl 4- cyanobenzoate (TCI), Sodium azide (Aldrich), Zinc bromide (Alfa Aeser), Manganese Dichloride (Aldrich), and Ammonium formate (Aldrich), were used as purchased without any further purification.

The synthesis of 4-Tetrazol benzoic acid is conducted according to methodology

reported by literature1. Click reaction with starting material of methyl 4- cyanobenzoate (3.225 g, 20 mmol), and sodium azide with 10% excess (1.433 g, 22 mmol) are refluxed in 40 g of water with 4.5 g $ZnBr_2$ as Lewis acid for 8 hrs. When reaction completed, white precipitate was extracted with Ethyl-acetate followed by rotoevaporation. Further hydrolysis of the ester de-protection was carried in 200ml of 2 M NaOH (aq) under 90 ^oC overnight. Final product was precipitated around pH value of 2 adjusted by 4M hydrochloric acid.

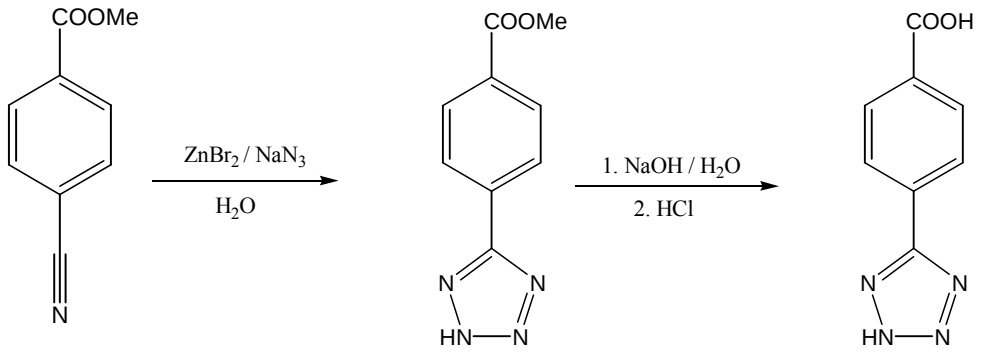

Figure 3.1. Ligand synthetic scheme.

3.2.2 Synthesis of CPF-5 Crystals

The CPF-5 reported in this study is synthesized under solvothermal conditions. By reacting a mixture of MnCl2 powder (100mg), 4- tetrazole benzoic acid (80 mg), ammonium formate (15 mg), in a solution of 1.8 g DMF and 200 mg water under 120oC for 3 days in a 23ml glass vial, colorless cubic crystal beautifully formed of 76% yield based on 4- tetrazole benzoic acid. The crystalline sample was collected after washing with dichloromethane. Data of the single crystal X-ray structure analysis, powder–XRD pattern, and TGA information, are all obtained from the sample as synthesized. Gas

adsorption measurements were performed on the samples with solvent exchange treatment in dichloromethane for 24 hours.

3.3 General Characterizations

3.3.1 Crystal Morphology

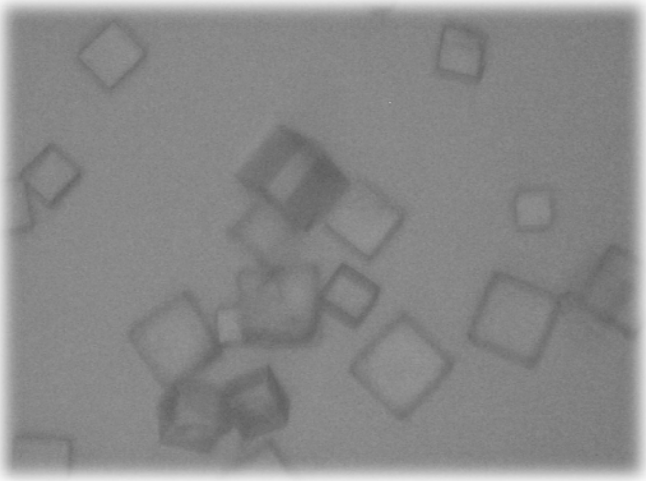

Figure 3.2. An optical image of crystals synthesized.

3.3.2 Bulk-phase X-Ray Diffraction Pattern

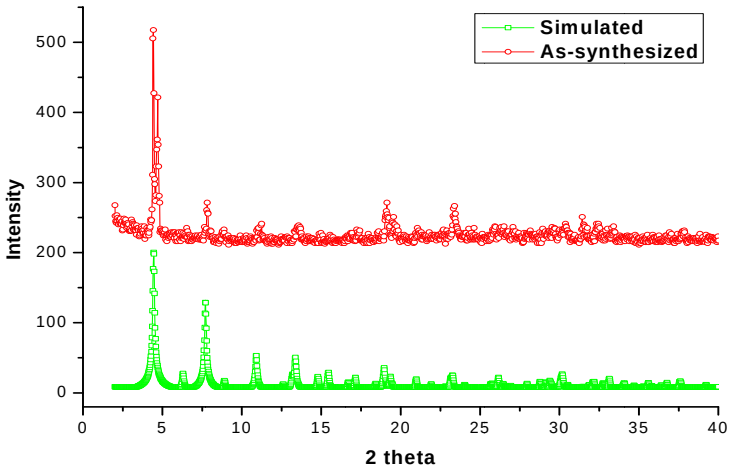

Figure 3.3. Measured and simulated powder XRD patterns for CPF-5.

3.3.3 Thermal Stability Test

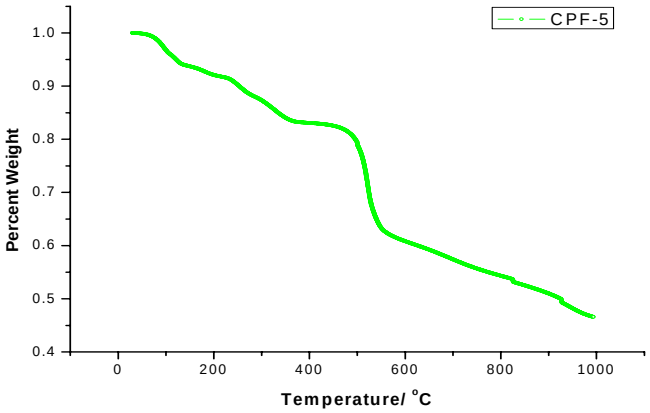

Figure 3.4. TGA plot of CPF-5 heated under nitrogen atmosphere.

TGA experiment was performed on STDQ-600 with initial temperature of 300K increased to 1000K with 10K per minute under nitrogen environment with a flow rate of 100 micro liters per minute.

3.3.4 IR Spectra of Synthesized Ligand and Crystals

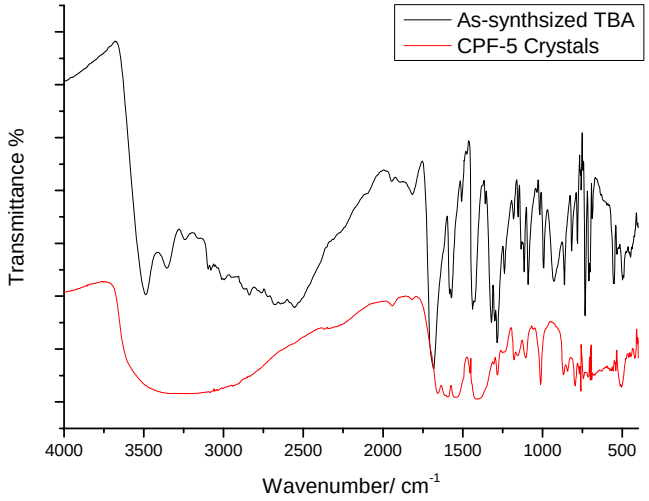

Figure 3.5. FT-IR of as-synthesized TBA ligand and CPF-5 crystal samples.

For the as-synthesized TBA ligand, the several strong and well separated IR bands were assigned to ν -NH at 3485 cm-1, ν -OH at 3360 cm-1, ν -CO at 1687 cm-1, and different stretching mode for NN and CN bond on the tetrazole five member ring at 1575, 1436, 1323 and 1286 cm-1, as well as ν -CH at 1091 cm-1 and ν -NH at 995 cm-1 according to literature report.2

For the crystallized CPF-5 sample, the framework bonded H2O covers a very large range from 3600 to 3000 cm-1, the rest of the absorption peaks are widened but still carry some obvious identities from the ligands such as characteristic absorption for ν -CO around 1700 and NCN, CNN, and NNN stretches at around 1630, 1550, and 1430 wavenumbers.

3.3.5 EPR Data of CPF-5 Crystals

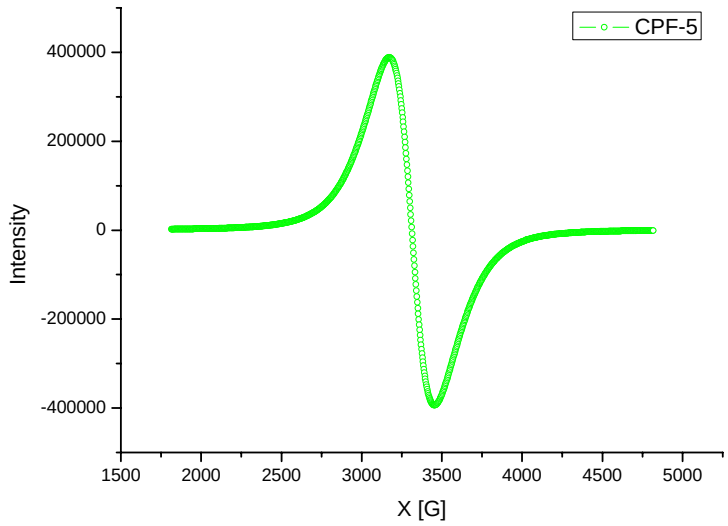

Figure 3.6 EPR spectra of as-synthesized crystals.

Since the Mn sites within the crystal is mixed with 6-coordinated and

5-coordinated geometry and experiencing 3 types of different chemical environment, a hyperfine structure with multi peak resolution was not obtained, and the EPR spectra shows a very broad band under the experiment condition of 100 K with frequency of 9.363 GHz.

3.3.6 Gas Adsorption Behaviors

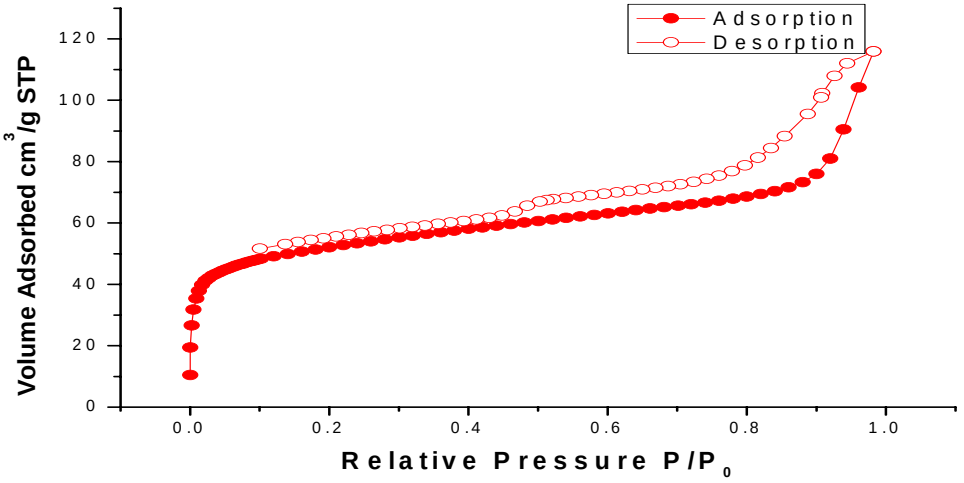

Figure 3.7. Nidrogen adsorption isotherm under 77K and 760mmHg for CPF-5.

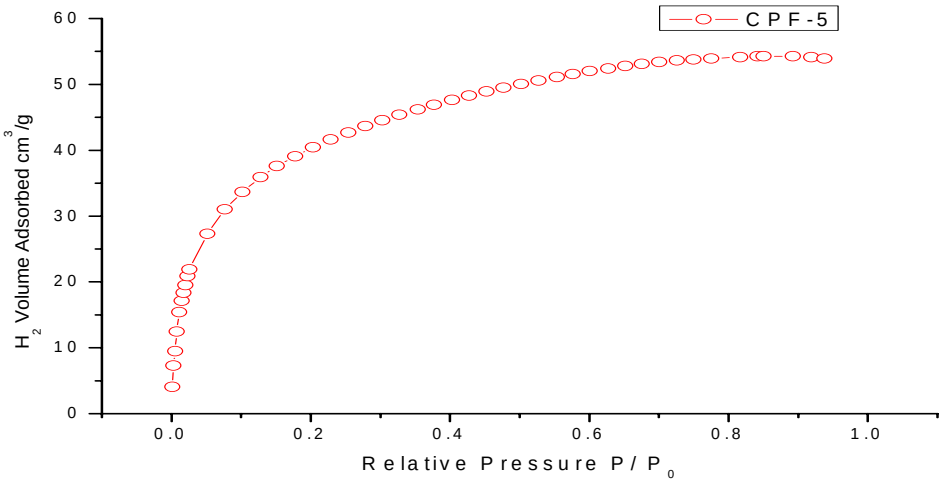

Figure 3.8. Hydrogen adsorption isotherm under 77K for CPF-5.

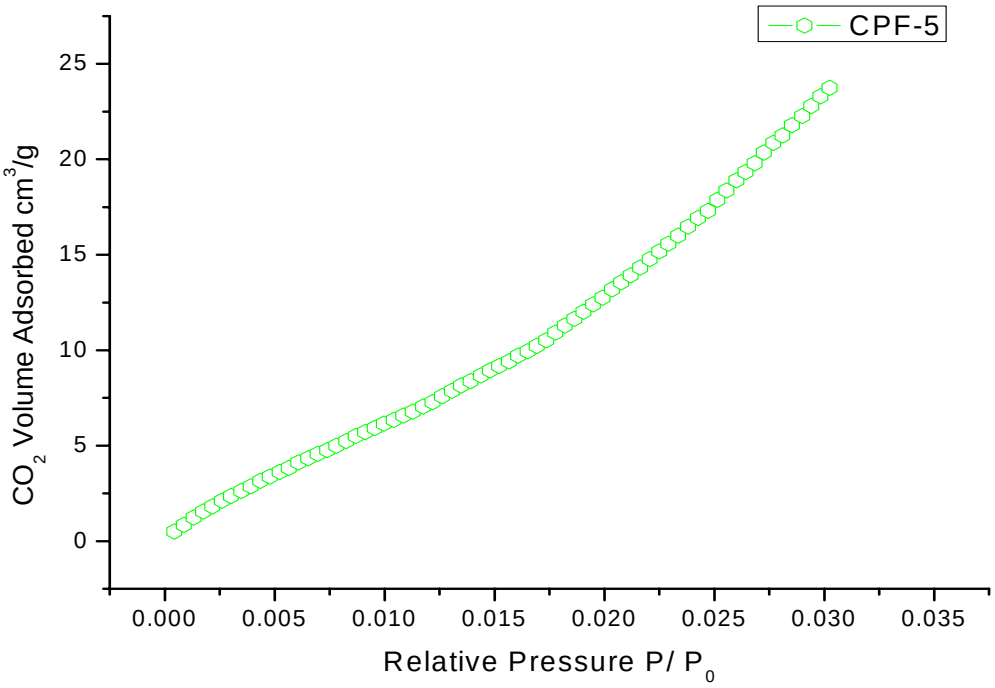

Figure 3.9. Carbon dioxide adsorption isotherm under 273K for CPF-5.

3.3.7 Magnetic Property Characterizations

Measurements of magnetic properties were conducted using a Quantum Design XL7SQUID magnetometer. Synthesized samples were first evacuated under 100oC and then incorporated into a diamagnetic eicosane (Alfa Aesar) matrix and loaded into a polycarbonate capsule. The background contribution from the sample mounting (straw, capsule, eicosane) was measured separately and subtracted from the measured sample net magnetic moment. Magnetization was measured in a constant applied magnetic field of 1kOe as the sample was cooled down from 300K to 2K.

3.3.8 Bond Valence Calculation for Mn Atoms Based on Crystal Data

Table 3.1. Bond valence calculation for different Mn sites

Mn1, corner	Mn-O	Mn-O	Mn-O	Mn-N	Mn-N	Mn-N	
	2.254	2.254	2.254	2.284	2.284	2.284	
Valence Assumed	Valence Contribution						Valence SUM
Mn II	0.285346	0.285346	0.285346	0.326633	0.326633	0.326633	1.835935
Mn III	0.263123	0.263123	0.263123	0.326633	0.326633	0.326633	1.769266
Mn IV	0.258191	0.258191	0.258191	0.326633	0.326633	0.326633	1.754472
Mn2, core	Mn-O	Mn-O	Mn-O	Mn-N	Mn-N	Mn-N	
	2.144	2.144	2.144	2.304	2.304	2.304	
Valence Assumed	Valence Contribution						Valence SUM
Mn II	0.384137	0.384137	0.384137	0.309446	0.309446	0.309446	2.080747
Mn III	0.35422	0.35422	0.35422	0.309446	0.309446	0.309446	1.990996
Mn IV	0.347581	0.347581	0.347581	0.309446	0.309446	0.309446	1.971081
Mn3, bridge	Mn-N	Mn-N	Mn-N	Mn-O	Mn-O	Mn-O	
	2.255	2.122	2.159	2.122	2.235	2.367	
Valence Assumed	Valence Contribution						Valence SUM
Mn II	0.284575	0.40767	0.368875	0.40767	0.300381	0.260998	2.03017
Mn III	0.262412	0.37592	0.340147	0.37592	0.276987	0.260998	1.892385
Mn IV	0.257495	0.368875	0.333772	0.368875	0.271796	0.260998	1.861811

3.4 Results and Discussion

3.4.1 Structural Description

Herein, the report multi-hierarchical MOF structure is constructed by a super-supertetrahedral metal-ligand cluster with twenty metal sites. It has a cubic unit cell with the formula of $[Mn_5(TBA)_3(HCOO)_3(OH)(H_2O)_2]_4 \bullet 6DMF$ (denoted as CPF-5, CPF = Crystalline Porous Framework; H_2TBA= 4-tetrazole-benzoic acid). In CPF-5, each tetrazolate uses three of its four N-donors to assemble five metal ions into a supertetrahedral T2-like cluster (Fig. 3.10). Within the T2 cluster, three tetrazolate groups

are arranged on three adjacent edges of the tetrahedron that share the same corner Mn, while the other three edges are occupied by formate groups, forming the $Mn_3(HCOO)_3$ 3-ring. One O site of the formate group is bonded to only one Mn^{2}+ site of the triangle, while the other O site bridges one Mn^{2+} site of the triangle with the core Mn^{2+} site. Thus, the core Mn is 6-coordinated, to three N atoms of three different tetrazolate groups and three O atoms of different formate groups (Fig. 3.10.a).

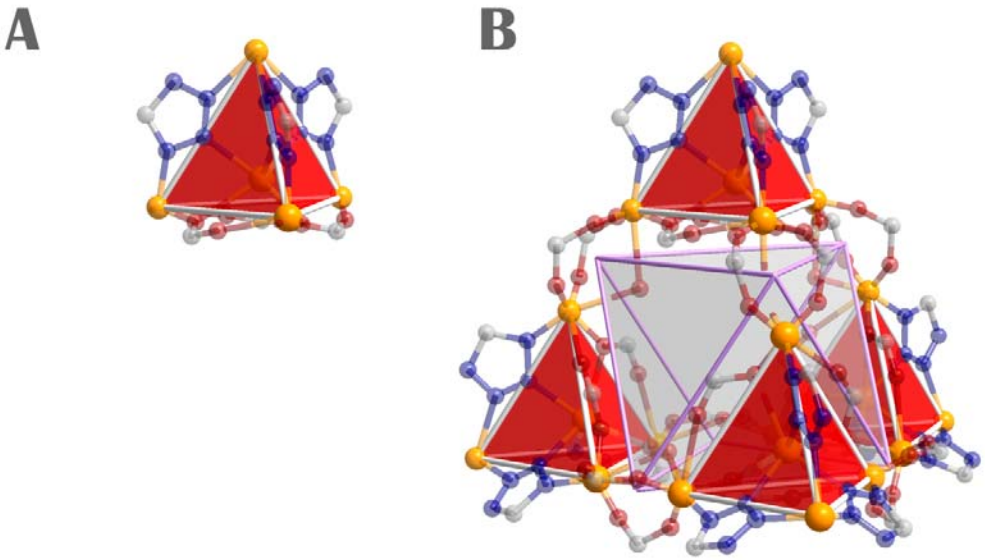

Figure 3.10. (A). Five Mn atoms are aggregated into a [Mn5(TBA)3(HCOO)3] supertetrahedral T2-like cluster. Six edges of the T2 cluster is occupied by 3 TBA and 3 formate groups. (B). Four T2 clusters are further linked into a super-supertetrahedral T2,2 cluster by carboxylate groups and DMF oxygen. Orange: Mn; Red: O; Blue: N; Grey: C.

Four T2 clusters are joined together by using two carboxyl groups and one DMF O donor to bridge two Mn2+ sites from two adjacent Mn-formate triangles, leading to a T2,2 cluster (Fig. 3.10.b). Within the T2,2 cluster, the Mn2+ sites in the Mn-formate triangle have a 5-coordinate environment. However, the four Mn atoms at the corner of T2,2 cluster possess 6-coordination by also bonding to three O atom with an average

bond length of 2.25 Å.

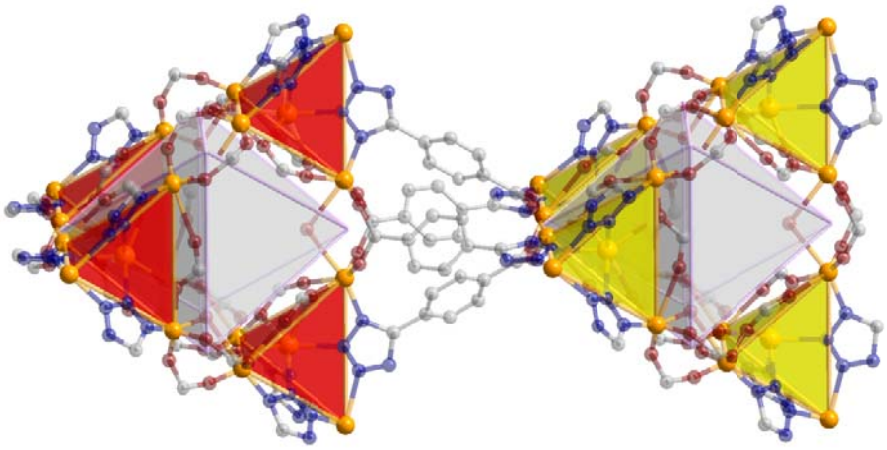

Figure 3.11. Two T2,2 clusters are connected together by a total of 4 ligands. Each TBA ligand runs from the edge center of one T2,2 cluster to the edge center of one T2 cluster within the other T2,2 cluster. Orange: Mn; Red: O; Blue: N; Grey: C.

This hierarchical self-assembly of the T2 cluster into T2,2 cluster drastically scales up the size of the building block. Interestingly, in CPF-5, T2,2 clusters are further assembled together through a special type of quadruple edge-to-edge connections (Fig. 3.11) into a 3D simple cubic topology (Fig. 3.12), which leads to the 4th-order of structural hierarchy (the 1st-order being the MnL5 and MnL6 complexes). This is highly unusual, not only because the overall framework involves four levels of hierarchical constructions, but also because the total connections between each T2,2 cluster and its six adjacent T2,2 clusters involve as many as 24 ligands.

While the overall framework topology resembles the well-known 6-connected MOF-5 structure, the 6-connected node in CPF-5 is far more complicated. In comparison

with MOF-5 with only four tetrahedral Zn atoms in its 6-connected node, the 6-connected node in CPF-5 has a total of 20 metal sites, organized into three levels of hierarchies with an accompanying hydrophilic cavity partially occupied by framework-bonded DMF molecules. A much larger void results from the cubic assembly of T2,2 clusters. The 3D interconnecting porous channels possess a hydrophilic central void of 14 Å in diameter with aperture of 11 Å. PLATON calculation indicates that the solvent accessible void space occupies a total of 56% of the crystal volume.

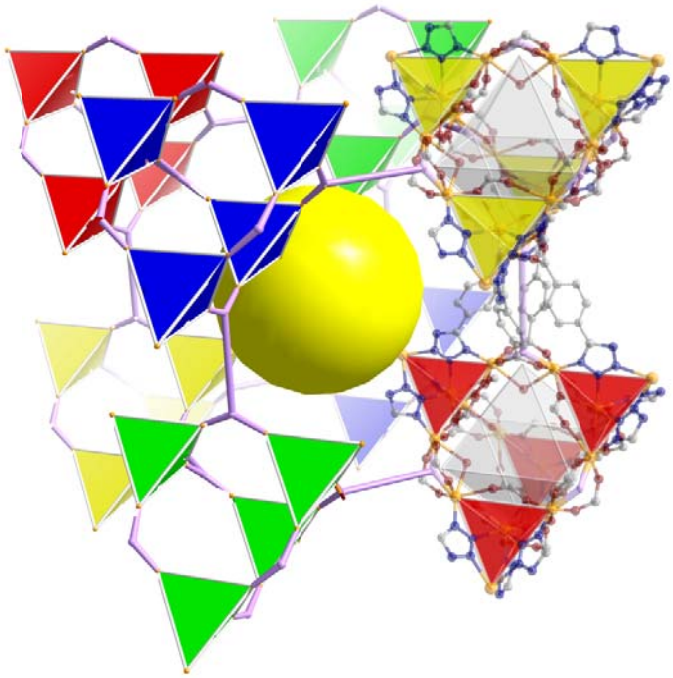

Figure 3.12. Eight T2,2 clusters aggregate into simple cubic packing. Each tetrahedron in this graph represents a T2 supertetrahedral cluster containing 5 Mn atoms. The four ligand connecting neighboring clusters are simplified as purple rods. Orange: Mn; Red: O; Blue: N; Grey: C.

3.4.2 General Material Properties and Pore Structure Evaluation

Thermogravimetric analysis shows that CPF-5 lost 15% of its weight at around 100oC due to the loss of uncoordinated solvent molecules, and continued to gradually

lose weight until 210^{o}C under N_2 atmosphere. Various degas temperatures were tested and 100^{o}C was found to provide the maximum adsorption uptake. Permanent porosity was confirmed by N_2 adsorption performed on Micromeritics ASAP 2020. N2 adsorption behavior of CPF-5 shows a small step before reaching the saturation and then followed by a hysteresis loop in the higher relative pressure region. The small step is quite typical for the materials with both micro and meso apertures. It likely resulted from the multi-layer adsorption of N_2 molecule in the larger channels and the hysteresis loop further confirmed there is capillary condensation in the larger pores even though the effect from the inter-particle pore near 1atm is evident. From the isotherm, Langmuir and BET surface areas were calculated to be 262.9m^2/g and 161.3m^2/g, respectively. This material also shows good adsorption ability for carbon dioxide (31.6cm^3/g at 273.15K under 784mmHg) and hydrogen (4.82mg/g) (Figures 3.8 and 3.9).

The three distinct regions, especially evident on the desorption branch (Fig. 3.13) represent three types of cavity: the octahedral cavity surrounded by the supramolecular Mn_5-tetrahedra, the large channel built by cubic packing of super-supertetrahedral Mn_{20}-T2,2 clusters, and macropore from macroscale particle packing. The presence of these multi-scale pores clearly demonstrates that by applying super-supramolecular clusters as building blocks, one could scale up the molecular architecture from atomic scale to meso-scale.

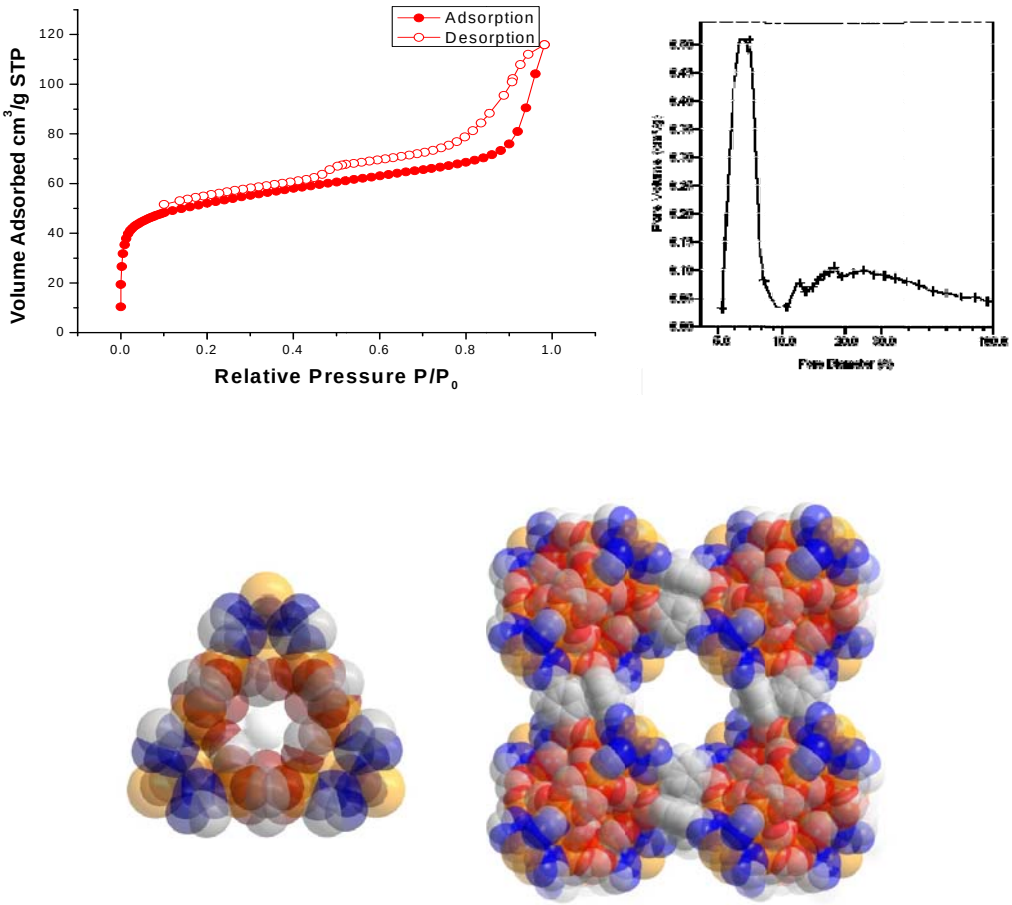

Figure 3.13. N_2 adsorption-desorption isotherm, BJH pore size distribution of adsorption branch and different sized pore windows of CPF-5 at 77K.

3.4.3 Magnetic Property

One advantage of using supramolecular clusters as the building block is the opportunity for incorporating other properties into the structure. A more densely aggregated metal-ligand cluster could offer desirable interactions such as magnetic exchange or other interactions that do not occur when the metal centers are separated significantly. The magnetic property measurement is carried out on Quantum Design XL7SQUID magnetometer on a degassed sample. The temperature dependent magnetic

susceptibility of CPF-5 is given in Fig. 3.14. Above 20K, the data follows a Curie-Weiss behavior with an effective magnetic moment (μeff) of 5.4μB per magnetic ion and a Weiss temperature (θ) of -23.7K. This 5.4μB per magnetic ion was derived by treating the mass of the crystal as the weight of the framework only. It is slightly smaller compared to the 5.9μB of Mn(II) ion, which indicates there is approximately 9% of the free solvent by weight still left in the open framework at this degas condition. Note that no maximum is observed in the susceptibility. Long-range AFM (χ-1mol vs. T minima) or fM (χ-1mol vs. T abscissa intercept) order is not observed down to 2K. The negative Weiss temperature (θ) is an indication that the magnetic moments have an antiparallel coupling as with an antiferro- (AFM) or ferri-magnet (fM). Considering the ordering temperature is at least an order of magnitude less than the Weiss temperature, a significant amount of magnetic frustration may be present. We conclude this is a spin glass system.

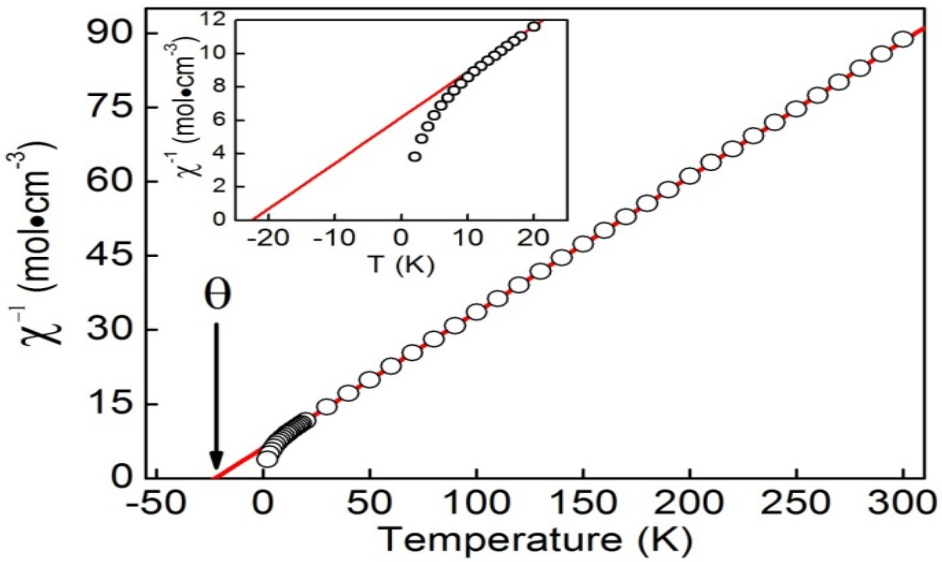

Figure 3.14. The inverse molar susceptibility (χ-1mol) versus temperature (T) for CPF-5. Below 20K, the inverse susceptibility descends faster than the Curie-Weiss relation.

The antiferromagnetic property of the material shows strong spin frustration character as stated above, and such resulted spin frustration is highly possible stemed from geometry spin frustration. In other words, the spin orientation ambiguity is originated from topological arrangement of the magnetic active atoms. A key feature for the material of CPF-5 is the odd number of magnetic atom in the same sub-building unit. Within the sub-building unit of the T2 supertetrahedral Mn-ligand cluster, the Mn atoms are considered to be in strong magnetic interactions. For antiferromagnetic materials without any spin frustration, the spin vertices have to be in anti-parallel pairs, and the spin atoms must be in even number within the repeating units throughout the unit cell. However, for the case of CPF-5, the 5 -member Mn(II) sub-building units could not find any possible spin arrangement to satisfy the anti-parallel pairing, hence finally results in spin frustration. One of the proposed scenarios showing the spin pairing ambiguity on core Mn is presented in figure 3.15.

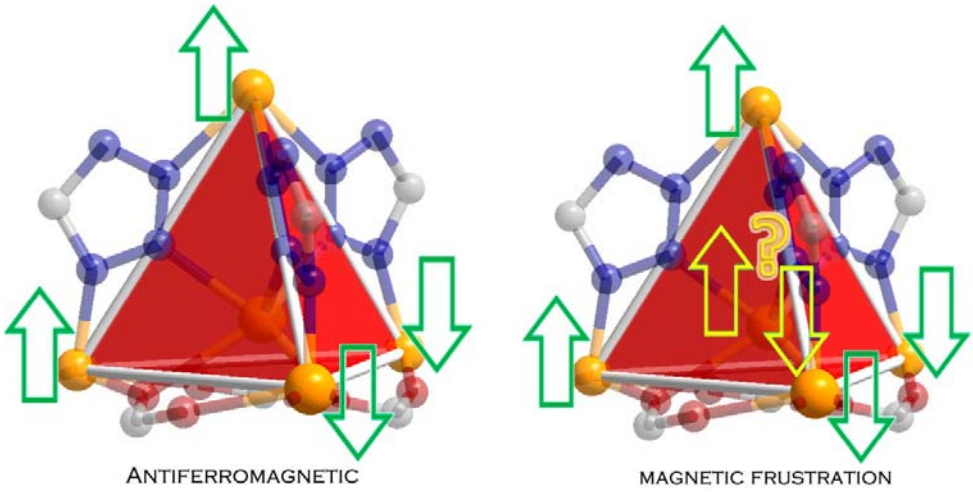

Figure 3.15. A possible spin-frustration mechanism based on the odd number magnetic atom composed building block in CPF-5.

3.6 Conclusive Remarks

In conclusion, this work shows that by utilizing supertetrahedral clusters as sub-building unit, one could push up the architectural scale from molecular to meso-scale with much larger void space. Moreover, once the magnetic active atoms are introduced into the framework, a more densely aggregated structure building block would result in interesting magnetic exchange such as geometric frustration.

3.7 Outlooks

Table 3.2. Composition of the proposed super-supertetrahedral metal-organic clusters

Denotation	T2,1	T2,2	T2,3
Composition	Mn5(ttz)6(OH)4(H2O)8	[Mn5(ttz)6]4(μ-O)6(CO2)12(OH)4(H2O)8	[Mn5(ttz)6]10(μ-O)16(CO2)36(OH)4(H2O)8
M.W. in Dalton	895	3568	8882
Available Spin Density	25	100	250
Cluster Size	6.36 Å	16.97 Å	29.56 Å

The work demonstrates the feasibility of constructing porous frameworks or discrete supramolecular aggregates based on higher-order supertetrahedral metal organic clusters. Considering there are many orders of supertetrahedral clusters such as T2,1 T2,2 T2,3… (figure 3.16) it is intriguing to speculate that other porous MOFs with multi-level hierarchical ordering may be produced by using triazolates or tetrazolates M_5L_6 supertetrahedral clusters. These clusters are of huge formula mass and join up a great number of magnetic atoms, most interestingly; they might carry the spin frustration

property as well.

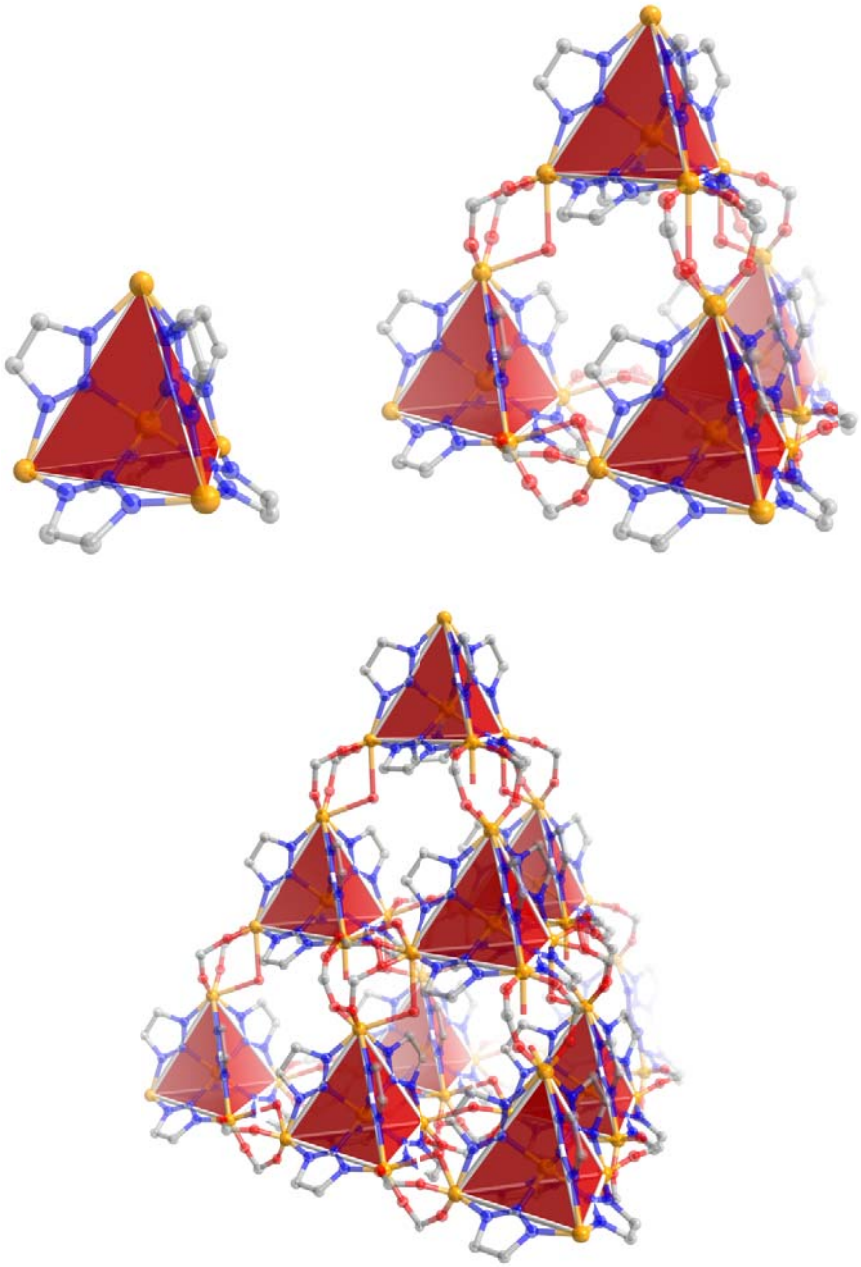

Figure 3.16. Proposed structure for T1, T2, and T3 tetrahedral metal organic cluster.

3.8 References

1 a) M. Fujita, M. Tominaga, A. Hori and B. Therrien. *Acc. Chem. Res.*, 2005, **38**, 369; b) B. F. Hoskins and R. Robson, *J. Am. Chem. Soc.*, 1999, **112**, 1546; c) R. Robson, *J. Chem. Soc. Dalton. Trans.*, 2000, 3735; (d) X.-C. Luo, D.-B. Luo, H.-M. Zeng, M.-C. Gong, Y.-Q. Chen, Z.-E. Lin, *Inorg. Chem.*, 2011, **50**, 8697; (e) Guo, H. Wu, G. Srinivas, Y. Zhou, S. Xiang, Z. Chen, Y. Yang, W. Zhou, M. O'Keeffe and B. Chen, *Angew. Chem. Int. Ed.*, 2011, **50**, 3178; (f) S.-H. Huang, C.-H. Lin, W.-C. Wu and S.-L. Wang, *Angew. Chem. Int. Ed.*, 2009, **48**, 6124. (g) A. Sonnauer, F. Hoffmann, M. Fröba, L. Kienle, V. Duppel, M. Thommes, C. Serre, G. Férey, N. Stock, *Angew. Chem*, **2009**, *121*, 3849-3852. (h) B. Yan, Y. Xu, X. Bu, N. K. Goh, L. S. Chia, G. D. Stucky, Dalton Trans., 2001, 2009-2014.

2 a) H. Li, M. Eddaoudi, M. O'Keeffe and O. M. Yaghi, *Nature*, 1999, **402**, 276; b) M. Eddaoudi, D. B. Moler, H. Li, B. Chen, T. M. Reineke, M. O'Keeffe and O. M. Yaghi, *Acc. Chem. Res.*, 2001, **34**, 319; c) O. M. Yaghi, M. O'Keeffe, N. W. Ockwig, H. K. Chae, M. Eddaoudi and J. Kim, *Nature*, 2003, **423**, 705. (d) F. Wang, Z.-S. Liu, H. Yang, Y.-X. Tan, J. Zhang, *Angew. Chem. Int. Ed.*, 2011, **50**, 450.

3 a) J.-R. Li, D. J. Timmons and H.-C. Zhou, *J. Am. Chem. Soc.* 2009, **131**, 6368; b) J.-R. Li and H.-C. Zhou, *Angew. Chem., Int. Ed.* 2009, **48**, 8465; c) J.-R. Li, A. A. Yakovenko, W. Lu, D. J. Timmons, W. Zhuang, D. Yuan and H.-C. Zhou, *J. Am. Chem. Soc.*, 2010, **132** 17599. d) J.-R. Li and H.-C. Zhou,

Nature Chem. 2010, **2**, 893, e) D. Yuan, D. Zhao, D. Sun and H.-C. Zhou, *Angew*. *Chem*., *Int*. *Ed*. 2010, **49**, 5357-5361.

4 a) A. J. Cairns, J. A. Perman, L. Wojtas, V. C. Kravstov, M. H. Alkordi, M. Eddaoudi and M. J. Zaworotko, *J*. *Am*. *Chem*. *Soc*. 2008, **130**, 1560; b) F. Nuoar, J. F. Eubank, T. Bousquet, L. Wojtas, M. J. Zaworotko, and M. Eddaoudi, *J*. *Am*. *Chem*. *Soc*. 2008, **130**, 1833; c) D. F. Sava, V. C. Kravtsov, J. Eckert, J. F. Eubank, F. Nouar and M. Eddaoudi, *J*. *Am*. *Chem*. *Soc*., 2009, **131** , 10394; d) M. H. Alkordi, J. A. Brant, L. Wojtas, V. C. Kravtsov, A. J. Cairns, and M. Eddaoudi, *J*. *Am*. *Chem*. *Soc*., 2009, **131**, 17753; e) S. Wang, T, Zhao, G. Li, L. Wojtas, Q. Huo, M. Eddaoudi and Y. Liu, *J*. *Am*. *Chem*. *Soc*., 2010, **132**, 18038.

5 a) B. Krebs and G. Henkel, *Angew*. *Chem*., *Int*. *Ed*. *Engl*. 1991, **30**, 769, b) R. W. J. Scott, M. J. MacLachlan and G. A. Ozin, *Curr*. *Opin*. *Solid State Mater*. *Sci*. 1999, **4**, 113, c) I. G. Dance and K. G. Fisher, *Prog*. *Inorg*. *Chem*. 1994, **41**, 637, d) P, Feng, X. Bu, N. Zheng, *Acc*. *Chem*. *Res*. 2005, **38**, 293.

6 a) N. Zheng, X. Bu, B. Wang and P. Feng, *Science*, 2002, **298**, 2366; b) H. Li, J. Kim, M. O'Keeffe and O. M. Yaghi, *Angew*. *Chem*., *Int*. *Ed*. 2003, **42**, 1819.

7 a) G. Ferey, C. Serre, F. Millange, C. Mellot-Draznieks, C. Surble, J. Dutour, and I. Margiolaki, *Angew*. *Chem*. *Int*. *Ed*., 2004, **43**, 6296; b) G. Ferey, C. Mellot-Draznieks, C. Serre, F. Millange, J. Dutour, G. Surble and I. Margiolaki, *Science*, 2005, **309**, 2040.

8 a) M. Murrie, D. Collison, C. D. Garner, M. Helliwell, P.A. Tasker, and S. S.

Turner, *Polyhedron* 1998, **17**, 3031; b) V. Tangoulis, C. P. Raptopoulou, and A. Terzis, *Inorg. Chem.*, 1998, **37**, 3142; c) Y.-L. Bai, J. Tao, R.-B. Huang and L.-S. Zheng, *Angew. Chem. Int. Ed.*, 2008, **47**, 5344.

9 a) Demko, Z. P.; Sharpless, K. B., Angew. Chem. Int. Ed. 2001, 41, 2010; b) Demko, Z.P.; Sharpless, K. B., Angew. Chem. Int. Ed. 2001, 41, 2013

10 a) Brown, D.; Altermatr, D., Acta Cryst., 1985, B41, 244; b) Brese, N. E.; O'Keeffe, M., Acta Cryst., 1991, B47,192

Chapter 4

Single Crystal X-ray Snapshots of Reaction Intermediates MOF Redox Catalyst

4.1 Introduction

Capturing the intermediates of chemical reactions for probing and understanding the reaction mechanisms have been an interesting and yet highly challenging pursuit for decades. Spectroscopic techniques are often used for such studies, even though such techniques often yield indirect evidences with more than one possible interpretation. Single crystal structure analysis as a powerful tool for unambiguously determining the structures at the atomic level has seen very limited use for probing and elucidating mechanistic aspects of catalytic reactions, because there are at least two major challenges. One is the requirement of the three-dimensional crystallographic ordering for the active sites. This is very difficult to meet, especially for redox catalysts in which redox active sites often exist at the dopant level in a non-active host matrix and can not achieve long-ranging ordering at all. The second requirement is the capture of reaction intermediates in the single-crystal matrix, with the perfect orientation so that the long-range ordering can also be accomplished for captured intermediates as well.

Porous materials are an ideal family of solids that may serve as the platform to address the above formidable challenges,[1-11] because the captured intermediates within channels and cavities of porous materials could, under ideal cases, adopt the three-dimensional periodicity of the cages or channels and therefore lend themselves

amenable to single crystal structure analysis. Recently, Fujita's group provided a elegant demonstration of this feasibility by capturing the transient intermediate states with sequential X-ray-based snapshots within a porous network material.[7,12] In their work, the framework itself does not possess catalytic site and instead it serves to host both catalytic species and reactants and to promote the catalytic process through the confinement effect of pores.

In the work presented hereby, by using vanadium as a structural building unit together with 1,3, 5-benzenetricarboxylic acid (H_3BTC), we have successfully synthesized porous materials with crystallographically ordered redox active centers embedded right on the porous framework. We demonstrate here that this novel material combines size selectivity with highly redox active catalytic sites. Most importantly, through epoxidation of alkene, this material allows the capture of a series of intermediates which can then be directly observed by single crystal X-ray analysis. Such direct observation not only provides insight into the catalytic process, but also makes it possible to pinpoint the exact active sites out of multiple crystallographically unique vanadium sites.

4.2 General Methodology

1,3,5-benzenetricaboxylic acid (btc) (TCI), vanadium(III) chloride anhydrate (Aldrich), cobalt(II) nitrate hexahydrate (Aldrich), nickel(II) chloride (Fisher), indium nitrate hydrate (Alfa Aeser), iron(III) chloride hexahydrate (Acros), hydrochloric acid (Alfa Aeser), 2, 4 biphenyldicarboxylic acid (bpdc) (Acros), sodium hexafluorosilicate (Aldrich), (+,-) 2-amino-1-butanol (Acros) and benzoic acid (Aldrich), were used as

purchased without any further purification.

Gas chromatography (GC) was performed on a Shimadzu 2010 gas chromatograph equipped with a (5% Phenyl)-95% Methoxpolysiloxane capillary column, flame ionization detector using He as the carrier gas. The thermogravimetric data were collected on a TA Q500 instrument. Powder XRD was measured on a Bruker D8 Advance Powder X-ray Diffraction instrument on monochromatic Cu Kα (λ = 1.54060 Å) radiation. Adsorption isotherms for nitrogen, hydrogen as well as carbondioxide were collected on a Micromeritics ASAP 2020 volumetric adsorption instrument.

4.2.1 Synthesis of CPF -28 Series

4.2.1.1 Synthesis of CPF-V-28

The CPF-V-28 ($V_3O(H_2O)_3V_3(H_2O)_3Cl_3(VO)_6(BTC)_6Cl_3$) reported hereby is synthesized under hydrothermal condition. By reacting a mixture of VCl3 powder (150mg), btc (100 mg), benzoate adduct benzoic acid (40 mg), in a solution of 4M hydrochloric acid aqueous solution (**CAUTION**: High acidity reaction system is extremely corrosive to steel autoclaves under high temperature, keep checking autoclaves condition frequently. Pre-damaged autoclaves are subjected to potential explosions though we have never encountered.) under 210^{o}C for 5-7 days in a 23ml Teflon-vial, emerald green crystals beautifully formed of 45% yield based on vanadium source. The crystalline sample was collected by centrifuge under 500 r/min for 30 seconds after washing with 95% ethanol to float away the amorphous benzoate adducts powder. The crystal for single crystal X-ray diffraction was picked from the batch using bpdc as adduct which helps to increase the crystal size. Noteworthy that adducts strongly effect

the crystal formation in the synthetic system (shown in Table 4.1), bpdc is the best adduct in forming large crystals. Data of the single crystal X-ray structure analysis, powder–XRD pattern, and TGA information, are all obtained from the sample as synthesized. Catalytic experiment, gas adsorption isotherms were performed on the samples with solvent exchange treatment in toluene for 24 hours followed by degas procedures under 140^{o}C.

Table 4.1 Supplementary reaction condition tuning on VCl3-btc-HCl system

Reaction conditions and Adducts	Product Morphology
/	Powder
1,4' bpdc	Large crystal
Benzoic acid	Micro crystal
1,3' bpdc	Micro crystal
1,3 bdc	Micro crystal
NaCl with lower acidity	Micro crystal
NH_4Cl with lower acidity	Micro crystal
180 ^{o}C	Amorphous powder

4.2.1.2 Synthesis of CPF-V-28-F

The CPF-V-28-F ($V_3O(H_2O)_3V_3(H_2O)_3F_3(VO)_6(BTC)_6Cl_3$) could be synthesized also with hydrothermal methods however under basic conditions which is autoclaves benign. By reacting a mixture of VCl_3 powder (150 mg), btc (100 mg) and sodium hexafluorosilicate (20 mg), in a 2 ml aqueous solution with 100 mg (+,-) 2-amino-1-butanol under 210^{o}C for 5 days in a 23ml Teflon-vial, large emerald green crystals beautifully formed of 41% yield based on vanadium source.

4.2.1.3 Synthesis of CPF-CoV-28

The CPF-CoV-28 is a mixed metal iso-structure to CPF-V-28. It could be synthesized under hydrothermal conditions similar to CPF-V-28-F. By reacting a mixture of VCl3 powder (120 mg), cobalt(II) nitrate hexahydrate (120 mg), btc (100 mg) and sodium hexafluorosilicate (20 mg), in a 2 ml aqueous solution with 100 mg (+,-) 2-amino-1-butanol under 210oC for 5 days in a 23ml Teflon-vial, purple-pink crystals are obtained.

4.2.1.4 Synthesis of CPF-NiV-28

The CPF-NiV-28 is a mixed metal iso-structure to CPF-V-28. It could be synthesized under hydrothermal conditions similar to CPF-V-28-F. By reacting a mixture of VCl3 powder (120 mg), nickel(II) chloride (120 mg), btc (100 mg) and sodium hexafluorosilicate (20 mg), in a 2 ml aqueous solution with 100 mg (+,-) 2-amino-1-butanol under 210oC for 5 days in a 23ml Teflon-vial, purple-pink crystals are obtained.

4.2.1.5 Synthesis of CPF-InV-28

The CPF-InV-28 is another mixed metal iso-structure to CPF-V-28. It could be synthesized by adding indium source to synthetic condition of CPF-V-28-F. By reacting a mixture of VCl3 powder (120 mg), indium nitrate hydrate (120 mg), btc (100 mg) and sodium hexafluorosilicate (20 mg), in a 2 ml aqueous solution with 100 mg (+,-) 2-amino-1-butanol under 210oC for 5 days in a 23ml Teflon-vial, pale green hexagonal pillar crystals are obtained.

4.2.1.6 Synthesis of CPF-FeV-28

The CPF-FeV-28 is another mixed metal iso-structure to CPF-V-28. It could be synthesized by adding iron source to synthetic condition of CPF-V-28-F. By reacting a mixture of VCl3 powder (120 mg), iron(III) chloride hexahydrate (120 mg), btc (100 mg) and sodium hexafluorosilicate (20 mg), in a 2 ml aqueous solution with 100 mg (+,-) 2-amino-1-butanol under 210oC for 5 days in a 23ml Teflon-vial, huge dark brown block crystals are obtained.

Table 4.2. Crystallographic data and structure refinement for CPF-V-28

	CPF-V-28	CPF-CoV-28	CPF-NiV-28	CPF-InV-28	CPF-FeV-28	CPF-V-28-F
Space Group	P-31c	P-31c	P-31c	P-31c	P-31c	P-31c
Unit Cell	a = 14.6993	a = 14.7029	a = 14.7231	a = 15.0821	a = 14.6716	a = 14.7123
	c = 31.8035	c = 31.8200	c = 31.8482	c = 31.8922	c = 31.8559	c = 31.7693
	α = 90	α = 90	α = 90	α = 90	α = 90	α = 90
	γ = 120	γ = 120	γ = 120	γ = 120	γ = 120	γ = 120
Cell Volume	5951.12	5957.12	5978.80	6282.59	5938.50	5955.24
Void Space (PLATON Cacd)	54.1%					
Temperature	296 K	296 K	296 K	296 K	296 K	296 K
Reflections Collected	3543	4631	3548	3648	4548	3527
Independent Reflections	2941	4210	3177	2866	3984	2526
GOOF	1.079	1.182	1.184	1.146	1.127	1.107
Final R1[a] [I > 2σ(I)]	0.0651	0.0636	0.0598	0.0809	0.0771	0.0857
Final wR2[b] [I > 2σ(I)]	0.1940	0.0676	0.0647	0.1009	0.0854	0.1157

4.2.2 General Characterizations

4.2.2.1 Morphology of CPF-V-28 crystals

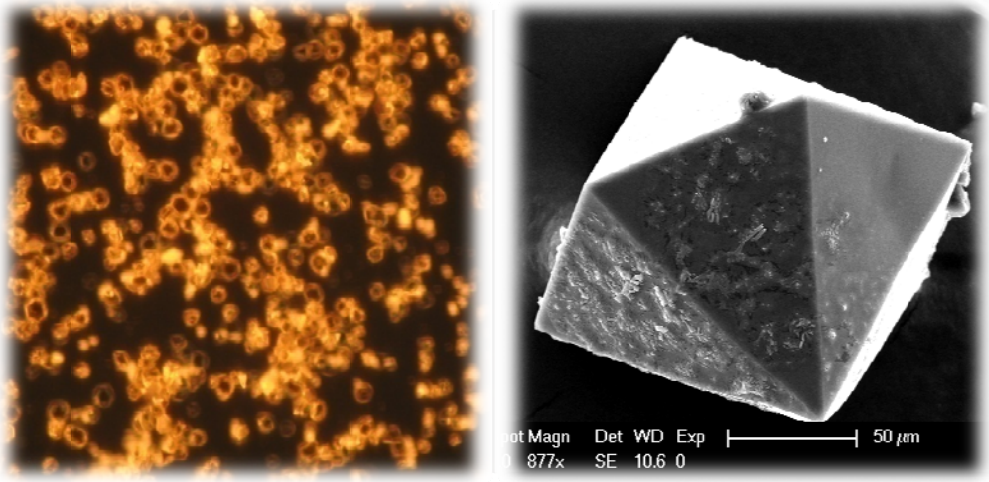

Figure 4.1. Left: dark field optical image of crystals synthesized; right: SEM image of single crystal CPF-V-28.

4.2.2.2 Powder XRD Patterns of CPF-V-28 Structure

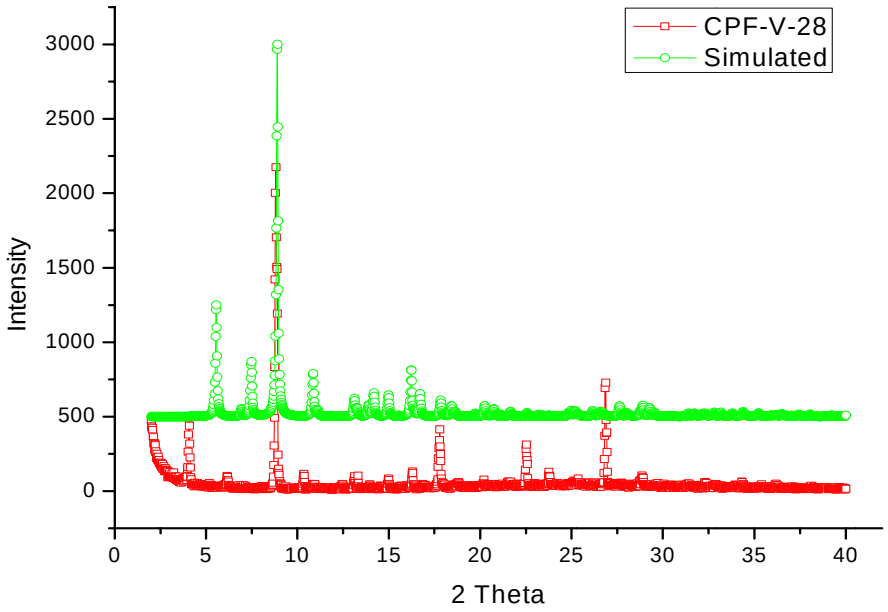

Figure 4.2. Powder-XRD patterns of as-synthesized CPF-V-28 sample and simulated diffractions.

4.2.2.3 Thermal Stability Test

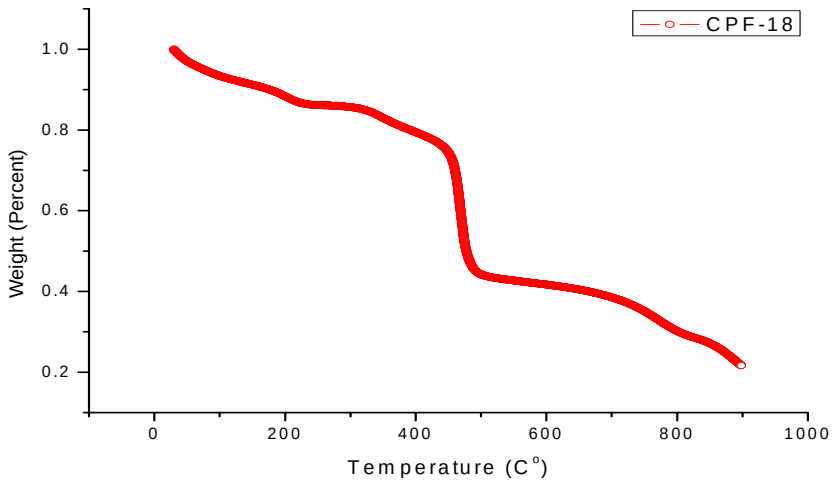

Figure 4.3. Thermogravimetric analysis of CPF-V-28 in nitrogen atmosphere.

4.2.2.4 XPS of CPF-V-28

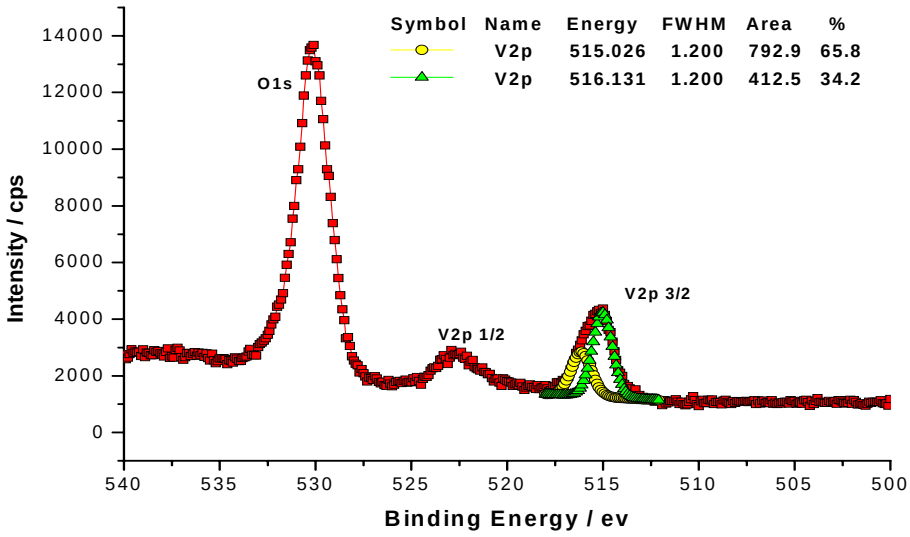

Figure 4.4. XPS of CPF-V-28.

The fresh CPF-V-28 crystals are washed with ethanol to eliminate the organic

acids not reacted. The samples are vacuum dried to prevent potential oxidation by air. The XPS data indicates vanadium in the sample is of mixed valence. Both V(III) (binding energy: 516 ev) and V(IV) (binding energy: 515 ev) are present in CPF-V-28 crystals.

4.2.2.5 Elemental Analysis on CPF-28 Series

The EDAX data proves the component variance on this structure is feasible once co-catalyst metal species are needed for other catalytic reactions. And this MOF catalyst with multi-metal cluster units is robust and tolerant enough on doping with other metal even with different valence. We believe the variable vanadium valence is responsible for this relatively higher self-adjusting ability comparing to other single-metal-node and single valence systems.

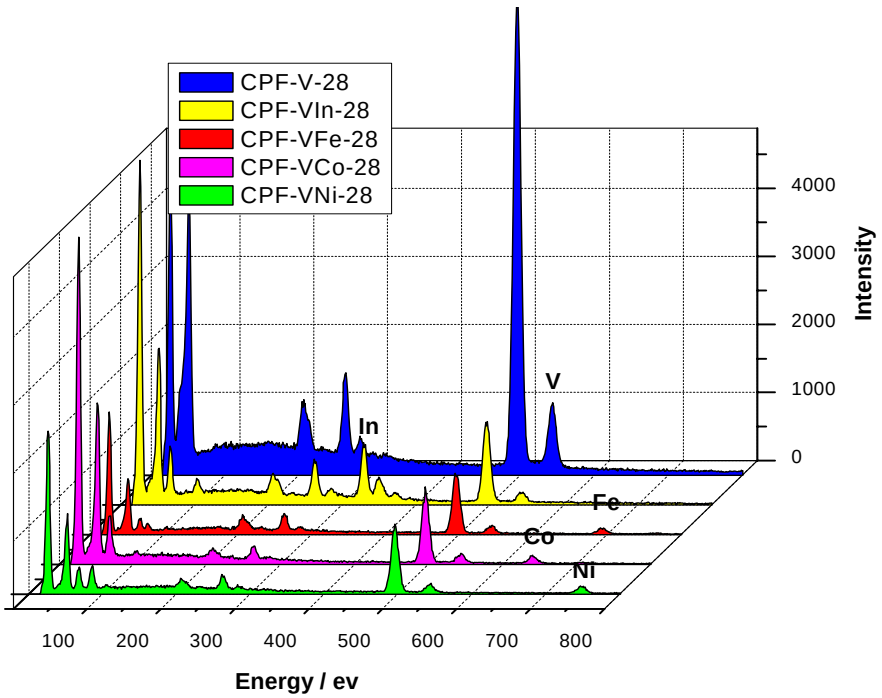

Figure 4.5. EDAX of CPF-28 series.

4.2.3 Gas Adsorption Behavior

4.2.3.1 Oxygen Adsorption of CPF-V-28

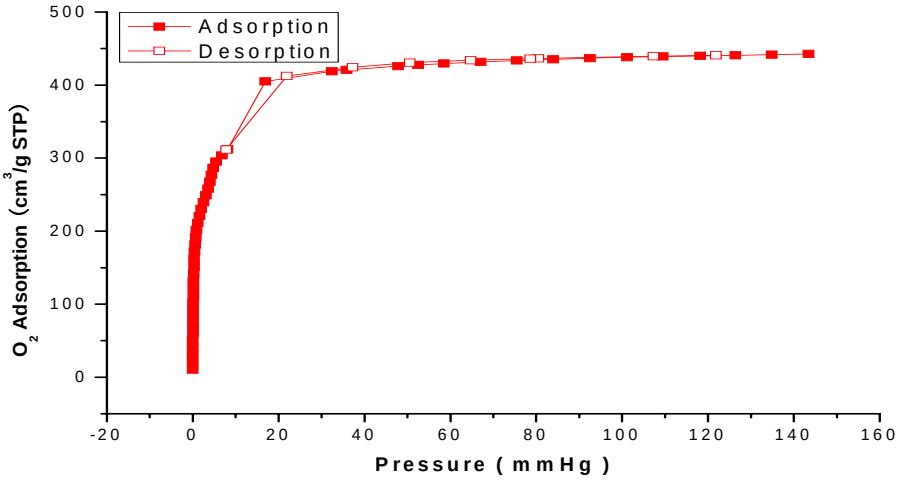

Figure 4.6. Oxygen adsorption isotherm of CPF-V-28 under 77K.

4.2.3.2 CO_2 Adsorption of CPF-V-28

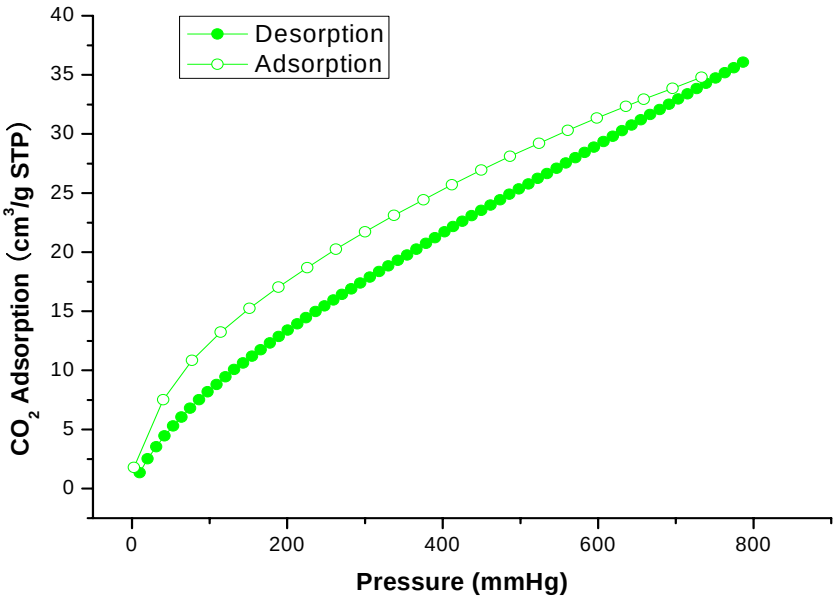

Figure 4.7. Carbon dioxide adsorption isotherm of CPF-V-28 under 273.15K.

4.2.3.3 H_2 Adsorption of CPF-V-28

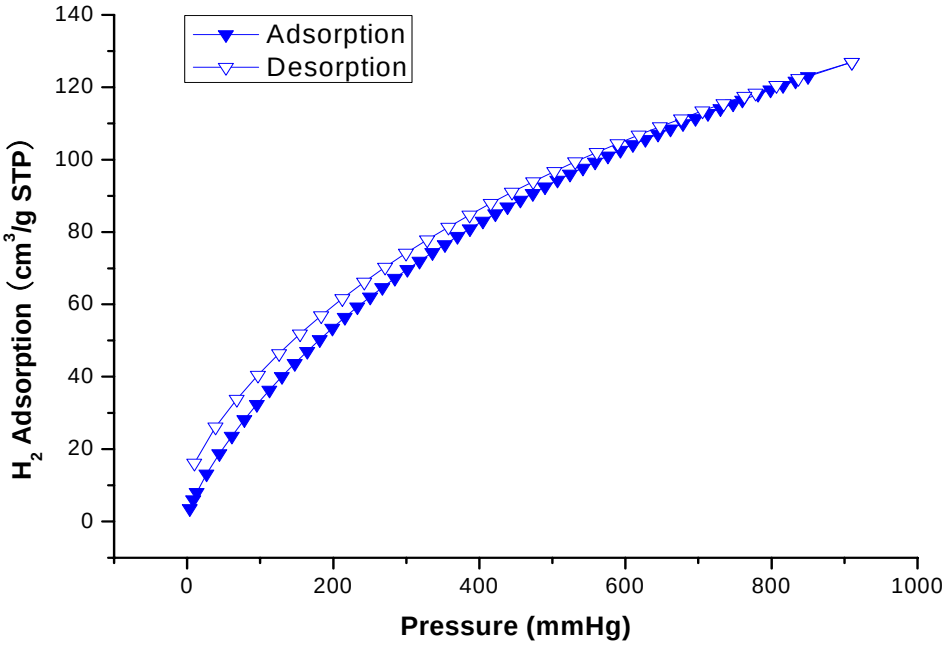

Figure 4.8. Hydrogen adsorption isotherm of CPF-V-28 under 77K.

4.3. Results and Disscussion

4.3.1 Structural Description

The material $V_3O(H_2O)_3V_3(H_2O)_3Cl_3(VO)_6(BTC)_6Cl_3$ denoted as CPF-V-28 is synthesized by hydrothermal method. Emerald green hexagonal shaped crystals were obtained that possess structural similarity with MIL-96. The material has two trimetal clusters with different chemical environments. The first type cluster is a trimeric oxo-centered carboxylate-bridged $V(III)_3(H_2O)O(OOCR)_6$. It is commonly obtained in many stand-alone molecular aggregates however still quite rare in the polymeric framework built by vanadium. The three six coordinated V(III) atoms shared a center μ3-O and linked by bridging carboxylate groups between one another through equatorial

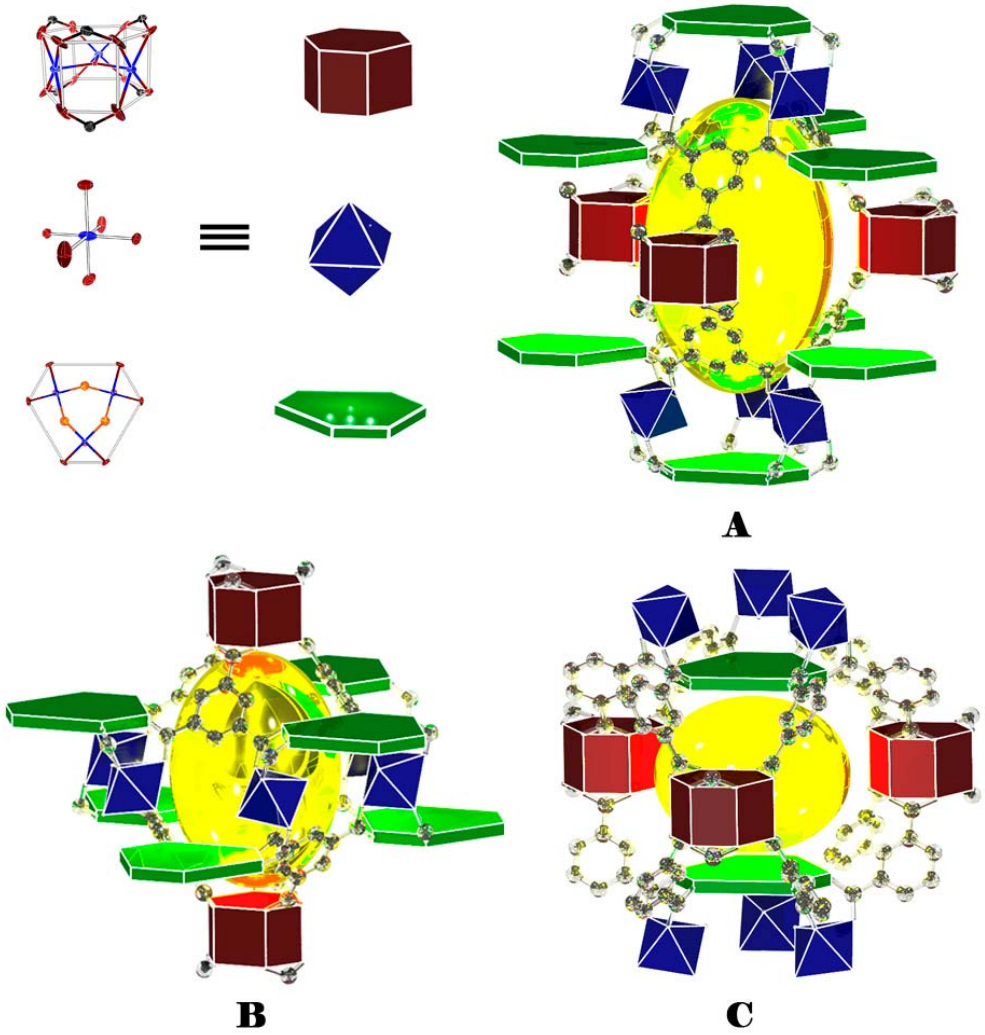

Figure 4.9. Three types of cages built by btc ligand and vanadium trimer building units. White: carbon; red: oxygen; green: chlorine; yellow polyhedral: vanadium.

position, leaving the last coordination site trans to the μ3-O occupied by an axial water molecule which is ready to be removed for generating active open-metal-site. Quite different from MIL-96 which having metal nodes all connected by oxygen atoms, the other type of vanadium trimer in CPF-V-28 is an unprecedented hexagonal planar $V(III)_3Cl_3(OOCR)_6$ cluster, the three V(III) ions are connected through three bridging

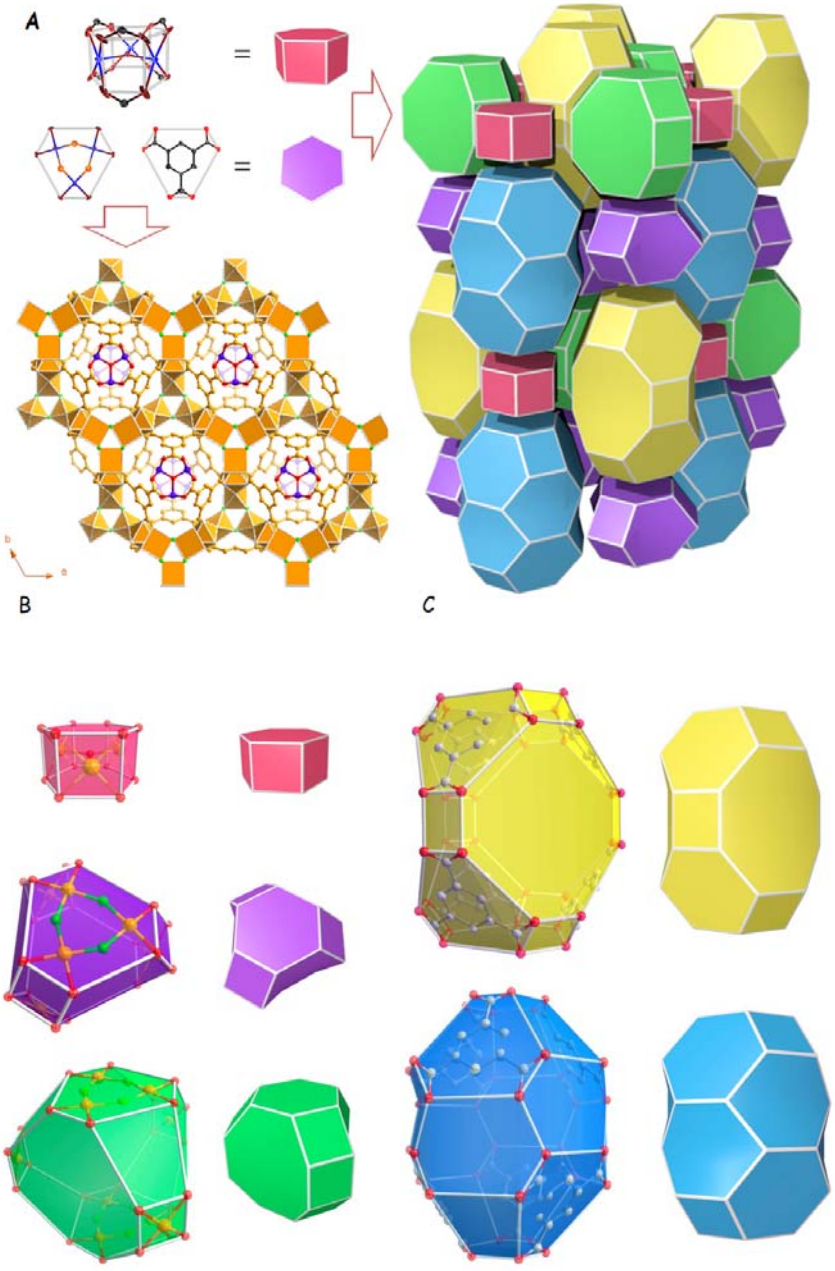

Figure 4.10. CPF-V-28 framework. A. Real molecular building units and geometrical simplifications. B. Structure viewed along c axis C. Natural tiling of overall topology. D. Structural comparison between individual actual molecular cages and their topological representation.

chloride anion to form a planar six-member ring. The V(III) ions in this trimetal cluster

are also six-coordinated with two sides of axial positions occupied by oxide anions and coordinated water respectively. The geometry of such chloride trimer bears close similarity with the structure fragment in solid state VCl_3. This may be related to the unusually high concentration of chloride anion in our synthetic system. Note worthy is that in both trimers the coordinated dangling oxygen atoms possess relatively longer bond length (2.05 and 1.92 angstrom) than that of oxide terminated vanadyl (1.57 angstrom V-O double bond), which indicates that the coordinated oxygen could be labile solvent molecule.

The two types of vanadium trimers are connected through btc ligand and six-coordinated vanadium atoms to form extended 3-D framework with three different cages (as shown in Figure 4.9). The cages A and B are identical with the ones in MIL-96, that have large void space and relatively small window openings. Two Cl- anions on the ends of cage B in CPF-V-28 crystal were identified for charge balancing. However very different from MIL-96-Al is that the cage C in CPF-V-28 has no dangling monomers blocking the catalytic sites. Thus it makes the generation of open-metal site much easier and leaves larger vacant space around the two types of vanadium trimer units for potential catalytic reactions. The material could be doped easily with other metal ions such as Fe, In, Co, and Ni.

4.3.2 Pore Structure Assessment on CPF-V-28 Catalyst

Permanent porosity of this material is confirmed by N_2 adsorption experiment which was performed on Micromeritics ASAP 2020. A series of degas conditions were tested and 140^{o}C to 200^{o}C temperature range could readily evacuate all the guest

molecules in the pore system to provide the maximum adsorption capacity without structural collapses. Nitrogen adsorption-desorption behavior of the activated material

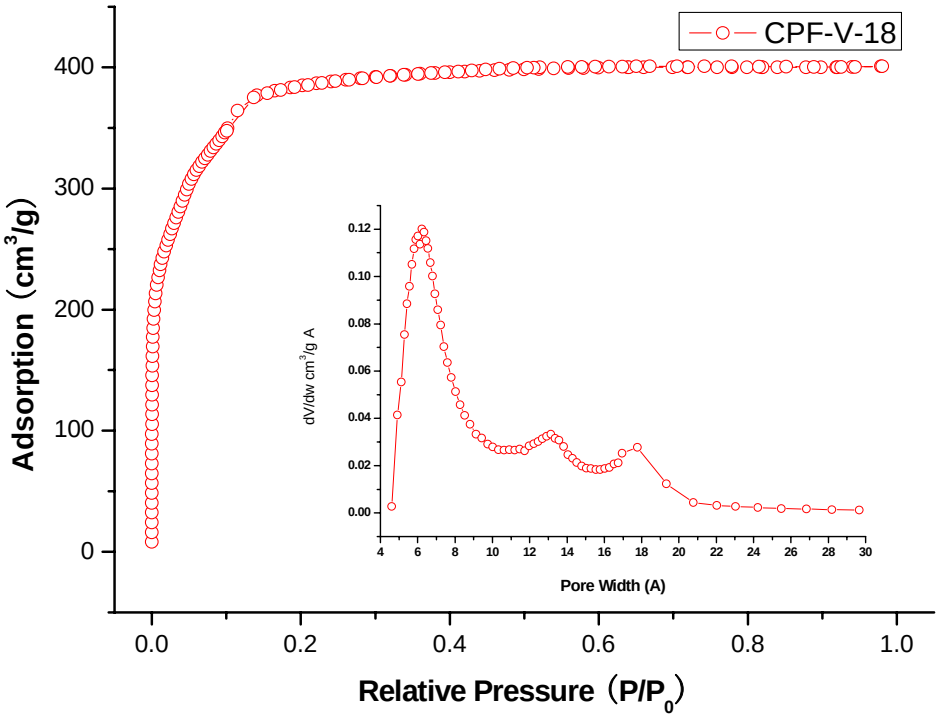

Figure 4.11. Nitrogen adsorption isotherm and pore distribution of CPF-V-28 under 77K.

clearly shows a reversible type-I isotherm (shown in Figure 4.11) with nitrogen uptake of 410 cm^3/g, which is equivalent to BET surface area of 1127 m^2/g and Langmuir surface area of 1787 m^2/g assuming monolayer coverage. Experiments for the adsorption of many other gas molecules were performed on this material. Noteworthy that very high uptake of oxygen adsorption under liquid nitrogen temperature on CPF-V-28 is observed (Figure 4.6) corresponding to the strong interactions between the gas molecule and framework. It is suggested by the stronger binding of oxygen molecule that, the open metal sites are present and they participate in the adsorption process. The general high

uptake for various guest molecules (shown in Figure 4.7, 4.8) is in well consistent with the PLATON calculated 54.1% void space within the crystal lattice. And such high surface area which is accessible to guest molecules is essential for the vanadium sites assisted catalytic reaction in confined space.

4.3.3 Catalytic Activity Assessment on CPF-V-28

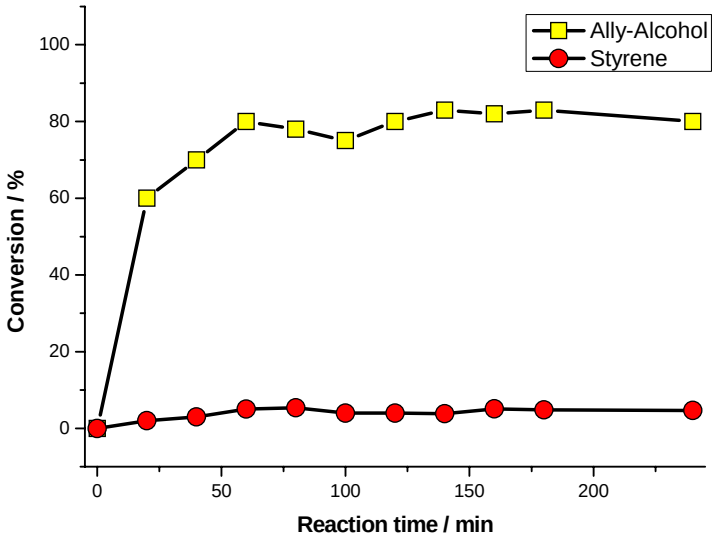

Figure 4.12. Reactivity bias on different sized olefin substrates.

As illustrated above, the existence of vanadium open metal sites is proved, and these active sites are readily accessible to small molecules. We hereby select the olefin epoxidation as the prototype reaction since vanadium is among the literature assessed best candidate for this reaction.[13] A series of olefin substrates are screened to evaluate the catalytic behavior of CPF-V-28. The substrate molecule sizes increased from smaller allyl-alcohol to larger ones as styrene. Among the various substrates, the smallest molecule as allyl-alcohol shows highest reaction rate. It is readily converted to epoxide product with 100% selectivity and 98% conversion rate within only 20 minutes which

corresponds to a turnover frequency of 30 per hour. This conversion rate is much faster comparing to the conventional active vanadium dopants assisted heterogeneous porous reactors since the vanadium based MOF is believed to be more effectively exposing active sites. However, the reaction rate decreased fast when the substrate becomes bulky. And it dropped to only 5.4% in conversion rate over 6 hours for largest chosen molecule

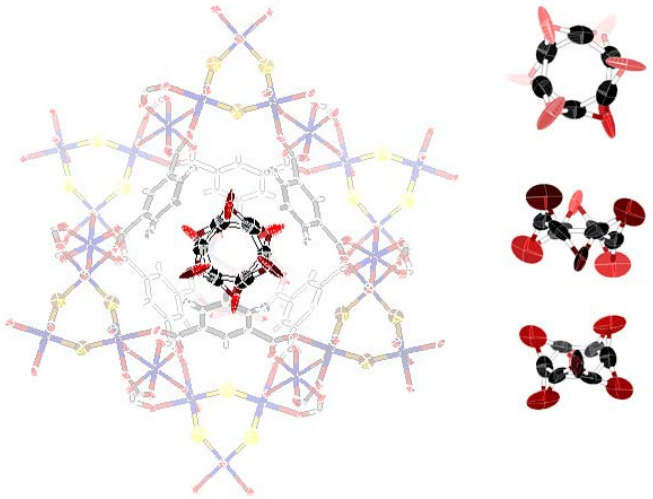

Figure 4.13. The observed epoxide product to cyclohexene in cage A of CPF-V-28.

as styrene (Figure 4.12). This size dependent reaction rate suggests the catalytic reaction is taking place within pore structure rather than just happening on the surface. The largest active substrate to the CPF-V-28 catalyst is cyclohexene, and its epoxide product is observed to be rotating along c axis freely in cage A (Figure 4.13) of the catalyst. This proves the permeability of pore structure to this product, its substrate and other smaller molecules. The uniform small sized channel windows inhibit the contact of larger substrates from the active centers which located within crystal lattice. The styrene molecule could not be located crystallographically even after the crystal emerged in its

concentrated toluene solution for days. We believe it is because of the solvated styrene molecule possessing a larger kinetic diameter than to the 6 angstrom channel window determined by nitrogen adsorption data (Figure 4.11), and therefore quite reasonable to appear almost inert. Moreover, to better illustrate the size selectivity induced by pore window regulation, the catalytic reaction upon mixed substrate is conducted, the reaction on the smaller sized molecules proceeds as intact however the larger sized substrate remains as inspector molecules (reactivity bias as shown in Figure 4.12). Very interestingly, the desiccated CPF-V-28 deep blue-green crystals changed to yellow-green during the reaction process, and recovered its original color when the reaction is finished. This suggests the catalytic center possibly experiences the oxidation state change and coordination environment change during the reaction process. This color-reversible phenomenon also suggests the reaction is taking place in a catalytic manner.

4.3.4 Active Sites Determination

Comparing to other chemical reaction matrix materials with trapped molecular catalyst or doped active metals where people generally experiencing difficulties in exactly positioning the active components, it is an intrinsic advantage that the local chemical environment of the active sites in MOF systems is precisely defined and aligned highly ordered. This gives rise to the opportunity of observing the local structure to the active intermediates by X-ray crystallography. To our best knowledge, even though the vanadium catalyzed olefin epoxidation is extensively studied; it is the first catalytic active vanadium MOF with open metal sites. It is well believed in molecular catalysis that the catalytic center usually undergoes coordination environment variation, hence we hereby

attempt to capture some direct evidence of such local structure change by single-crystal X-ray crystallography to a series of crystals under different reaction stage.

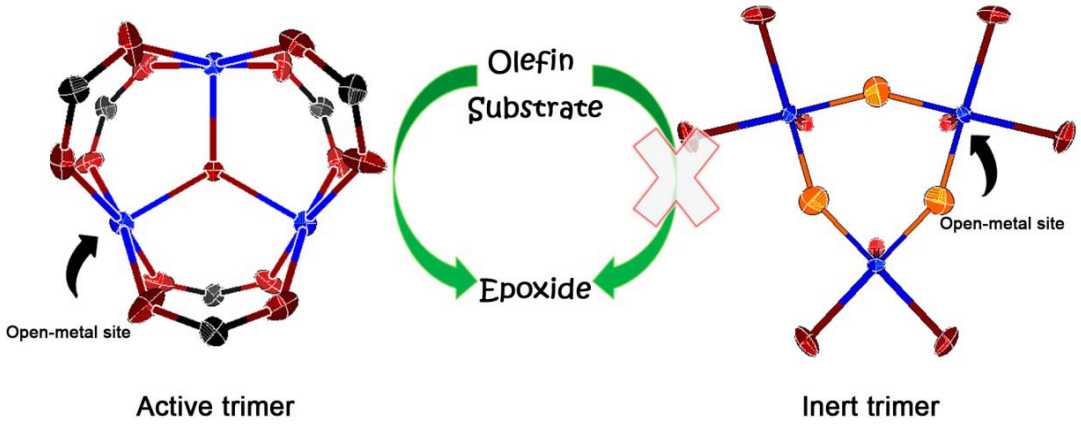

Figure 4.14. Local chemical environment and catalytic activity difference on two types of vanadium open-metal sites.

First important finding is the catalytic activity difference on the vanadium open-metal sites. The two types of open-metal sites present in CPF-V-28 differ from each other a lot both compositionally and geometrically. Hence they behave very differently in catalytic activity, and X-Ray resolved structures also confirmed our speculation. Residue peaks of closely bonded reactants and intermediate species are allocated on the open-metal site of trimeric oxo-centered carboxylate-bridged $V(III)_3(H_2O)O(OOCR)_6$ clusters that clearly prove their participation in the catalytic process. However, for the hexagonal planar $V(III)_3Cl_3(OOCR)_6$ clusters, we did not observed any coordinated reactive species, the axial position is steadily occupied by oxygen atoms and only shown a gradually bond lengths shrinkage as reaction proceeded which indicates potential oxidation on vanadium(III) active site however very slow. Therefore, we believe the material's activity should be contributed majorly form the can type $V(III)_3(H_2O)O(OOCR)_6$ trimers but the planar chloride trimers are almost inert (Figure

4.14).

4.3.5 Reaction Intermediates Capture

After determining the reaction sites responsible for the catalytic activity, we further investigated the local coordination environment of the oxo-centered active trimer. It is being widely accepted that the TBHP oxidant is the first reagent to make contact with the catalytic center and initiate the reaction; therefore the local geometry of such active site is of great importance for mechanistic study. However the conformation to this very initial stage is proposed differently in the literature. In our experiment, the local coordination geometry of TBHP oxidant is unambiguously determined. The axial position previously occupied by water is now replaced by the oxygen that on hydroxide end of TBHP. The V-O bond length is significantly shortened to 1.98 Å compared to the initial 2.05 Å of water coordination, which indicates the possibly loss of proton and the formation of a V(IV) peroxide complex with much stronger binding (Figure 5). The other oxygen atom on t-butyl end of TBHP occupies a side position with the very same bond length and leaves the t-butyl group wrapped in a crowded space between two benzene rings from btc ligands. Although the two oxygen atoms are of the same bond length hence possess comparable affinity towards the vanadium catalyst, comparing to this t-butyl-oxygen with too much steric hindrance, the hydroxide-oxygen on the axial position is more accessible to other guest molecules in the pore channels hence should be more reactive.

Knowing the catalytic turnover time rage is on the scale up to tens of minutes, we further exposed the fresh oxidant bonded crystal to allyl chloride toluene solution shortly

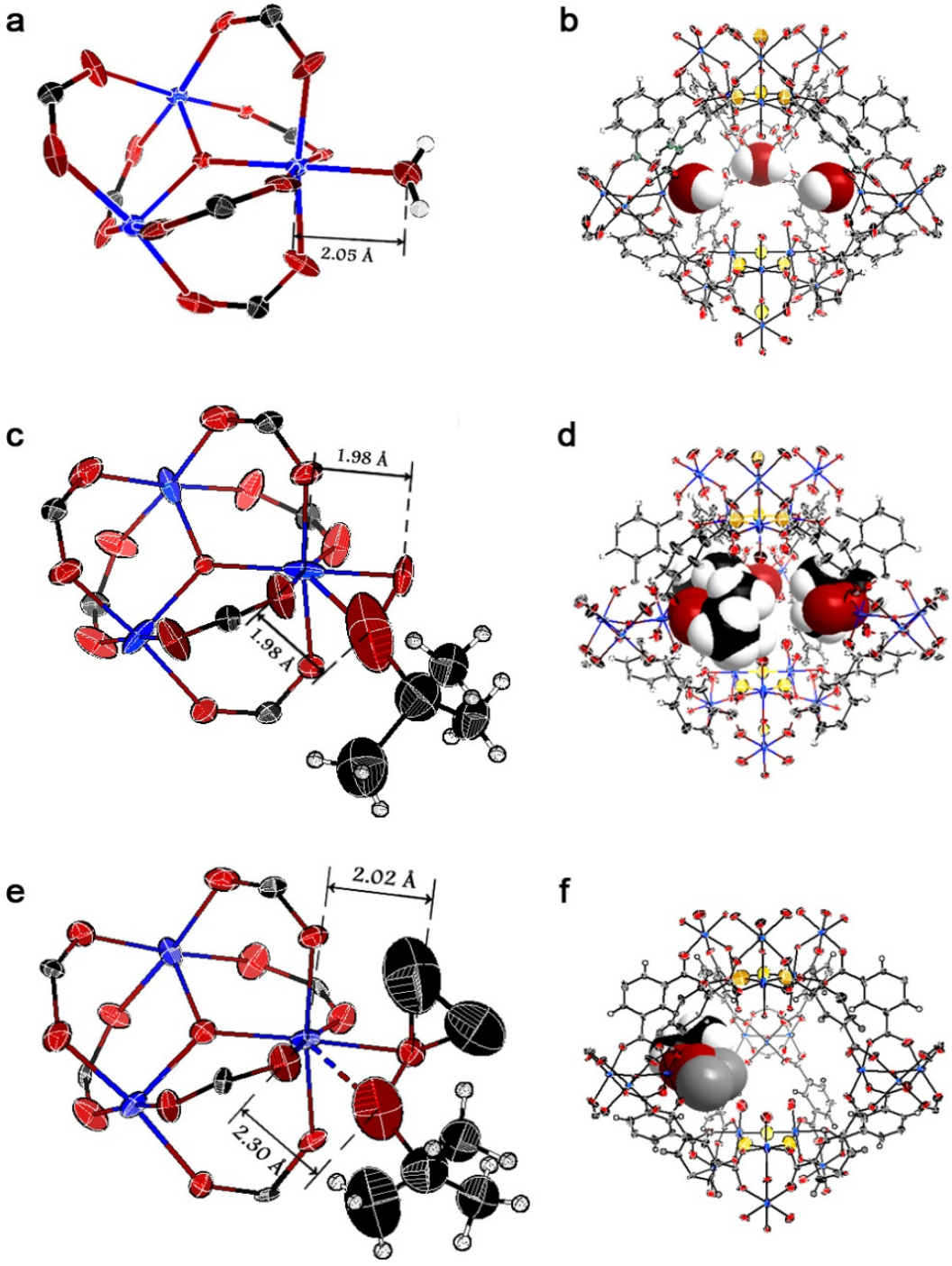

Figure 4.15. Local chemical environment on active vanadium open-metal site at different reaction stages. A: pre-catalytic state; c: oxidant activated state; e: epoxidation intermediate state; b, d and f represent space filling mode of guest molecule trapped in catalytic cage on different reaction stages respectively.

intermediate capturing turns to be very successful with the help of liquid nitrogen flow freezing. The crystal data clearly shows an epoxide fragment formed on the hydroxide to allow the contact between olefin substrate and activated TBHP. The ex-situ intermediate capturing turns to be very successful with the help of liquid nitrogen flow freezing. The crystal data clearly shows an epoxide fragment formed on the hydroxide oxygen side. This reactivity bias on the tow oxygen atoms is consistent to our expectation since the chemical environment at the t-butyl side oxygen is too crowded. Other than to the steric consideration, simulated frontier orbital of the oxidized catalyst also shows the hydroxide side oxygen is more reactive electronically (Figure 4.16).

It is of great necessity to point out that the V-O bond length between vanadium active center and epoxide oxygen is 2.02 Å, which is obviously elongated comparing to 1.98 Å on the previous reaction stage. The V-O distance for t-butyl attached oxygen is even elongated to 2.30 Å. The longer bond lengths on both oxygen atoms are quite reasonable because the current guest molecules on the active sites are electronically rich and generally believed to have more electrons populated in the V-O anti-bonding orbitals. They are readily to be substituted by new oxidants once there are available ones nearby. And the observed labile interaction between t-butyl side oxygen and vanadium center with such long distance of 2.30 Å also suggests the t-butanol possibly would first leave the active site after the O-O bond cleavage leaving behind the product bonded active center. Worth noticing that there is no obvious carbon-vanadium interaction, instead the olefin double bond is interacting directly to the vanadium bonded oxygen making the vanadium peroxide oxygen atoms triangle, and epoxide triangle being in “butterfly”

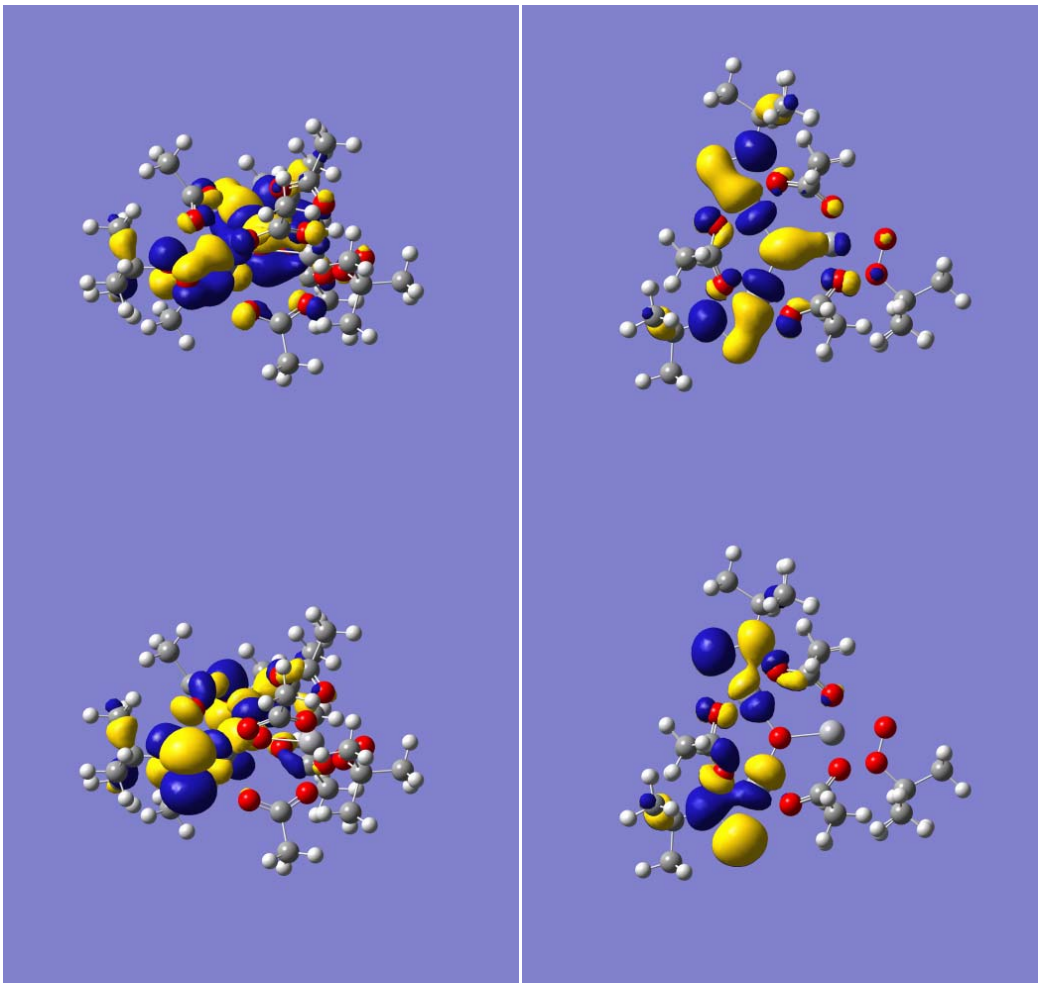

Figure 4.16. The frontier orbital of TBHP oxidized active sites. Up: HOMO; down: LUMO.

conformation and nearly co-planar (Figure 4.15). Such observed intermediate conformation bares very close similarity towards Bartlett's "butterfly" intermediate for olefin epoxidation by percarboxylic acids and is also in very well agreement with the mechanism proposed by Sharpless on several of similar vanadium carboxylate based catalysts.[15] The rest of the atoms on the chosen olefin substrate is highly disordered hence not located due to the lack of bonding constrains; however the captured core structure has already evidently revealed the conformation of the intermediate state. To our best knowledge, this is the first X-ray resolved reaction intermediate to catalytic epoxidation

process and we believe it would provide some basic clues to other similar epoxidation catalysts.

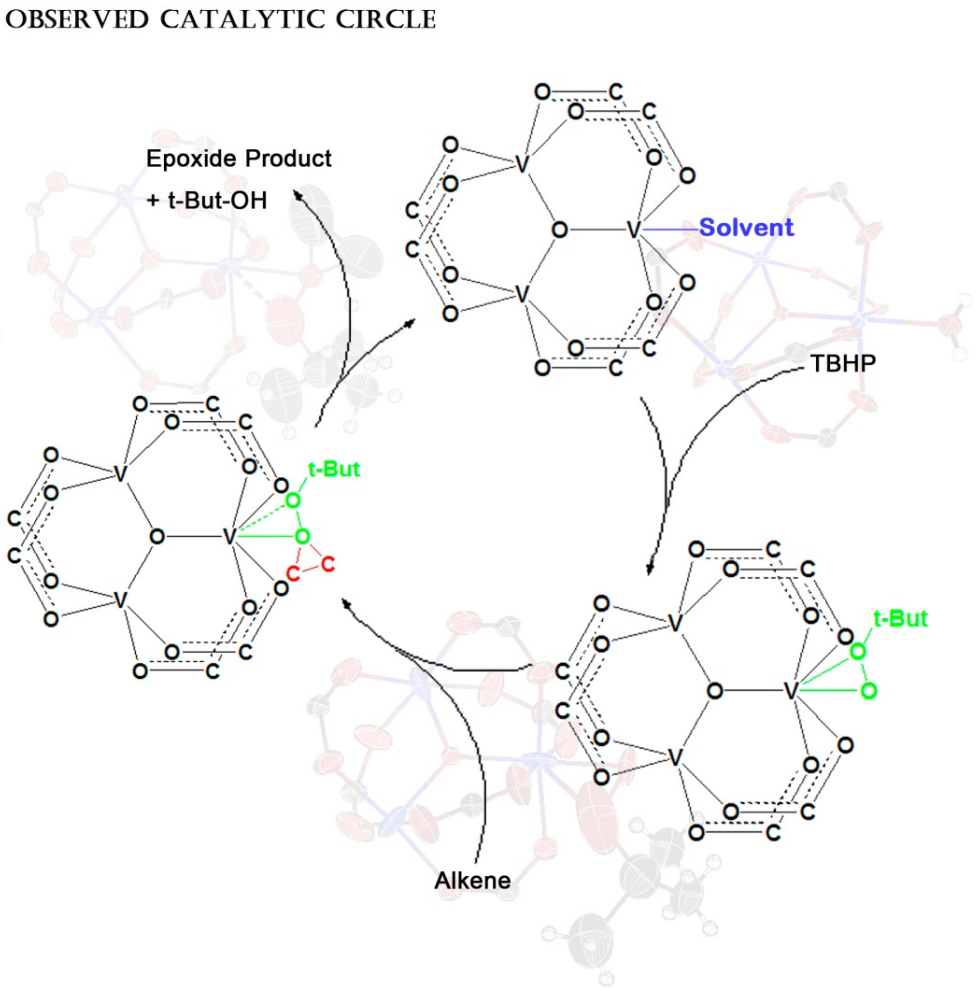

Figure 4.17. The proposed mechanism based on crystallography observations.

In addition to studying the catalytic intermediates by TBHP oxidant, we also applied the same methodology for the aerobic epoxidation reaction. Isobutyraldehide was introduced as co-catalyst, and the interaction conformation between co-catalyst and vanadium active site is captured. The determined structure to the pre-catalyst stage is in well agreement with the mechanism proposed for typical Mukaiyama process (Figure

S13).[19] This success shows the methodology of determining reaction intermediate states on highly ordered parallel reaction arrays trapped in MOF structures is general and very promising for the multi component reactions with long turnover periods. However due to the difficulty of oxygen exclusion in current ex-situ experiments, further investigation by in-situ data collection is under progress and will be reported elsewhere.

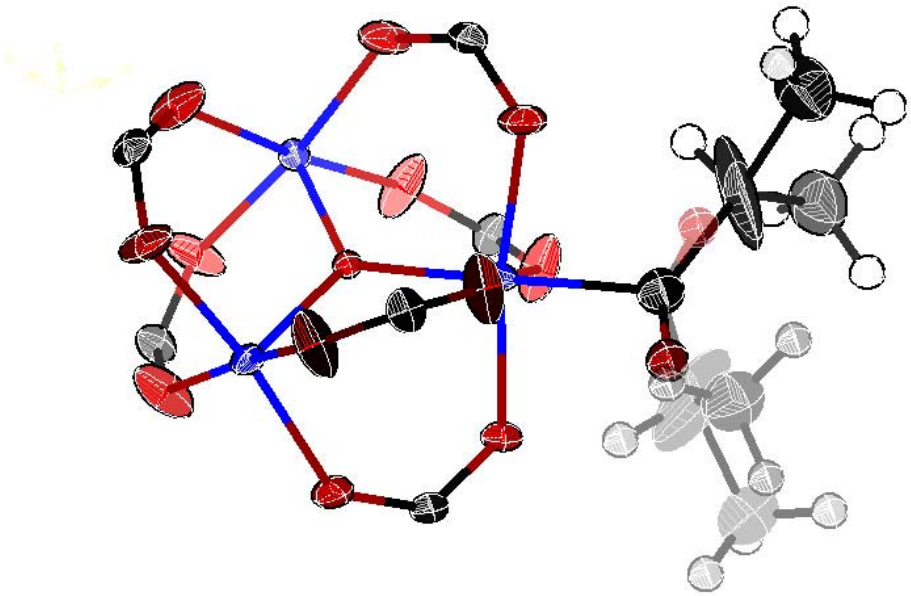

Figure 4.18. The observed local structure of the pre-catalytic stage in Mukaiyama process.

4.4 Conclusion

In conclusion, a conceptual experiment has been performed to capture the epoxidation intermediates on a novel crystalline porous vanadium catalyst. We have demonstrated that MOF as a unique type of crystalline open structures to bridge the gap between molecular and heterogeneous catalysts. MOF could serve as matrix materials that provide opportunities for detailed structural analysis on catalytic processes, for the X-ray crystallography as the direct structural analysis method could be applied to

unambiguously determine the conformation of intermediate species on each reaction stage. This method is advantageous especially for the d-orbitals participated catalytic processes as in many cases, when the introduced low activation energy barriers between different possible intermediate states hampers the exact prediction of the catalytic mechanism. Such solid proved structures would eliminate some ambiguities in the proposed mechanism and serve as good model compounds for further catalyst design.

4.5 Outlooks for Designing Other Redox MOF Materials

Encouraged by the stated work above, we believe the redox MOF material is of great potential in catalytic intermediates capture as well as performing size selective catalytic reactions. We are particularly interested in designing new redox active MOF materials with various pore sizes and channel geometries in order to examine other catalytic processes and to achieve the right pore size in distinguishing different substrates.

However for this type of redox MOF material, it is a widely accepted fact that the metals such as vanadium, chromium, titanium and zirconium with the desired functionality are binding to the ligand with very slow ligand exchange rates thus prohibits the formation of large single-crystals. However the metals such as zinc, copper, indium etc. are generally incapable in performing redox tasks even though they possess very fast ligand exchange rates and forms frameworks with very high crystallininty. Here I propose one possible general idea which is to utilize the early transition metal to form metal-ligand aggregates while apply another metal with faster ligand exchange rate to link up these preformed aggregates and build up the framework in a reversible way that allows self-refining in crystallization process.

4.6 References

(1) (a) Tranchemontagne, D. J.; Mendoza-Cortes, J. L.; O'Keeffe, M.; Yaghi, O. M., Chem. Soc. Rev. 2009, 38, 1257-1283;

(2) Ferey, G.; Serre, C., Chem. Soc. Rev. 2009, 38, 1380-1399;

(3) Kitagawa, S.; Kitaura, R.; Noro, S., Angew. Chem. Int. Edit. 2004, 43, 2334-2375;

(4) Wilmer, C. E.; Leaf, M.; Lee, C. Y.; Farha, O. K.; Hauser, B. G.; Hupp, J. T.; Snurr, R. Q., Nat. Chem. 2012, 4, 83-89.

(5) Rosi, N. L.; Eckert, J.; Eddaoudi, M.; Vodak, D. T.; Kim, J.; O'Keeffe, M.; Yaghi, O. M., Science 2003, 300, 1127-1129; (b) Duren, T.; Sarkisov, L.; Yaghi, O. M.; Snurr, R. Q., Langmuir 2004, 20, 2683-2689; (c) Kuppler, R. J.; Timmons, D. J.; Fang, Q. R.; Li, J. R.; Makal, T. A.; Young, M. D.; Yuan, D. Q.; Zhao, D.; Zhuang, W. J.; Zhou, H. C., Coordin. Chem. Rev. 2009, 253, 3042-3066.

(6) Inokuma, Y.; Kawano, M.; Fujita, M., Nat. Chem. 2011, 3, 349-358; (b) Inokuma, Y.; Arai, T.; Fujita, M., Nat. Chem. 2010, 2, 780-783; (c) Inokuma, Y.; Yoshioka, S.; Fujita, M., Angew. Chem. Int. Edit. 2010, 49, 8912-8914; (d) Inokuma, Y.; Ning, G. H.; Fujita, M., Angew. Chem. Int. Edit. 2012, 51, 2379-2381.

(7) (a) Chen, B. L.; Liang, C. D.; Yang, J.; Contreras, D. S.; Clancy, Y. L.; Lobkovsky, E. B.; Yaghi, O. M.; Dai, S., Angew. Chem. Int. Edit. 2006, 45, 1390-1393; (b) Britt, D.; Furukawa, H.; Wang, B.; Glover, T. G.; Yaghi, O. M., P. Natl. Acad. Sci. USA 2009, 106, 20637-20640.

(8) (a) Ma, S. Q.; Sun, D. F.; Wang, X. S.; Zhou, H. C., Angew. Chem. Int. Edit. 2007, 46, 2458-2462; (b) Li, J. R.; Kuppler, R. J.; Zhou, H. C., Chem. Soc. Rev. 2009, 38,

1477-1504; (c) Li, J. R.; Sculley, J.; Zhou, H. C., Chem. Rev. 2012, 112, 869-932.

(9) (a) Barcia, P. S.; Bastin, L.; Hurtado, E. J.; Silva, J. A. C.; Rodrigues, A. E.; Chen, B. L., Separ. Sci. Technol. 2008, 43, 3494-3521; (b) Chen, B. L.; Xiang, S. C.; Qian, G. D., Accounts. Chem. Res. 2010, 43, 1115-1124; (c) Xiang, S. C.; Zhang, Z. J.; Zhao, C. G.; Hong, K. L.; Zhao, X. B.; Ding, D. R.; Xie, M. H.; Wu, C. D.; Das, M. C.; Gill, R.; Thomas, K. M.; Chen, B. L., Nat. Commun. 2011, 2.

(10) (a) Corma, A., Chem. Rev. 1997, 97, 2373-2419; (b) Corma, A.; Garcia, H.; Xamena, F. X. L., Chem. Rev. 2010, 110, 4606-4655.

(11) (a) Ikemoto, K.; Inokuma, Y.; Fujita, M., J. Am. Chem. Soc. 2011, 133, 16806-16808; (b) Kawamichi, T.; Inokuma, Y.; Kawano, M.; Fujita, M., Angew. Chem. Int. Edit. 2010, 49, 2375-2377; (c) Ohara, K.; Inokuma, Y.; Fujita, M., Angew. Chem. Int. Edit. 2010, 49, 5507-5509.

(12) (a) Song, F. J.; Wang, C.; Falkowski, J. M.; Ma, L. Q.; Lin, W. B., J. Am. Chem. Soc. 2010, 132, 15390-15398; (b) Song, F. J.; Zhang, T.; Wang, C.; Lin, W. B., P. Roy. Soc. a-Math. Phy. 2012, 468, 2035-2052; (c) Wanderley, M. M.; Wang, C.; Wu, C. D.; Lin, W. B., J. Am. Chem. Soc. 2012, 134, 9050-9053.

(13) Kawamichi, T.; Haneda, T.; Kawano, M.; Fujita, M., Nature 2009, 461, 633-635.

(14) (a) Barthelet, K.; Riou, D.; Ferey, G., Chem. Commun. 2002, 1492-1493; (b) Ferey, G.; Mellot-Draznieks, C.; Serre, C.; Millange, F.; Dutour, J.; Surble, S.; Margiolaki, I., Science 2005, 309, 2040-2042; (c) Dan-Hardi, M.; Serre, C.; Frot, T.; Rozes, L.; Maurin, G.; Sanchez, C.; Ferey, G., J. Am. Chem. Soc. 2009, 131, 10857-10859.

(15) (a) Loiseau, T.; Lecroq, L.; Volkringer, C.; Marrot, J.; Ferey, G.; Haouas, M.; Taulelle, F.; Bourrelly, S.; Llewellyn, P. L.; Latroche, M., J. Am. Chem. Soc. 2006, 128, 10223-10230; (b) Volkringer, C.; Loiseau, T., Mater. Res. Bull. 2006, 41, 948-954; (c) Volkringer, C.; Loiseau, T.; Ferey, G.; Morais, C. M.; Taulelle, F.; Montouillout, V.; Massiot, D., Micropor. Mesopor. Mat. 2007, 105, 111-117.

(16) (a) Gould, E. S.; Hiatt, R. R.; Irwin, K. C., J. Am. Chem. Soc. 1968, 90, 4573-4579; (b) Itoh, T.; Kaneda, K.; Teranishi, S., Chem. Comm. 1976, 421-422; (c) Ritter, R. H.; Cohen, T., J. Am. Chem. Soc. 1986, 108, 3718-3725.

(17) (a) Oldroyd, R. D.; Sankar, G.; Thomas, J. M.; Hunnius, M.; Maier, W. F., J. Chem. Soc. Faraday. T. 1998, 94, 3177-3182; (b) Shylesh, S.; Singh, A. P., J. Catal. 2005, 233, 359-371.

(18) (a) Chong, A. O.; Sharpless, K. B., J. Org. Chem. 1977, 42, 1587-1590; (b) Michaelson, R. C.; Palermo, R. E.; Sharpless, K. B., J. Am. Chem. Soc. 1977, 99, 1990-1992.

(19) (a) Mukaiyama, T., Aldrichim. Acta. 1996, 29, 59-76; (b) Wentzel, B. B.; Alsters, P. L.; Feiters, M. C.; Nolte, R. J. M., J. Org. Chem. 2004, 69, 3453-3464.